2002-12

Performance of IEEE 802.11a wireless LAN standard over frequency-selective, slowly fading Nakagami channels in a pulsed jamming environment

Kosa, Irfan

Monterey California. Naval Postgraduate School

NAVAL POSTGRADUATE SCHOOL
Monterey, California

THESIS

PERFORMANCE OF *IEEE 802.11a* WIRELESS LAN STANDARD OVER FREQUENCY-SELECTIVE, SLOWLY FADING NAKAGAMI CHANNELS IN A PULSED JAMMING ENVIRONMENT

by

Irfan Kosa

December 2002

Thesis Advisor:	R. Clark Robertson
Second Reader:	Tri Ha

Approved for public release; distribution is unlimited

THIS PAGE INTENTIONALLY LEFT BLANK

REPORT DOCUMENTATION PAGE			Form Approved OMB No. 0704-0188
Public reporting burden for this collection of information is estimated to average 1 hour per response, including the time for reviewing instruction, searching existing data sources, gathering and maintaining the data needed, and completing and reviewing the collection of information. Send comments regarding this burden estimate or any other aspect of this collection of information, including suggestions for reducing this burden, to Washington headquarters Services, Directorate for Information Operations and Reports, 1215 Jefferson Davis Highway, Suite 1204, Arlington, VA 22202-4302, and to the Office of Management and Budget, Paperwork Reduction Project (0704-0188) Washington DC 20503.			
1. AGENCY USE ONLY ***(Leave blank)***	**2. REPORT DATE** December 2002	**3. REPORT TYPE AND DATES COVERED** Master's Thesis	
4. TITLE AND SUBTITLE: Performance of *IEEE 802.11a* Wireless LAN Standard over Frequency-Selective, Slowly Fading Nakagami Channels in a Pulsed Jamming Environment			**5. FUNDING NUMBERS**
6. AUTHOR(S) Irfan Kosa			
7. PERFORMING ORGANIZATION NAME(S) AND ADDRESS(ES) Naval Postgraduate School Monterey, CA 93943-5000			**8. PERFORMING ORGANIZATION REPORT NUMBER**
9. SPONSORING /MONITORING AGENCY NAME(S) AND ADDRESS(ES) N/A			**10. SPONSORING/MONITORING AGENCY REPORT NUMBER**
11. SUPPLEMENTARY NOTES The views expressed in this thesis are those of the author and do not reflect the official policy or position of the Department of Defense or the U.S. Government.			
12a. DISTRIBUTION / AVAILABILITY STATEMENT Approved for public release; distribution is unlimited.			**12b. DISTRIBUTION CODE**

13. ABSTRACT ***(maximum 200 words)***

Wireless local area networks (WLAN) are increasingly important in meeting the needs of the next generation broadband wireless communication systems for both commercial and military applications. In 1999, the *Institute of the Electrical and Electronics Engineers (IEEE) 802.11a* working group approved a standard for a 5 GHz band WLAN that supports a variable bit rate from 6 to 54 Mbps, and orthogonal frequency-division multiplexing (OFDM) was chosen because of its well-known ability to avoid multipath effects while achieving high data rates by combining a high order sub-carrier modulation with a high rate convolutional code. This thesis investigates the performance of the OFDM based *IEEE.802.11a WLAN* standard in frequency-selective, slowly fading Nakagami channels in a pulsed-noise jamming environment. Contrary to expectations, the signal-to-interference ratio (SIR) required to achieve a specific P_b does not monotonically decrease when the bit rate decreases. Furthermore, the results show that the performance is improved significantly by adding *convolutional coding* with *Viterbi decoding*, and thus highlights the importance of forward error correction (FEC) coding to the performance of wireless communications systems.

14. SUBJECT TERMS *IEEE 802.11a* standard, WLAN, OFDM, BPSK, QPSK, QAM, probability of bit error, frequency-selective fading, fast fading, slow fading, Nakagami fading, Viterbi algorithm, convolutional code, hard decision decoding, soft decision decoding, coding gain, pulsed jamming			**15. NUMBER OF PAGES** 129
			16. PRICE CODE
17. SECURITY CLASSIFICATION OF REPORT Unclassified	**18. SECURITY CLASSIFICATION OF THIS PAGE** Unclassified	**19. SECURITY CLASSIFICATION OF ABSTRACT** Unclassified	**20. LIMITATION OF ABSTRACT** UL

NSN 7540-01-280-5500 Standard Form 298 (Rev. 2-89)
Prescribed by ANSI Std. 239-18

THIS PAGE INTENTIONALLY LEFT BLANK

Approved for public release; distribution is unlimited

PERFORMANCE OF *IEEE 802.11a* WIRELESS LAN STANDARD OVER FREQUENCY-SELECTIVE, SLOWLY FADING NAKAGAMI CHANNELS IN A PULSED JAMMING ENVIRONMENT

Irfan Kosa
Lieutenant Junior Grade, Turkish Navy
B.S., Turkish Naval Academy, 1997

Submitted in partial fulfillment of the
requirements for the degree of

MASTER OF SCIENCE IN ELECTRICAL ENGINEERING

from the

NAVAL POSTGRADUATE SCHOOL
December 2002

Author: Irfan Kosa

Approved by: R. Clark Robertson
Thesis Advisor

Tri Ha
Second Reader

John Powers
Chairman, Department of Electrical and Computer Engineering

THIS PAGE INTENTIONALLY LEFT BLANK

ABSTRACT

Wireless local area networks (WLAN) are increasingly important in meeting the needs of the next generation broadband wireless communication systems for both commercial and military applications. In 1999, the *IEEE 802.11a* working group approved a standard for a 5 GHz band WLAN that supports a variable bit rate from 6 to 54 Mbps, and orthogonal frequency-division multiplexing (OFDM) was chosen because of its well-known ability to avoid multipath effects while achieving high data rates by combining a high order sub-carrier modulation with a high rate convolutional code. This thesis investigates the performance of the OFDM based *IEEE.802.11a WLAN* standard in frequency-selective, slowly fading Nakagami channels in a pulsed-noise jamming environment. The benefit of such an analysis is to assess the performance of an existing OFDM standard and to gain some insight into how well these systems will perform in military applications when subjected to hostile jamming. Contrary to expectations, the signal-to-interference ratio (SIR) required to achieve a specific P_b does not monotonically decrease when the bit rate decreases. Furthermore, the results show that the performance is improved significantly by adding *convolutional coding* with *Viterbi decoding*, and thus highlights the importance of forward error correction (FEC) coding to the performance of wireless communications systems.

THIS PAGE INTENTIONALLY LEFT BLANK

TABLE OF CONTENTS

LIST OF FIGURES

LIST OF TABLES

THIS PAGE INTENTIONALLY LEFT BLANK

ACKNOWLEDGMENTS

First of all I am grateful to my love, my wife, Hanife, for the sacrifices she made and for being so patient in support of completing this thesis.

I want to express my deepest appreciation to my thesis advisors, Professor R. Clark Robertson and Professor Tri Ha for their ever informative, insightful mentoring and for their endless hours of help, support and advice during the development of this thesis.

Thanks go out as well to Ron Russell for his help in editing my thesis.

Finally, I want to thank my country for giving me the opportunity to obtain such a priceless education at the Naval Postgraduate School.

THIS PAGE INTENTIONALLY LEFT BLANK

EXECUTIVE SUMMARY

The objective of this thesis was to investigate the performance of the OFDM based *IEEE.802.11a WLAN* standard in frequency-selective, slowly fading Nakagami channels in a pulsed-noise jamming environment. Prior to the analysis, we discuss *multipath fading* to examine how the system's performance and the transmission data rates are determined for wireless communications. We also introduce four different types of small-scale fading: *frequency-selective* fading, *flat* fading, *fast* fading, and *slow* fading.

The Nakagami-m distribution is chosen as a statistical model because of its ability to emulate fading channels whose conditions are more severe than the Rayleigh model. We then introduce the physical layers of the *IEEE 802.11a* standard, the fundamentals of OFDM, and the reasons why OFDM type multiple-carrier systems are adopted for transmission.

In order to perform the analysis, we derived analytic expressions for all sub-carrier modulation techniques used in the *IEEE 802.11a* standard: BPSK, QPSK, 16QAM and 64QAM. After the derivation, we assume the channel coherence bandwidth is such that we have 48 independent sub-carriers for large office buildings and 24 independent sub-carriers for small/medium-size office buildings.

Next, we investigate the uncoded *IEEE 802.11a* based OFDM performance for both pure and composite Nakagami fading channels with either 48 or 24 independent sub-carriers in the presence of pulsed-noise jamming so that we can obtain the coding gain by comparing these results to those with FEC coding. As expected, the performance of uncoded BPSK/QPSK modulated OFDM in the presence of pulsed-noise jamming is better than uncoded 16QAM and 64QAM; however, the performance is not acceptable regardless of the modulation type or the number of independent sub-carriers without FEC.

After the evaluation of uncoded *IEEE 802.11a* based OFDM, we investigate the performance with FEC coding by employing convolutional encoding and Viterbi decoding. The effect of Viterbi hard decision decoding (HDD) is analyzed for all the modulation schemes used in the *IEEE 802.11a* standard, while the effect of Viterbi soft

decision decoding is analyzed only for BPSK and QPSK owing to the complexity of analyzing the probability of bit error for SDD of a binary code transmitted with a non-binary modulation scheme. In addition, due to the difficulty of analyzing the probability of bit error for two different noise levels (i.e., when the pulsed-noise jammer is on or off) for SDD with BPSK/QPSK, perfect side information is assumed.

For the performance of *IEEE 802.11a* based OFDM with HDD, the performance is improved significantly by adding FEC coding. The absolute performance in SIR ranges from 6.2 to 19.34 dB. Also, as expected, for a specific modulation type, regardless of the channel conditions, the SIR required to achieve a fixed probability of bit error increases as the code rate increases. However, contrary to expectations, the SIR required to achieve a specific P_b does not monotonically decrease when the bit rate decreases.

For the performance of *IEEE 802.11a* with SDD, for BPSK/QPSK with code rate $r = 1/2$, SDD improves performance by 8.3 dB over a composite Nakagami fading channel with jamming. For BPSK/QPSK with code rate $r = 3/4$, SDD improves performance by 3 dB over a composite Nakagami fading channel with jamming. On the other hand, we assume that the receiver has perfect side information for SDD. Thus, if we compare the performance of BPSK/QPSK with SDD versus HDD, we cannot make a direct comparison since the HDD analysis does not assume the availability of side information.

We observe that the performance difference between 48 and 24 independent sub-carriers decreases as more effective coding techniques are used.

I. INTRODUCTION

A. OBJECTIVE

Wireless local area networks (WLAN) are increasingly important in meeting the needs of the next generation broadband wireless communication systems for both commercial and military applications. In 1999, the *IEEE 802.11a* working group approved a standard for a 5-GHz band WLAN that supports a variable bit rate from 6 to 54 Mbps, and orthogonal frequency-division multiplexing (OFDM) was chosen because of its well-known ability to avoid multipath effects while achieving high data rates by combining a high order sub-carrier modulation with a high rate convolutional code. OFDM is a multi-carrier transmission technique in which the data signal is divided among 48 separate sub-carriers, each one modulated by a low rate data stream. OFDM is used with either phase-shift-keying (BPSK/QPSK) or M-ary quadrature modulation (16 and 64-QAM) to modulate the digital signal to achieve appropriate channel transmission data rates. The objective of this thesis was to investigate the performance of the OFDM based *IEEE.802.11a WLAN* standard in frequency-selective, slowly fading Nakagami channels in a pulsed-noise jamming environment. For military applications, analyzing the effect of jamming on wireless communication systems is very important. Furthermore, the performance when applying forward error correction (FEC) coding using both hard decision Viterbi decoding (HDD) and soft decision Viterbi decoding (SDD) is also investigated. However, SDD with M-QAM modulation is beyond the scope of this thesis owing to the complexity of analyzing the probability bit error for SDD of a binary code transmitted with a non-binary modulation. In addition, due to the difficulty of analyzing the probability of bit error for two different noise levels (i.e., when the pulsed-noise jammer is on or off) for SDD with BPSK/QPSK, perfect side information is assumed.

B. RELATED RESEARCH

Because of its reliability, *IEEE 802.11a* standards for the operation of WLAN technology in the 5-GHz band have been developed in Europe, North America and Japan. With the rapidly growing demand for reliable and higher data rates in WLANs, numerous

studies focus on the performance of OFDM for many different fading channel characteristics. For example:

- Frequency non-selective, fast Rayleigh and Ricean fading channels [1, 2]
- Frequency-selective, Rayleigh fading channels [3]
- Frequency-selective, slow Ricean fading channels [4] and
- Frequency-selective, slow Nakagami fading channels [5].

These are just a few of the many related studies. Unlike the above referenced work, the performance of the *IEEE 802.11a* standard over frequency-selective, slowly fading Nakagami channels in a worst-case, pulsed jamming environment is analyzed in this thesis. Until recently the effects of pulsed-noise jamming on an *IEEE 802.11a* system have not been addressed. In this thesis we derive analytic expressions for the probability of bit error for BPSK/QPSK, 16QAM and 64QAM in Nakagami fading channels in order to analyze the effects of the pulsed-noise jamming. The benefit of such an analysis is to assess the performance of an existing OFDM standard and to gain some insight into how well these systems will perform in military applications when subjected to hostile jamming.

C. THESIS ORGANIZATION

After the introduction, this thesis is organized into five additional chapters. In Chapter II we discuss *multipath fading* to examine how the system's performance and the transmission data rates are determined for wireless communications. Although in this thesis the channel is modeled as a frequency-selective, slow Nakagami fading channel, a thorough discussion of small scale fading is given because it is important to understand the effect of intersymbol interference (ISI) and to also understand why the signal amplitude is modeled as a Nakagami random variable. The *IEEE 802.11a* standard for WLAN Medium Access Control (MAC) and Physical Layer (PHY) specifications [6] are introduced in Chapter III, and the reasons why OFDM type multiple-carrier systems are important are discussed. Furthermore, OFDM concepts, such as *orthogonality* and *multicarrier* techniques, major OFDM parameters, and OFDM signal processing topics,

are also covered in Chapter III. The performance of OFDM without FEC coding in Nakagami channels under the effect of worst-case, pulsed-noise jamming is examined in Chapter IV. The analysis begins with the sub-carrier modulation techniques for OFDM as specified in the *IEEE 802.11a* standard, which are BPSK, QPSK, 16QAM and 64QAM, and then proceeds to evaluate composite OFDM performance for a Nakagami fading channel under the attack of a hostile pulsed-noise jammer. OFDM performance with FEC coding and Viterbi hard decision decoding (HDD) with BPSK, QPSK, 16QAM and 64QAM is examined in Chapter V; however, Viterbi soft decision decoding (SDD) is only considered with BPSK and QPSK assuming that the receiver has perfect side information. The results will be compared to those of Chapter IV in order to obtain the coding gain. Finally, this thesis concludes with Chapter VI and a brief review of the results obtained in the previous chapters, followed by recommendations for further research.

THIS PAGE INTENTIONALLY LEFT BLANK

II. MULTIPATH FADING CHANNELS

Unlike wired channels that are stationary and predictable, many wireless communication channels neither have a line-of-sight (LOS) transmission path nor offer easy analysis. Instead, a signal can travel from transmitter to receiver via a number of random and independent paths. This phenomenon is referred to as *multipath propagation*. Due to reflections from the ground and surrounding structures, a signal arrives at the receiver multiple times with different amplitudes, phases, and angles of arrival giving rise to the terminology *multipath fading*. Moreover, fading is caused by interference between two or more versions of the transmitted signal which arrive at the receiver at slightly different times. This chapter starts with the discussion of the two types of fading effects that characterize wireless communications and then focuses on small-scale fading. The last part of this chapter introduces Nakagami fading.

A. FADING CHANNELS

The effect of multipath fading can be roughly divided into two categories: large-scale fading and small-scale fading, as shown in Figure 1.

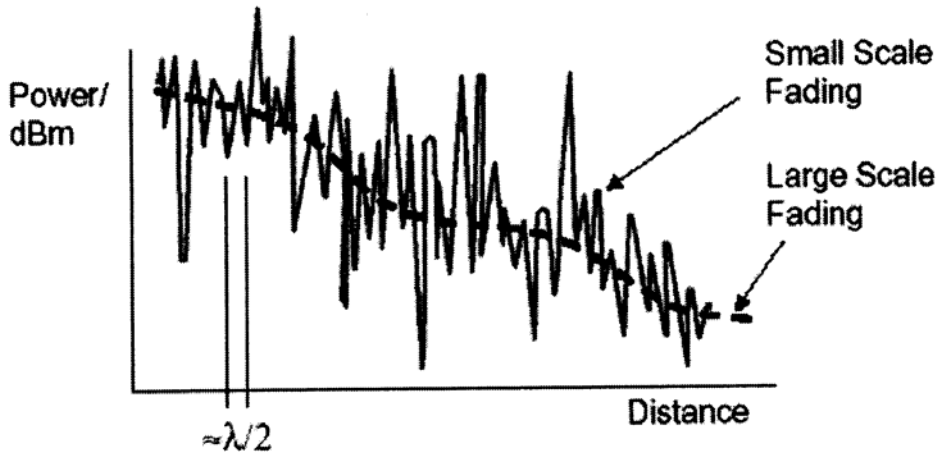

Figure 1. Large and small-scale fading. [From Ref. 7]

Large-scale fading represents the average signal power attenuation or the path loss over large transmitter-to-receiver (T-R) separation distances (several hundreds or

thousands of meters), whereas small-scale fading refers to the rapid fluctuations of the received signal strength over very short travel distances (an order of half a wavelength change) or short time durations (on the order of seconds). Large-scale fading is often modeled as log-normal fading because the received signal amplitude can be modeled as a random variable that has a log-normal probability density function (PDF). Small-scale fading is usually modeled as either Nakagami or Rayleigh fading. All indoor wireless communication systems experience small-scale fading. In this chapter, we will discuss the effects of small-scale fading since OFDM is conceived and employed to combat the multipath effects encountered in indoor environments [8].

B. SMALL-SCALE FADING

Small-scale fading manifests itself in two mechanisms: *time spreading of the signal due to multipath* and *time variance of the channel due to Doppler spread*. While multipath delay spread leads to either *frequency-selective fading* or *flat fading*, Doppler spread leads to either *fast fading* or *slow fading*.

1. Time Spreading of the Signal Due to Multipath

Time spreading of the signal causes the transmitted signal to undergo either flat or frequency selective fading. There are two parameters used to describe the time spreading mechanism: *coherence bandwidth* and *maximum excess delay*.

The coherence bandwidth B_c is a statistical measure of the range of frequencies over which the channel transfer function remains virtually constant. In other words, the coherence bandwidth represents the range of frequencies over which two frequency components show $\geq 90\%$ correlation in their response. The coherence bandwidth is given by [8]

$$B_c \approx \frac{1}{T_m} \tag{2.1}$$

where T_m represents the maximum excess delay. The maximum excess delay is defined in terms of the multipath intensity profile (MIP), illustrated in Figure 2. This function

shows how the average power of the received signal $S(\tau)$ varies as a function of time delay τ. The maximum excess delay T_m is the time-difference-of-arrival for which received signal power is essentially zero.

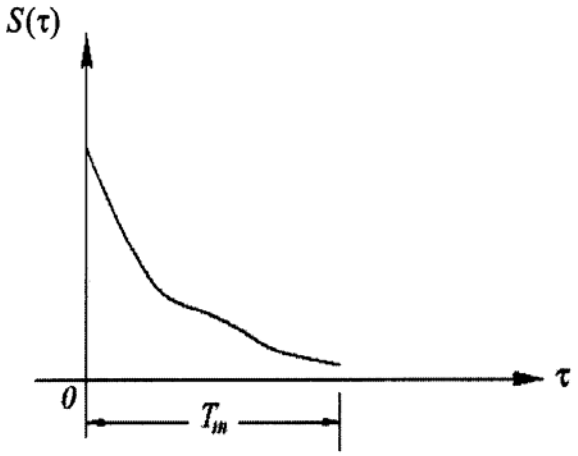

Figure 2. Multipath intensity profile. [After Ref. 8]

The maximum excess delay T_m is not the best indicator of how any given system will perform when signals are transmitted on a channel because the MIP can change considerably for channels with the same T_m. Hence, a more useful parameter is the root-mean-square (rms) delay spread, defined as [8]

$$\sigma_\tau = \sqrt{\overline{\tau^2} - \left(\overline{\tau}\right)^2} \tag{2.2}$$

where $\overline{\tau}$ is the mean excess delay and $\overline{\tau^2}$ is the mean-square excess delay, or second moment. The rms delay spread and coherence bandwidth are inversely proportional to one another, although their exact relationship is related to the channel's multipath characteristics. If the coherence bandwidth B_c is defined as the bandwidth over which the frequency correlation function is greater than 0.9, then an emperical formula that is used is [7]

$$B_c = \frac{1}{50 \cdot \sigma_\tau}. \tag{2.3}$$

If the definition is relaxed so that the frequency correlation function is greater than 0.5, then the coherence bandwidth is approximately [7]

$$B_c = \frac{1}{5 \cdot \sigma_\tau}. \tag{2.4}$$

According to [9], depending on the existence or absence of a clear LOS path, the reported rms delay spread values are 30 ns for small/medium-size office buildings and less than 120 ns for large office buildings.

a. Frequency-Selective Fading

If the coherence bandwidth B_c is smaller than the bandwidth W of the transmitted signal, then the channel is referred to as frequency-selective, that is, a signal undergoes frequency-selective fading if

$$B_c < W \tag{2.5}$$

or

$$T_m > T_s \tag{2.6}$$

since $B_c \approx 1/T_m$ and $W \approx 1/T_s$, where T_s is the symbol duration. When a channel is specified as a frequency–selective fading channel, the received signal consists of multiple versions of the transmitted waveform which are attenuated and delayed in time. Consequently, the channel induces intersymbol interference (ISI). The typical frequency-selective fading case is shown in Figure 3(a).

b. Flat Fading

If the coherence bandwidth B_c is greater than the bandwidth W of the transmitted signal, then the channel is referred to as flat; that is, a signal undergoes flat fading if

$$B_c > W \tag{2.7}$$

or equivalently,

$$T_m < T_s. \tag{2.8}$$

In flat fading, due to fluctuations in the gain of the channel caused by multipath, the amplitude of the received signal changes with time. The typical flat fading case is shown in Figure 3(b).

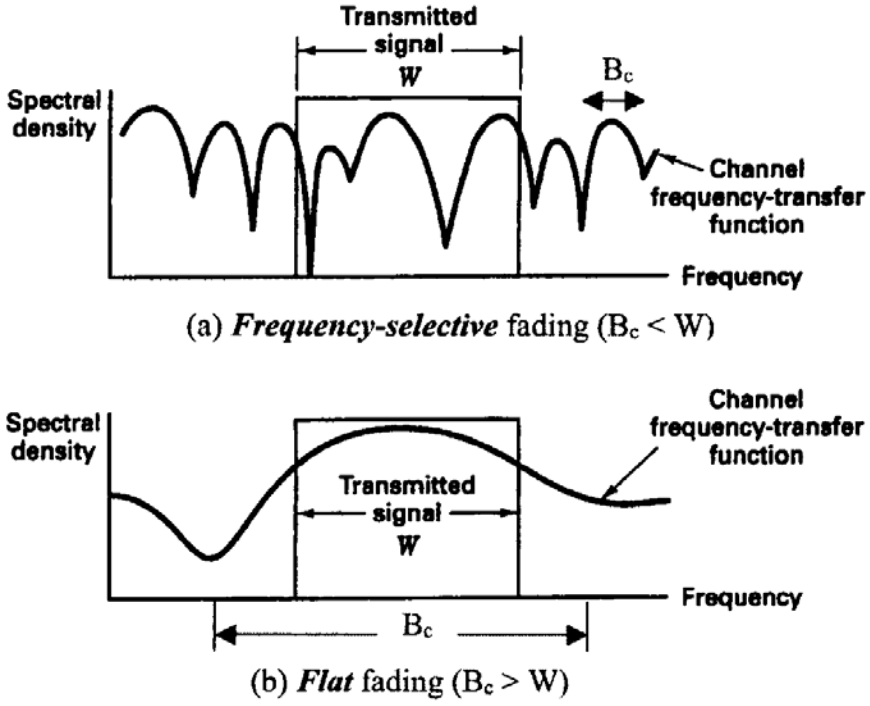

Figure 3. Typical frequency-selective and flat fading case. [After Ref. 8]

2. Time Variance of the Channel Due to Doppler Spread

Due to the relative motion between a transmitter and receiver or other objects within the channel, the time variance causes the transmitted signal to undergo either *fast* or *slow fading*. There are two parameters used to describe the time-variant mechanism: *Doppler spread* and *coherence time*.

The Doppler spread is defined as the range of frequencies over which the received Doppler spectrum is essentially non-zero. When a pure sinusoidal tone of frequency f_c is

transmitted, the received signal spectrum will have components in the range of $f_c - f_d$ to $f_c + f_d$, where f_d is the Doppler shift given by [7]

$$f_d = \frac{\nu}{\lambda} \cdot \sin\phi \tag{2.9}$$

where λ represents the signal wavelength, ν represents the relative velocity of the transmitter with respect to the receiver, and ϕ represents the spatial angle between the direction of the motion of the receiver and the direction of arrival of the signal. The value of f_d depends on the direction of the objects whether they are moving toward or away from each other.

Coherence time T_c is a statistical measure of the time duration over which the channel characteristics are considered to be static. Furthermore, coherence time is the time duration over which two received signals have a strong potential for amplitude correlation. The coherence time is inversely proportional to the Doppler spread given by [7]:

$$T_c \approx \frac{1}{f_d}. \tag{2.10}$$

a. Fast Fading

If the coherence time T_c is smaller than the transmitted symbol period, then the channel is referred to as fast; that is, a signal undergoes fast fading if

$$T_c < T_s \tag{2.11}$$

or

$$f_d > W \tag{2.12}$$

since $f_d \approx 1/T_c$ and $W \approx 1/T_s$, where T_s is the symbol duration. In a fast fading channel, the channel impulse response changes rapidly during the transmitted symbol duration, which leads to signal distortion. In practice, fast fading only occurs for very low data rates.

b. Slow Fading

Contrary to fast fading, if the coherence time T_c is greater than the transmitted symbol period, then the channel is referred to as slow; that is, a signal undergoes slow fading if

$$T_c > T_s \tag{2.13}$$

or equivalently,

$$f_d < W. \tag{2.14}$$

3. Summary of Small-Scale Fading

The relation between the various multipath parameters and the type of fading experienced by the signal are summarized in Figure 4, where B_c is the coherence bandwidth, W is the signal bandwidth, T_c is the coherence time, T_m is the maximum excess delay, T_s is the symbol duration, and f_d is the Doppler spread.

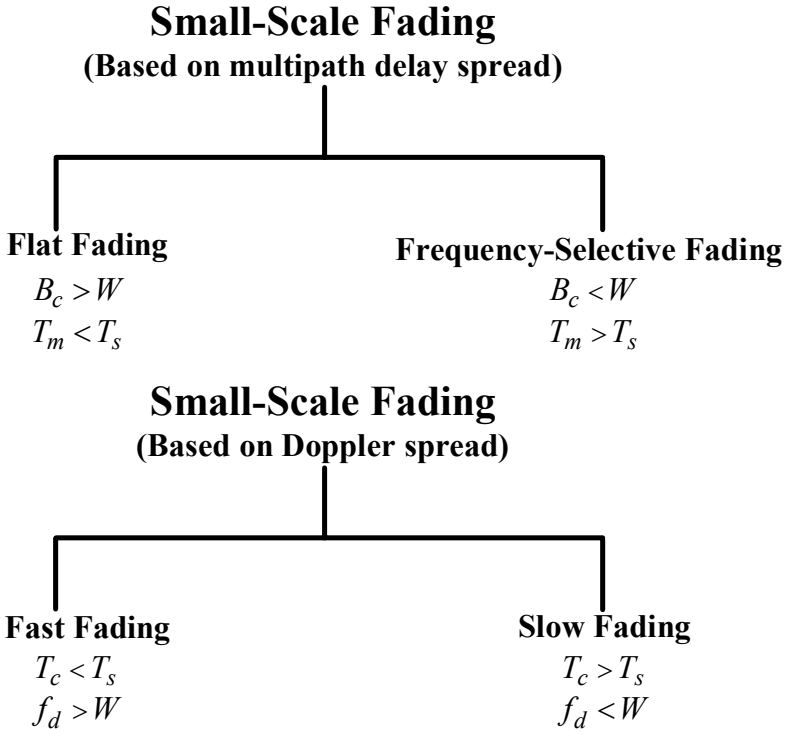

Figure 4. Types of small-scale fading. [After Ref. 7]

C. THE NAKAGAMI CHANNEL MODEL

As mentioned in the previous section, fading is observed in wireless communications channels due to multipath. A variety of statistical models derived from probability theory have been suggested to explain the nature of the wireless channels. If the received signal amplitude levels can be predicted based on these models, then the required transmitter power, system architecture, modulation schemes, and other parameters can be adjusted to compensate for the channel.

The Rayleigh distribution is frequently used to describe the statistical time-varying nature of the received signal in which no line-of-sight (LOS) is available and there are numerous multipath components; however, it fails to describe long-distance fading effects with sufficient accuracy. On the other hand, the Ricean distribution is generally used when there is a LOS present but there remain some multipath due to secondary reflections.

Like other distributions, the Nakagami-m distribution is used to describe the fluctuations in the received signal envelope due to multipath fading. The choice of the Nakagami model for the transmission channel in this thesis is based upon the fact that the Nakagami-m distribution models more severe conditions than the Rayleigh model for $m < 1$ and has been found to best match observed signal statistics in fading environments [10]. The second reason for this choice is that the Nakagami model is more general than many others such as the Rayleigh or Ricean model. This offers us a greater flexibility to investigate various degrees of fading conditions by simply adjusting certain model parameters. In fact, the Rayleigh distribution is a special case of the Nakagami-m distribution.

The Nakagami-m probability density function, which is a function of two parameters, is given by [10]:

$$p_R(r) = \frac{2}{\Gamma(m)}\left(\frac{m}{\Omega}\right)^m r^{2m-1} e^{-\frac{mr^2}{\Omega}} \tag{2.15}$$

where Ω is defined as

$$\Omega = E[R^2]. \tag{2.16}$$

$\Gamma(m)$ is the Gamma function defined as

$$\Gamma(m) = \int_0^\infty t^{m-1} e^{-t} dt \qquad m > 0 \tag{2.17}$$

and the parameter m, the fading figure, is defined as the ratio of moments

$$m = \frac{\Omega^2}{E[(R^2 - \Omega)^2]}, \qquad m \geq \frac{1}{2}. \tag{2.18}$$

When $m = 1$, Equation (2.15) reduces to the Rayleigh PDF given by

$$p_R(r) = \frac{r}{\sigma^2} e^{-\frac{r^2}{2\sigma^2}}, \qquad r \geq 0. \tag{2.19}$$

This is why we consider the Rayleigh distribution to be a special case of the Nakagami-m distribution. In Figure 5, we plot the Nakagami-m PDF as a function of R for various values of m with $\Omega = 1$.

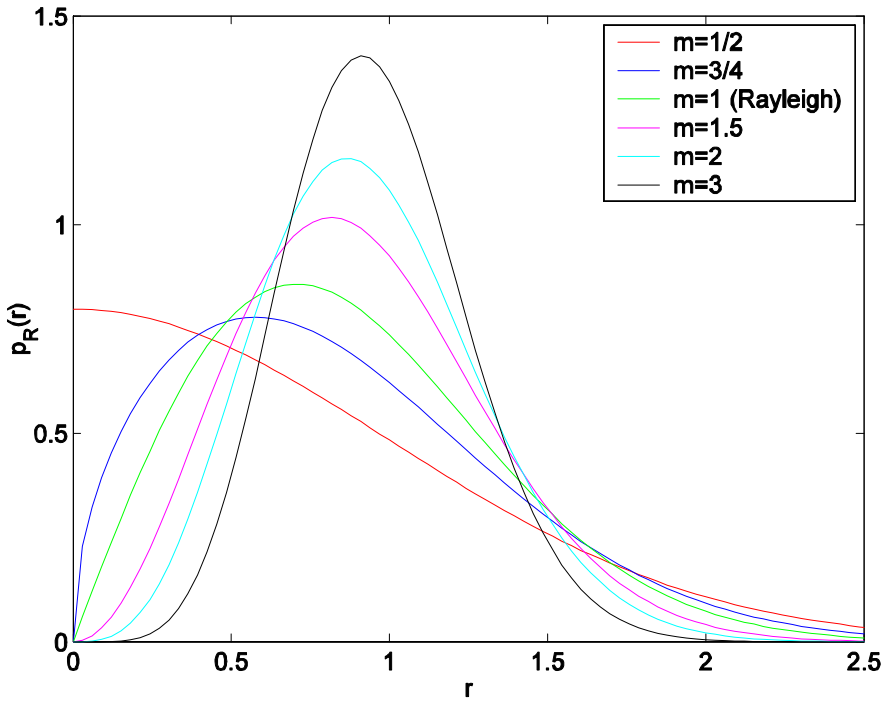

Figure 5. The Nakagami PDF for $\Omega = 1$.

The fading figure m controls the severity of the fading of the received signal amplitude. For $m < 1$, the Nakagami-m distribution approaches that of a one-sided Gaussian distribution and models very severe fading conditions with no LOS. In addition, the Nakagami-m distribution with $m \leq 1$ is accurate in modeling high frequency (HF) transmissions over long distances. For $m > 1$, the distribution models a moderate fading condition in which LOS communications are possible, similar to Ricean fading. It is this flexibility that gives the Nakagami-m distribution its added value.

D. SUMMARY OF MULTIPATH FADING CHANNELS

In this chapter, we addressed multipath fading and introduced different types of small-scale fading channels: frequency-selective fading, flat fading, fast fading, and slow fading. Multipath fading induces intersymbol interference (ISI). OFDM is conceived and employed to combat the multipath effects encountered in indoor environment. In the next chapter, we will investigate OFDM parameters and OFDM signal processing topics.

III. OFDM-BASED *IEEE 802.11A* STANDARD

A. WHY OFDM?

As discussed in Chapter II, a channel is referred to as frequency-selective if the coherence bandwidth B_c is smaller than the bandwidth W of the transmitted signal. When a channel is specified as a frequency-selective fading channel, the received signals are distorted and overlapped due to the multipath time delay spread. Consequently, the channel induces intersymbol interference (ISI), which degrades system performance because it leads to irreducible errors; that is, increasing the received signal-to-noise ratio (SNR) does not reduce the number of errors caused by ISI. There are several major ways to mitigate the effects of ISI. The first method is to reduce the symbol rate, but then the data rate is also reduced. The second method is to use equalizers, but equalization increases the complexity of the system since it needs a signal processing operation that minimizes ISI. Finally, OFDM was conceived and is employed to combat multipath effects encountered in indoor environment since it has none of the drawbacks of the previous techniques.

OFDM is a multi-carrier transmission technique in which the data signal is divided among N separate sub-carriers, each one modulated by a low-rate data stream. Therefore, the symbol rate for one sub-carrier is $R_{sc} = R_s / N$. In other words, the bandwidth of each sub-carrier is reduced by a factor of N as compared with the bandwidth required when a single sub-carrier is used. In this case, the channel coherence bandwidth B_c will be greater than the bandwidth of the transmitted sub-carrier signal, $B_c \geq W_{SC} = W / N$, and the sub-carrier channel is flat, which eliminates ISI effects.

B. OFDM FUNDAMENTALS

With OFDM, the high-speed serial data stream is divided into N low-speed sub-carriers that the system transmits simultaneously at different frequencies. Hence, OFDM is referred to as a multi-carrier modulation system. In this section, we will discuss the concept of single/multi-carrier modulation, FDM/OFDM, and the orthogonality principle.

1. Single/Multi-carrier Modulation

Single-carrier modulation systems transmit data symbols over a single carrier frequency. Compared to multi-carrier modulation, single-carrier modulation has several advantages. For instance, it is less sensitive to phase noise and frequency offset. In addition, excessive peak-to-average power problems associated with multi-carrier schemes do not occur in single-carrier modulation. However, the main disadvantage of single-carrier modulation is that a single fade or interference can render the entire system useless since it uses only one carrier.

Multi-carrier modulation systems transmit data symbols over N parallel sub-carriers, resulting in longer symbol durations. OFDM-based *IEEE 802.11a* uses 48 sub-carriers to transmit data. Multi-carrier modulation has the additional benefit of superior performance in frequency-selective fading channels or in the presence of interference because only a small portion of the sub-carriers in the OFDM system will encounter distortion, not the whole system. However, any multi-carrier system requires reliable synchronization; that is, it is vulnerable to phase noise and frequency offset [7].

2. FDM/OFDM

The classical multi-carrier transmission system is nothing more than a frequency-division-multiplexing (FDM) system. FDM is a multiplexing technique in which numerous signals are combined for transmission on a single communications line or channel. Each signal is assigned a different carrier frequency within the main channel. The assigned carrier frequencies are separated by the guard bands, which act as buffer zones to reduce the inter-carrier-interference (ICI), or cross talk, from adjacent spectral regions. However, this separation in the spectrum wastes the available bandwidth.

Contrary to FDM, OFDM uses overlapped orthogonal sub-carriers to divide a broadband frequency-selective channel into a number of flat fading channels, which yields tremendous bandwidth savings as illustrated in Figure 6.

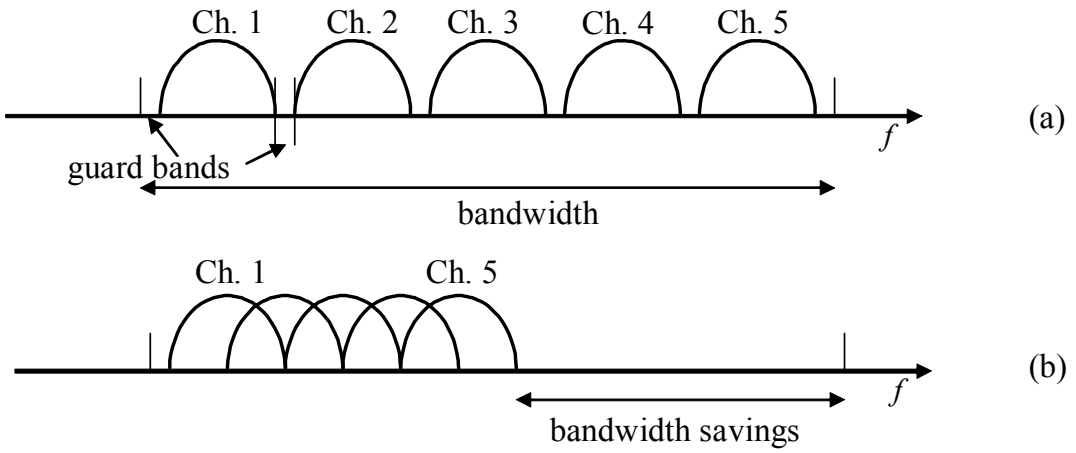

Figure 6. FDM (a) vs. OFDM (b). [From Ref. 5]

As we can see from Figure 6, OFDM saves almost 50 percent of the available bandwidth compared to FDM. On the other hand, the major advantage of FMD is its simplicity.

3. Orthogonality

Mathematically, two vectors are orthogonal if, when multiplied together and averaged over time, the result is zero. In other words, two vectors perpendicular to each other are orthogonal and their *dot product* is equal to zero. In communications, orthogonality means two signals are uncorrelated or independent over a symbol interval. When two signals are orthogonal, building a receiver that responds to one while completely rejecting the other is possible. In OFDM, cross talk among the sub-carriers is prevented by the orthogonality principle, that is, each sub-carrier must be spaced at intervals of $1/T_s$ where T_s is the symbol duration for each sub-carrier. As long as orthogonality is maintained, recovering the individual sub-carriers' signals despite their overlapping spectrums is still possible. A representative OFDM signal spectrum with $N = 4$ is shown in Figure 7. Obviously the spectra of the subcarriers are not separated but overlap. Also, note that the orthogonal carriers are spaced in frequency by integer multiples of $1/T_s$.

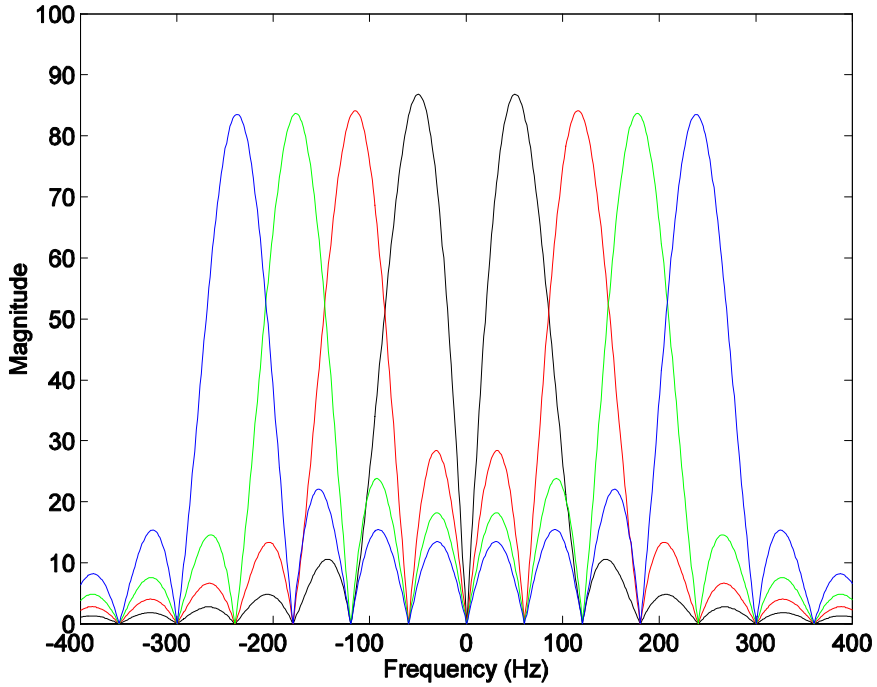

Figure 7. Orthogonally spaced carriers in frequency domain. [After Ref. 5]

C. OFDM BASED *802.11A* PARAMETERS

Previously, we have explained why OFDM is employed to combat the multipath effects encountered in indoor environments while achieving high data rates. In this section, we address the details of the OFDM based *IEEE 802.11a* standard. The major parameters of the OFDM PHY are listed in Table 1.

Information data rate	**6, 9, 12, 18, 24, 36, 48 and 54 Mbit/s (6, 12 and 24 Mbit/s are mandatory)**
Modulation	BPSK OFDM QPSK OFDM 16-QAM OFDM 64-QAM OFDM
Error correcting code	K = 7 (64 states) convolutional code
Coding rate	1/2, 2/3, 3/4
Number of subcarriers	52
OFDM symbol duration	4.0 μs
Guard interval	0.8 μs[a] (T_{GI})
Occupied bandwidth	16.6 MHz

Table 1. Major parameters of the OFDM PHY. [From Ref.6]

1. Guard Interval

Guard interval T_{GI} is the most important parameter in *IEEE 802.11a* PHY because it provides robustness to rms delay spreads up to several hundreds of nanoseconds depending on the code rate and the modulation used in any indoor wireless application. In order to minimize ISI, which decreases orthogonality and has an effect that is similar to inter-channel-interference, T_{GI} is inserted between two consecutive OFDM symbols. T_{GI} should be larger than the expected rms delay spread, otherwise the impact of ISI will be significant. From [9], the reported rms delay spread values can be up to 200 ns for small/medium-size office buildings and 300 ns for large office buildings. As can be seen from Table 1, the guard interval T_{GI} for each OFDM symbol is $0.8\ \mu s$, which is greater than 300 ns.

2. OFDM Symbol Duration and Sub-Carrier Spacing

As mentioned above, guard interval T_{GI} is an important parameter which eliminates ISI; however, there is an inverse relationship between T_{GI} and OFDM effective symbol duration; that is, when T_{GI} increases, the OFDM effective symbol duration decreases. Hence, T_{GI} cannot be chosen too large. The total symbol duration chosen in *802.11a* is four microseconds. Taking the inverse of the symbol duration less the inverse of the guard time of 0.8 microseconds results in the sub-carrier spacing of 312.5 kHz.

3. Number of Sub-Carriers

There are a total of 52 sub-carriers for each OFDM symbol. However, four pilot sub-carriers are used to assist timing and carrier tracking tasks during data symbols after the two preambles. Hence, the remaining 48 sub-carriers are used to carry the data stream.

4. Error Correcting Code and Coding Rate

FEC coding is applied in order to improve overall system performance; otherwise, the error probability will generally be determined by weaker sub-carriers due to fading conditions. The convolutional encoder employed by the *IEEE 802.11a* standard for the rate $1/2$ code uses industry-standard generator polynomials $g_0 = 133_8$ and $g_1 = 171_8$ with constraint length 7; that is, six linear shift registers comprise the memory components of the encoder as shown in Figure 8.

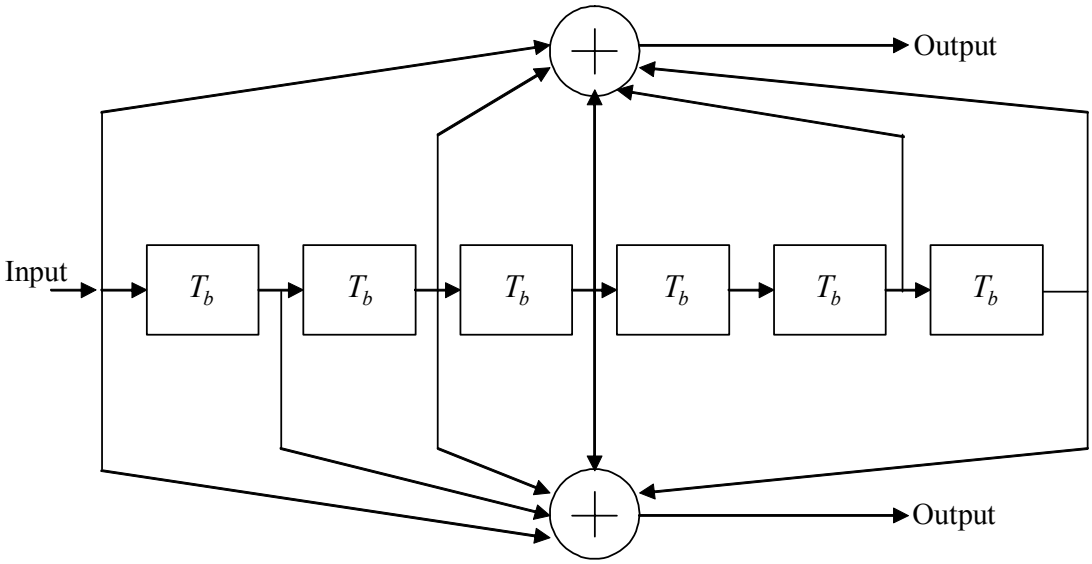

Figure 8. Convolutional encoder with constraint $\nu = 7$. [From Ref. 6]

Higher coding rates of $2/3$ and $3/4$ are obtained by puncturing the rate $1/2$ code. Puncturing is a procedure for omitting some of the encoded bits in the transmitter and inserting a dummy zero metric into the convolutional decoder on the receive side in place of the omitted bits [6]. Puncturing reduces the free distance of the convolutional code; however, the coding gain of the punctured codes is almost the same as that of the best code for that particular code rate. The rate-dependent parameters of *IEEE 802.11a* standard, which uses BPSK/QPSK, 16QAM, and 64QAM as sub-carrier modulation schemes in combination with rate $1/2$, $2/3$, and $3/4$ convolutional codes are listed in Table 2. Note that the rate $2/3$ code is only used with 64QAM to obtain a data rate of 48 Mbps.

Data rate (Mbits/s)	Modulation	Coding rate (R)	Coded bits per subcarrier (N_{BPSC})	Coded bits per OFDM symbol (N_{CBPS})	Data bits per OFDM symbol (N_{DBPS})
6	BPSK	1/2	1	48	24
9	BPSK	3/4	1	48	36
12	QPSK	1/2	2	96	48
18	QPSK	3/4	2	96	72
24	16-QAM	1/2	4	192	96
36	16-QAM	3/4	4	192	144
48	64-QAM	2/3	6	288	192
54	64-QAM	3/4	6	288	216

Table 2. Rate-dependent parameters. [From Ref. 6]

D. OFDM SIGNAL PROCESSING

The general block diagram of the transmitter and receiver for the OFDM PHY is shown in Figure 9 [6].

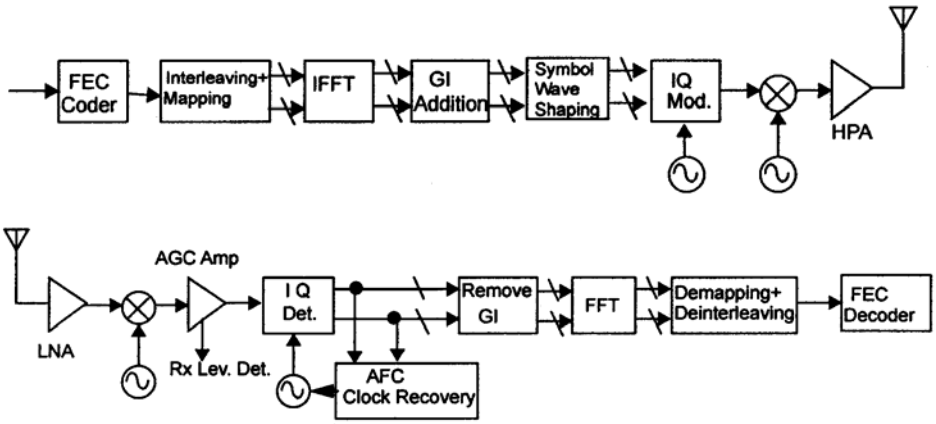

Figure 9. OFDM PHY transceiver block diagram. [From Ref. 6]

In the transmitter, the input data are encoded using a half-rate convolutional encoder with a constraint length 7. The code rate can be changed by using the puncturing process with respect to the desired data rate. Then the coded data are interleaved and mapped. The fading channels tend to introduce errors in bursts. The interleaver spreads sequential coded bits out in time in such a way that the bursty channel is transformed at

the receiver into a channel having independent errors; thus, the convolutional decoder can correct these independent errors. After interleaving, the coded binary bits are mapped into PSK/QAM constellation points. The constellation schemes for BPSK, QPSK, 16QAM and 64QAM are all shown in Figure 10.

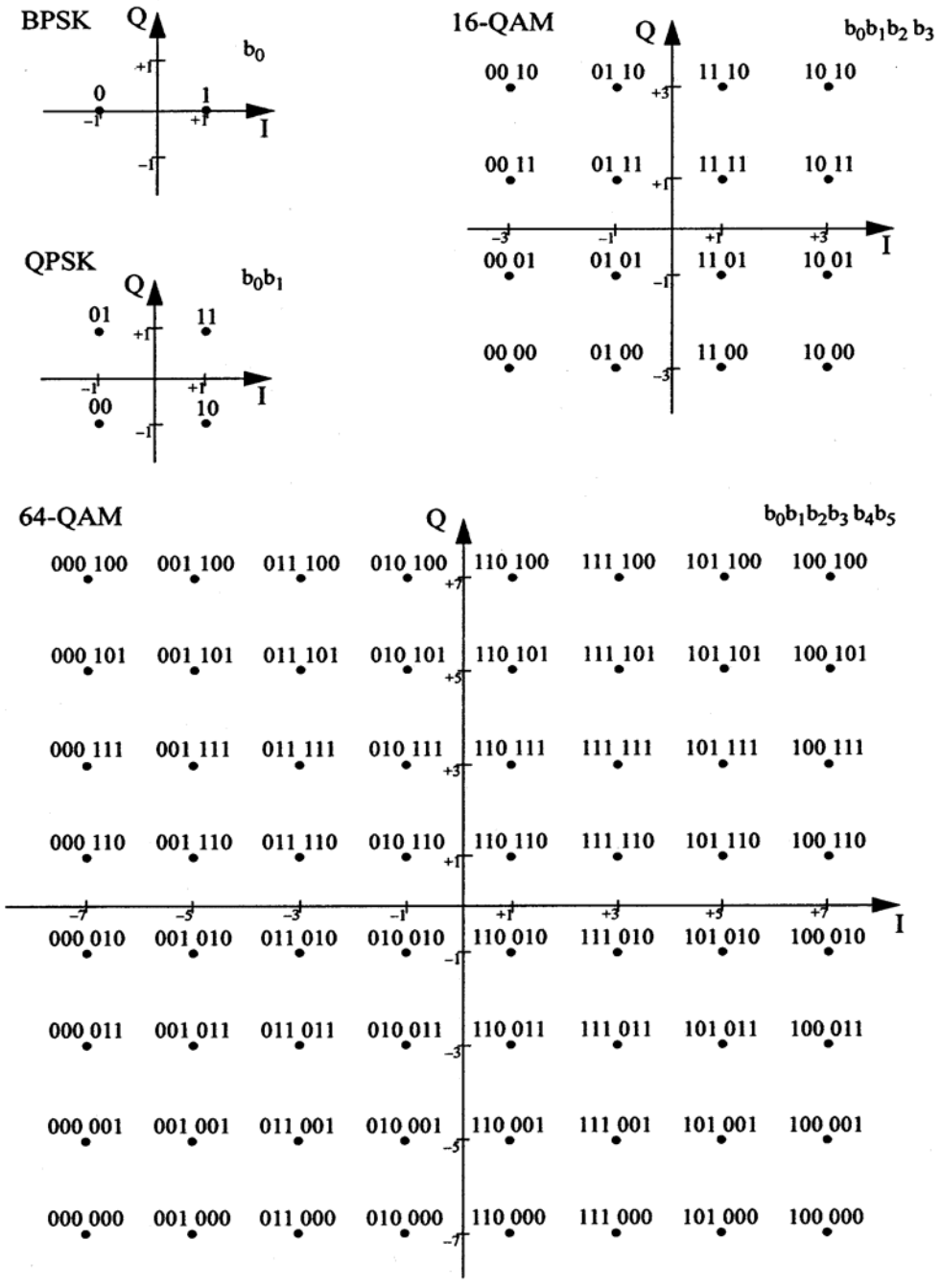

Figure 10. Constellation for BPSK, QPSK, 16QAM and 64QAM. [From Ref. 6]

In order to assist timing and carrier tracking in coherent detection, four pilot tones are added to each 48 data symbols to make one OFDM symbol. After serial-to-parallel conversion, each OFDM symbol is modulated over 52 sub-carriers by applying an inverse fast Fourier transform (IFFT). A cyclic extension is added to the guard interval to prevent frequency domain ICI and to maintain orthogonality. In theory, the guard interval could be a "no signal" extension of the OFDM symbol, and this would be sufficient to eliminate ISI. However, if the guard interval has no signal, then ICI increases because the carriers are no longer orthogonal. In other words, the number of cycles per interval between any two arriving symbols is not an interger. Hence, orthogonality is compromised as shown in Figure 11.

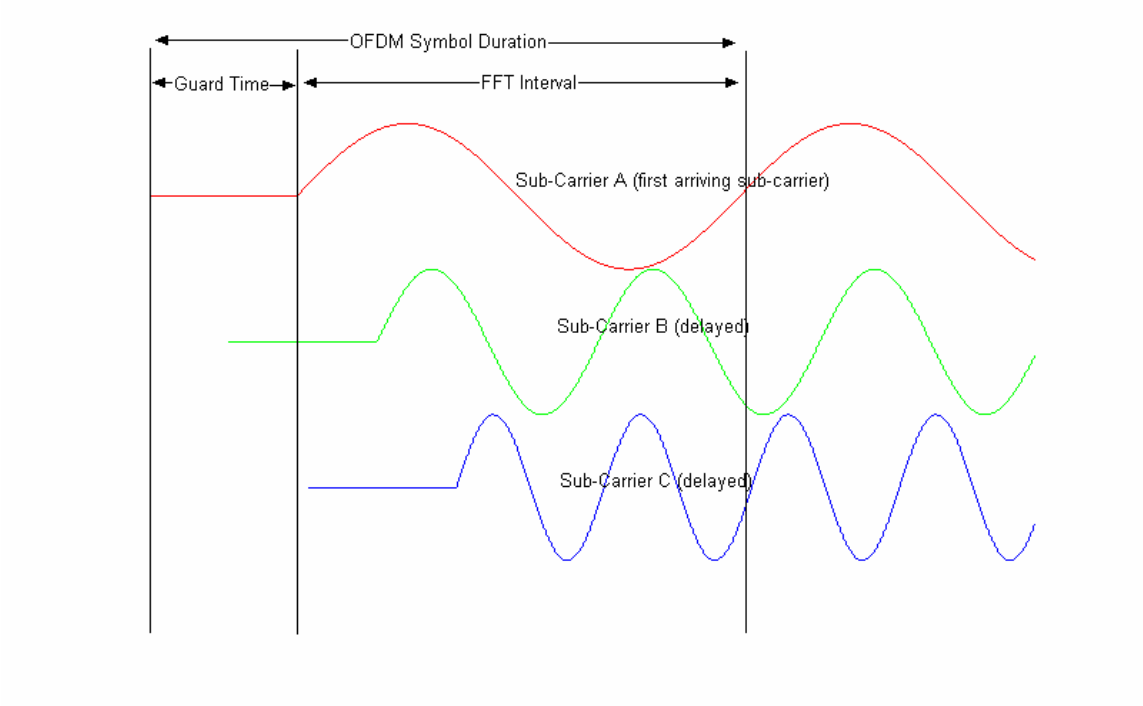

Figure 11. Effect of no cyclic extension in the guard interval. [From Ref. 5]

On the other hand, by adding delayed replicas of the OFDM symbol within the guard interval, each sub-carrier has an integer number of cycles over the OFDM symbol. Hence, there will be no ICI among the sub-carriers in the frequency domain. This is demonstrated in Figure 12.

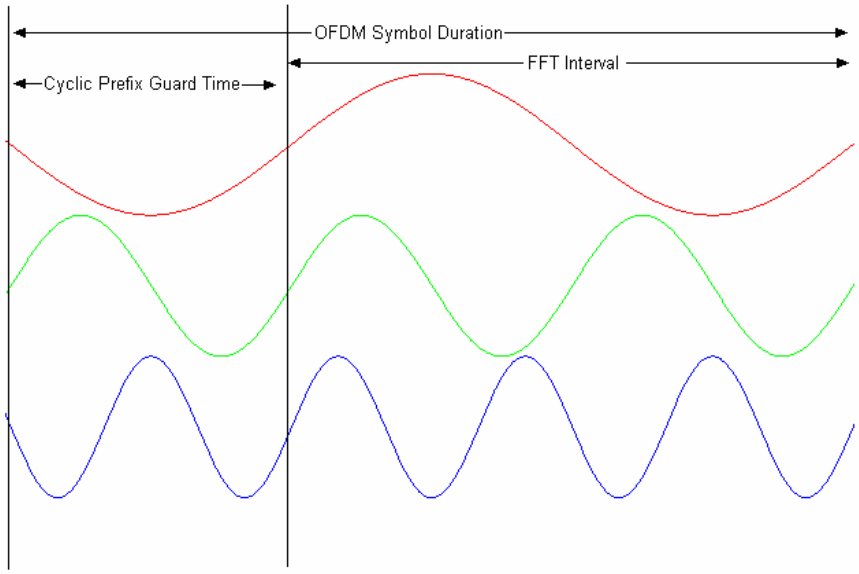

Figure 12. OFDM symbol with cyclic extension. [From Ref. 5]

Further, windowing is applied to smooth the transition region from symbol to symbol to get a narrower output spectrum. The I/Q modulation process transforms the digital OFDM symbol into an analog waveform. This waveform is then up-converted to the 5-GHz band for amplification and transmission through the antenna.

On the receiver side, the reverse operations are performed with the exception of adding a low-noise amplifier (LNA) and automatic gain control (AGC). The LNA reduces the effective noise temperature of the receiver, while the AGC estimates the power of the received pilot tone and controls the power at the demodulator input. Basically, what is done on the transmitter side is undone on the receiver side.

So far, we have introduced the basic concepts of multipath fading and OFDM based *IEEE 802.11a* standard. We are now ready to investigate the performance of the OFDM based *IEEE.802.11a WLAN* standard in frequency-selective, slowly fading Nakagami channels in a pulsed-noise jamming environment.

IV. PERFORMANCE WITHOUT FEC CODING

The performance of uncoded OFDM signals transmitted over Nakagami fading channels in a pulsed jamming environment is examined in this chapter. The analysis begins with the sub-carrier modulation techniques for OFDM as specified in the *IEEE 802.11a* standard, which are BPSK, QPSK, 16QAM and 64QAM and proceeds to composite OFDM system performance over a Nakagami fading channel that is attacked by a hostile pulsed-noise jammer. In this chapter, each modulation technique will be independently evaluated and the probability of bit error analytically derived.

A. PERFORMANCE IN AWGN WITH PULSED-NOISE JAMMER

1. BPSK/QPSK Modulation

The performance of BPSK and QPSK in AWGN are the same, and in [10] it is shown that the bit error probability P_b for a coherently demodulated BPSK/QPSK system is

$$P_b = Q\left(\sqrt{\frac{2E_b}{N_0}}\right) \tag{4.1}$$

where E_b / N_o is the ratio of average energy per bit-to noise power spectral density. E_b is represented by $A_c^2 \cdot T_b$, where A_c^2 is the received signal power and T_b is the bit duration. The symbol $Q(.)$ is the Q-function, defined as

$$Q(z) = \frac{1}{2\pi}\int_z^\infty \exp\left(\frac{-\lambda^2}{2}\right). \tag{4.2}$$

Suppose the communication system is attacked by a band-limited, noise-like signal that is turned on and off systematically, and let us define a parameter ρ $(0 < \rho \le 1)$ that represents the fraction of time the jammer is turned on. Since the noise jammer increases the noise power spectral density from N_o to $N_o + N_I$, where N_I is the jammer power spectral density, the bit error probability with noise jamming is

$$P_b = Q\left(\sqrt{\frac{2A_c^2 \cdot T_b}{N_o + N_I}}\right). \tag{4.3}$$

If we make the assumption that the overall average power transmitted by the jammer is the same whether the jammer is pulsed or not, then the interference power spectral density with pulsed-noise jamming is

$$N_I^{'} = N_I / \rho. \tag{4.4}$$

Now the probability of bit error with pulsed-noise jamming is obtained by using Equation (4.1) through Equation (4.4):

$$\begin{aligned} P_b &= P_r(\text{pulse jammer on})P_b(\text{pulse jammer on}) \\ &\quad + P_r(\text{pulse jammer off})P_b(\text{pulse jammer off}) \\ &= \rho \cdot Q\left(\sqrt{\frac{2E_b}{N_o + N_I/\rho}}\right) + (1-\rho) \cdot Q\left(\sqrt{\frac{2E_b}{N_o}}\right). \end{aligned} \tag{4.5}$$

We can ask if there is a value of $\rho = \rho_{wc}$ that maximizes the probability of bit error. In order to make some simplifications, we assume that $E_b / N_o >> 1$ and $N_I / \rho >> N_o$. The first assumption allows us to neglect the second term in Equation (4.5), and the second assumption allows us to neglect N_o in the first term. Therefore, Equation (4.5) can be rewritten as

$$P_b \approx \rho \cdot Q\left(\sqrt{\frac{2\rho E_b}{N_I}}\right). \tag{4.6}$$

We know that [16]

$$[zQ(z)]_{\max} = 0.1657 \tag{4.7}$$

where $z = 1.44$. As a consequence, for $z = \dfrac{2E_b \cdot \rho_{wc}}{N_I}$ we get

$$\rho_{wc} = \frac{0.72}{E_b / N_I}. \tag{4.8}$$

Substituting Equation (4.8) into (4.6), we can evaluate the probability of bit error for the worst case pulsed-noise jamming:

$$P_{b_{\max}} = \frac{0.08285}{E_b / N_I}. \tag{4.9}$$

2. 16QAM/64QAM Modulation

In order to obtain data rates between 24 and 54 Mbps, *IEEE 802.11a* uses the bandwidth efficient M-ary QAM. For square QAM constellations, the probability of bit error is [11]

$$P_b \approx \frac{4\left(\sqrt{M}-1\right)}{q\sqrt{M}} Q\left(\sqrt{\frac{3q \cdot E_b}{(M-1)\cdot N_0}}\right) \tag{4.10}$$

where M is the number of possible combinations of q bits and q is the number of bits per symbol. As a result, $q = 4$ corresponds to 16QAM and $q = 6$ corresponds to 64QAM, respectively. If the system is attacked by a pulsed-noise jammer, the probability of bit error P_b can be obtained by making the same assumptions that we discussed in the derivation of Equation (4.5). Hence,

$$P_b = \frac{\rho \cdot 4\left(\sqrt{M}-1\right)}{q\sqrt{M}} Q\left(\sqrt{\frac{3qE_b}{(M-1)\cdot(N_0 + N_I/\rho)}}\right) + (1-\rho)\cdot\frac{4\left(\sqrt{M}-1\right)}{q\sqrt{M}} Q\left(\sqrt{\frac{3qE_b}{(M-1)N_0}}\right) \tag{4.11}$$

For practical purposes, we can make the assumption that $E_b / N_o >> 1$ and $N_I / \rho >> N_o$, with the aim of evaluating $\rho = \rho_{wc}$ that maximizes the probability of bit error. Again the first assumption allows us to neglect the second term in Equation (4.11), and the second assumption allows us to neglect N_o in the first term. Therefore, Equation (4.11) can be rewritten as

$$P_b \approx \frac{\rho \cdot 4\left(\sqrt{M}-1\right)}{q\sqrt{M}} Q\left(\sqrt{\frac{3q \cdot E_b}{(M-1)\cdot N_I/\rho}}\right). \tag{4.12}$$

Setting $z = \dfrac{3qE_b \cdot \rho_{wc}}{N_I \cdot (M-1)}$ in Equation (4.7), we get

$$\rho_{wc} = \frac{0.48 \cdot (M-1)}{q \cdot E_b / N_I}. \tag{4.13}$$

Hence, we can evaluate the probability of bit error for the worst case pulsed-noise jamming by substituting Equation (4.13) into Equation (4.12):

$$P_{b_{\max}} = \frac{0.221 \cdot (M-1)}{q \cdot E_b / N_I} \cdot \frac{\left(\sqrt{M}-1\right)}{\sqrt{M}}. \tag{4.14}$$

With Equation (4.5) and (4.11), we plot the performance of BPSK/QPSK, 16QAM, and 64QAM in AWGN with pulsed-noise jamming versus signal-to-interference ratio (SIR) assuming $E_b / N_o = 16$ dB and $\rho = 0.5$ as shown in Figure 13. As we expect, the performance of BPSK/QPSK is superior to the performance of 16QAM, and the performance of 16QAM is superior to that of 64QAM.

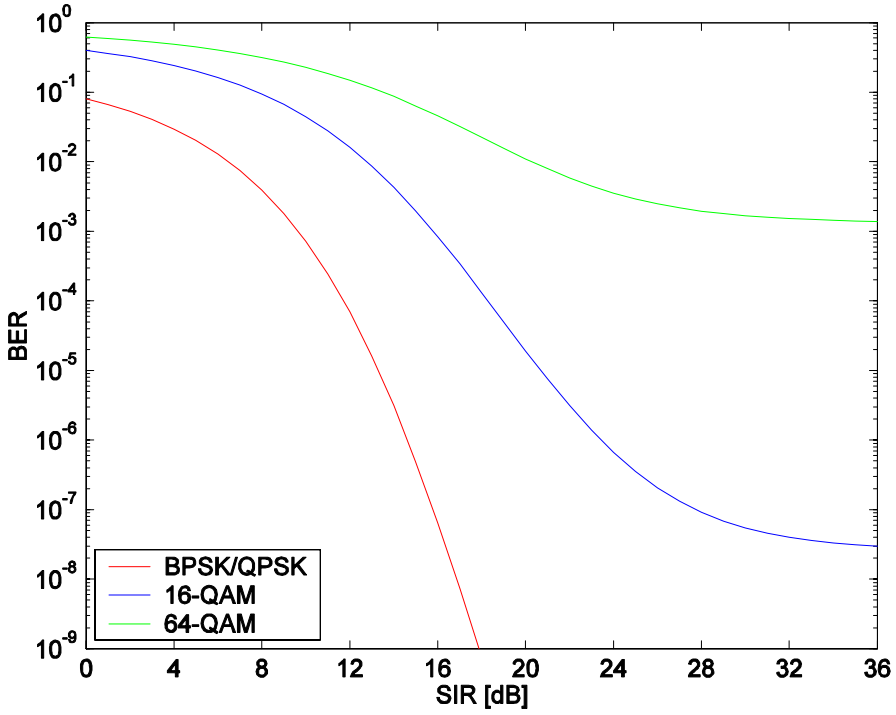

Figure 13. Performance of BPSK/QPSK, 16QAM and 16QAM in AWGN with pulsed-noise jamming, $SNR = 16$ dB and $\rho = 0.5$.

We plot the performance of all modulations discussed in this chapter under the effect of worse case pulsed-noise jamming in Figure 14. The effect of worst case pulsed-noise jamming is to change the dependence of P_b on E_b / N_I from an exponential one to an inverse one. As E_b / N_I increases, worst-case pulsed-noise jamming requires shorter duration pulses and higher peak jamming power since ρ_{wc} gets smaller. However, if we consider practical limitations, the pulsed-noise jammer may not be able to transmit for as short duration as called for when ρ is small.

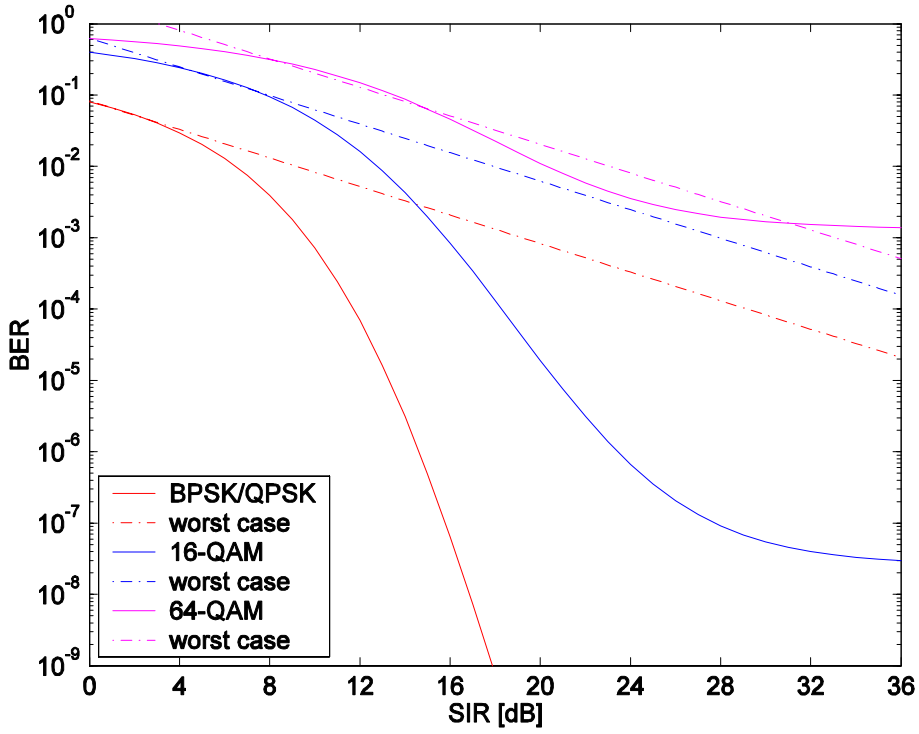

Figure 14. Performance of BPSK/QPSK, 16QAM and 16QAM in AWGN with pulsed-noise jamming.

B. PERFORMANCE IN NAKAGAMI FADING CHANNELS

The probability of bit error of all sub-carrier modulation formats that we have analyzed are functions of $E_b = A_c^2 \cdot T_b$, where A_c is modeled as a constant parameter. In fading channels, because of the multipath effects discussed in Chapter II, the received signal amplitude fluctuates and cannot be modeled as a constant parameter but must be

modeled as a random variable a_c. More specifically for this study, we model a_c as a Nakagami random variable. Hence, $E_b = a_c^2 \cdot T_b$ is also a random variable. For this reason Equation (4.1) and (4.10) are now conditional probabilities $P_b(a_c)$. In this case, we need to find the average probability of bit error for all sub-carrier modulations.

1. BPSK/QPSK Modulation

The probability of bit error for BPSK/QPSK with pulsed-noise jamming is given by Equation (4.5). In Nakagami fading channels, Equation (4.5) is a conditional probability which can be expressed as

$$P_b(a_c) = \rho \cdot Q\left(\sqrt{\frac{2a_c^2 \cdot T_b}{N_o + N_I/\rho}}\right) + (1-\rho) \cdot Q\left(\sqrt{\frac{2a_c^2 \cdot T_b}{N_o}}\right) \tag{4.15}$$

In order to obtain the probability of bit error when a_c is modeled as a random variable, we must average the conditional probability of bit error over the probability density function (PDF) as described in [10]; that is,

$$P_b = \int_0^\infty P_b(a_c) \cdot f_{A_c}(a_c)\, da_c \tag{4.16}$$

where $f_{A_c}(a_c)$ is the Nakagami-m PDF given by Equation (2.19), rewritten here as

$$f_{A_c}(a_c) = \frac{2}{\Gamma(m)}\left(\frac{m}{\Omega}\right)^m a_c^{2m-1} e^{-\left(\frac{ma_c^2}{\Omega}\right)} \quad a_c \geq 0. \tag{4.17}$$

If we define

$$e_b = a_c^2 \cdot T_b, \tag{4.18}$$

then

$$a_c = \sqrt{\frac{e_b}{T_b}} = \sqrt{e_b \cdot R_b} \tag{4.19}$$

where R_b is the signal data rate. It is clear that at this point we must obtain the PDF of e_b from the PDF of a_c given in Equation (4.17) from:

$$f_{E_b}(e_b) = \frac{1}{\left|de_b / da_c\right|} f_A(a_c)\Big|_{a_c = f^{-1}(e_b)}. \tag{4.20}$$

Next, we obtain the differential term,

$$\frac{de_b}{da_c} = \frac{2a_c}{R_b}. \tag{4.21}$$

When we substitute Equations (4.19) and (4.21) into (4.20), we obtain

$$f_{E_b}(e_b) = \frac{R_b}{2 \cdot a_c} \frac{2}{\Gamma(m)} \left(\frac{m}{\Omega}\right)^m \left(\sqrt{e_b \cdot R_b}\right)^{2m-1} e^{-\frac{m\left(\sqrt{e_b \cdot R_b}\right)^2}{\Omega}} = \frac{m^m}{\Gamma(m)} \frac{{e_b}^{m-1}}{\Omega^m} \mathrm{e}^{-\frac{m(e_b \cdot R_b)}{\Omega}}. \tag{4.22}$$

Since $\Omega = E\left[a_c^2 \cdot T_b\right] = E_b$ we obtain,

$$f_{E_b}(e_b) = \frac{m^m}{\Gamma(m) {E_b}^m} {e_b}^{m-1} e^{-\frac{me_b}{E_b}} \tag{4.23}$$

which is the PDF that we require.

We now obtain an expression for the probability of bit error for a single BPSK-modulated OFDM sub-carrier that encounters Nakagami-m distributed fading. Substituting Equations (4.15) and (4.23) into (4.16), we get

$$P_b = \int_0^\infty \left\{ \rho \cdot Q\left(\sqrt{\frac{2a_c^2 \cdot T_b}{N_o + N_I / \rho}}\right) + (1-\rho) \cdot Q\left(\sqrt{\frac{2a_c^2 \cdot T_b}{N_o}}\right) \right\} \cdot \frac{m^m}{\Gamma(m) {E_b}^m} {e_b}^{m-1} e^{-\frac{me_b}{E_b}} de_b. \tag{4.24}$$

In order to obtain an analytic solution, we compare Equation (4.24) with the following identity

$$\frac{a^b}{\Gamma(b)} \int_0^\infty d \cdot e^{-at} t^{b-1} Q\left(\sqrt{ct}\right) dt = \sqrt{\frac{\psi}{1+\psi}} \frac{\Gamma\left(b+\frac{1}{2}\right)}{2\sqrt{\pi}\Gamma(b+1)(1+\psi)^b} {}_2F_1\left(1, b+\tfrac{1}{2}; b+1; \frac{1}{1+\psi}\right) \tag{4.25}$$

where ${}_2F_1$ is Gauss' hyper-geometric function and is defined as

$$ {}_2F_1\left(1, b+\tfrac{1}{2}; b+1; z\right) = \sum_{k=0}^{\infty} \frac{\left(b+\frac{1}{2}\right)_k z^k}{\left(b+1\right)_k} \tag{4.26} $$

with

$$ z = \frac{1}{1+\psi} \tag{4.27} $$

and

$$ \begin{aligned} \left(r\right)_k &= \frac{\Gamma\left(r+k\right)}{\Gamma\left(r\right)} = r(r+1)\cdots(r+k-1) \\ \left(r\right)_0 &= 1. \end{aligned} \tag{4.28} $$

Equation (4.28) is known as Pochhammer's Symbol [22], and we can rewrite Equation (4.28) as

$$ \frac{\Gamma\left(r+k\right)}{\Gamma\left(r\right)} = \prod_{n=0}^{k-1}\left(r+n\right). \tag{4.29} $$

If we now compare variables from the integrand in Equation (4.24) to those of Equation (4.25), set $b_1 = m$, $a_1 = m/E_b$, $c_1 = \dfrac{2}{N_o + N_I/\rho}$, $t_1 = e_b$, $d_1 = \rho$, $\psi_1 = c_1/2a_1 = \dfrac{E_b}{\left(N_o + N_I/\rho\right)\cdot m}$ for the first term of the integrand and $b_2 = m$, $a_2 = m/E_b$, $c_2 = \dfrac{2}{N_o}$, $t_2 = e_b$, $d_1 = \left(1-\rho\right)$, $\psi_2 = c_2/2a_2 = \dfrac{E_b}{N_o \cdot m}$ for the second term, Equation (4.24) is now in a form suitable for analytical resolution by comparison with Equation (4.25). If we define $SNR = \dfrac{E_b}{N_o}$ as the signal-to-noise ratio and $SIR = \dfrac{E_b}{N_I}$ as the signal-to-interference ratio, respectively, then we obtain

$$P_{b_{BPSK/QPSK}} = \frac{\rho}{\sqrt{1+m\left(SNR^{-1}+SIR^{-1}/\rho\right)}} \cdot \frac{\Gamma\left(m+0.5\right)}{2\sqrt{\pi}\Gamma\left(m+1\right)\left(1+\frac{1}{m\left(SNR^{-1}+SIR^{-1}/\rho\right)}\right)^{m}}$$
$$\times\left(\sum_{k=0}^{\infty}\frac{\left(m+0.5\right)_k\left(\frac{1}{1+\left[m\left(SNR^{-1}+SIR^{-1}/\rho\right)\right]^{-1}}\right)^{k}}{\left(m+1\right)_k}\right) \tag{4.30}$$
$$+\frac{\left(1-\rho\right)}{\sqrt{1+m\cdot SNR^{-1}}}\cdot\frac{\Gamma\left(m+0.5\right)}{2\sqrt{\pi}\Gamma\left(m+1\right)\left(1+SNR/m\right)^{m}}\left(\sum_{k=0}^{\infty}\frac{\left(m+0.5\right)_k\left(\frac{1}{1+SNR/m}\right)^{k}}{\left(m+1\right)_k}\right).$$

By substituting Equations (4.28) and (4.29) into (4.30), we get the more concise expression

$$P_{b_{BPSK/QPSK}} = \frac{\rho}{\sqrt{1+m\left(SNR^{-1}+SIR^{-1}/\rho\right)}}\frac{\Gamma\left(m+0.5\right)}{2\sqrt{\pi}\Gamma\left(m+1\right)\left(1+\frac{1}{m\left(SNR^{-1}+SIR^{-1}/\rho\right)}\right)^{m}}$$
$$\times\left(1+\sum_{k=0}^{\infty}\frac{\prod_{n=0}^{k-1}\left(m+0.5+n\right)\left(\frac{1}{1+\left[m\left(SNR^{-1}+SIR^{-1}/\rho\right)\right]^{-1}}\right)^{k}}{\prod_{n=0}^{k-1}\left(m+1+n\right)}\right) \tag{4.31}$$
$$+\frac{\left(1-\rho\right)}{\sqrt{1+m\cdot SNR^{-1}}}\frac{\Gamma\left(m+0.5\right)}{2\sqrt{\pi}\Gamma\left(m+1\right)\left(1+SNR/m\right)^{m}}\left(1+\sum_{k=0}^{\infty}\frac{\prod_{n=0}^{k-1}\left(m+0.5+n\right)\left(\frac{1}{1+SNR/m}\right)^{k}}{\prod_{n=0}^{k-1}\left(m+1+n\right)}\right).$$

We have obtained an analytic expression for the probability of bit error for a single BPSK/QPSK modulated OFDM sub-carrier under the conditions that the sub-carrier experiences flat, slow Nakagami fading in the presence of pulsed-noise jamming.

Because of the Nakagami-m distributed fading, Equation (4.9) is a conditional probability $P_{b_{\max}}\left(a_c\right)$; hence, in order to obtain the worst case probability of bit error

$P_{b_{\max}}$ when a_c is random, we must average the conditional probability of bit error over the probability density function (PDF)

$$P_{b_{\max}} = \int_0^{\infty} \frac{0.08285}{e_b / N_I} \cdot \frac{m^m}{\Gamma(m)(E_b)^m} e_b^{m-1} e^{-\frac{me_b}{E_b}} de_b. \tag{4.32}$$

This integral is evaluated numerically.

Since thermal noise is not neglected in Equation (4.31), now we need to estimate the required signal-to-noise ratio (SNR). Therefore, considering all modulations utilized in *IEEE 802.11a*, OFDM performance for 48 independent sub-carriers over composite Nakagami fading channels is plotted by using the results provided in [5] in Figure 15, where *m* is uniformly distributed between $0.5 < m < 3$.

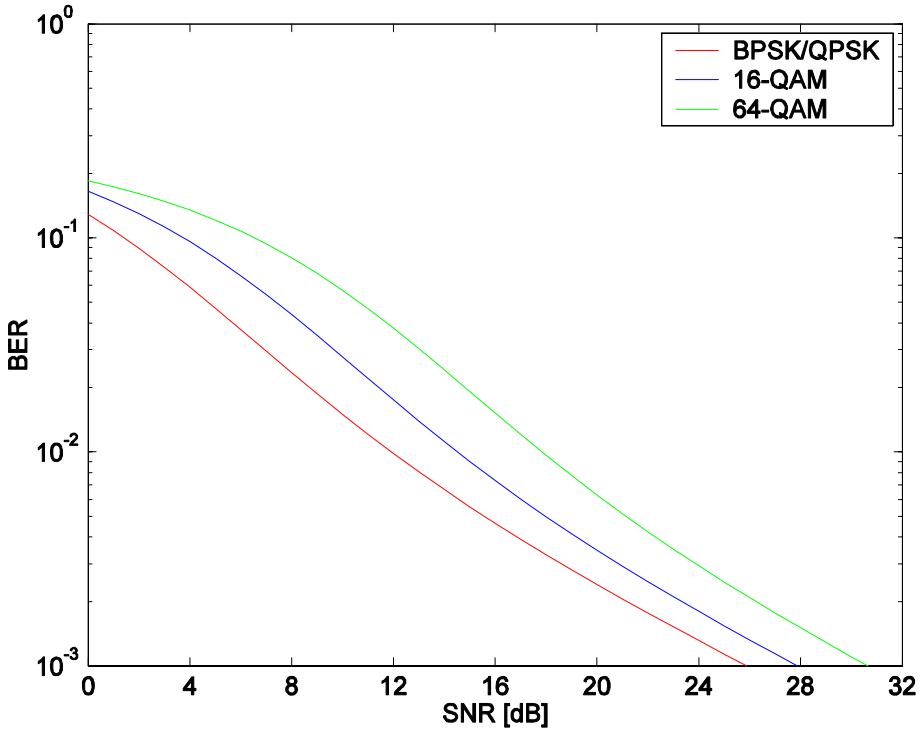

Figure 15. Performance of BPSK/QPSK, 16QAM and 16QAM in Nakagami fading.

It is well known that a channel $P_b = 10^{-3}$ is a good benchmark required by many wireless communications systems for practical applications. Consequently, $P_b = 10^{-3}$ is

chosen in order to be consistent with the practical applications. If we were to attempt to achieve a $P_b = 10^{-5}$, the required SNR would be very large, on the order of 70-80 dB. Therefore, $SNR = 26$ dB for $P_b = 10^{-3}$ is used in plotting Equation (4.31) with respect to average signal-to-interference ratio (SIR).

Figure 16 is plotted for multiple values of the fading figure m. As previously mentioned, the value of $m = 1$ corresponds to Rayleigh fading. Values $m > 1$ indicate better fading conditions than Rayleigh and usually specify a line of sight (LOS) is available between the workstation and the access point. Higher values of m indicate less severe fading. If we let $m \to \infty$, there is no fading and the performance is as shown in Figure 14 for BPSK and QPSK in AWGN with pulsed-noise jamming. For values $m < 1$, fading conditions are much more severe than the Rayleigh case, and there is a performance reduction as indicated in Figure 16.

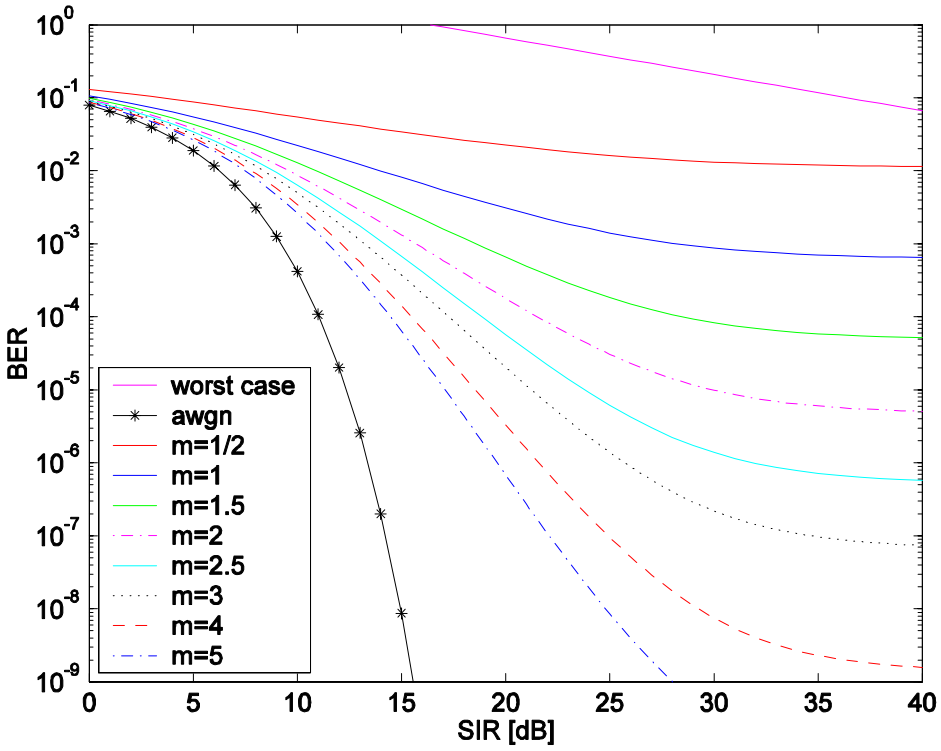

Figure 16. Performance of BPSK/QPSK with Nakagami fading in the presence of pulsed-noise jamming with $SNR = 26$ dB and $\rho = 0.5$.

Looking at Equation (4.30) more closely, we notice that for values of $\frac{1}{m\left(SNR^{-1}+SIR^{-1}/\rho\right)} \geq 3$ and $\frac{SNR}{m} \geq 3$ the first term in each summation dominates. Hence, a close approximation to Equation (4.31) can be made by setting

$$\left(1+\sum_{k=0}^{\infty}\frac{\prod_{n=0}^{k-1}(m+0.5+n)\left(\frac{1}{1+\left[m\left(SNR^{-1}+SIR^{-1}/\rho\right)\right]^{-1}}\right)^{k}}{\prod_{n=0}^{k-1}(m+1+n)}\right)\approx 1 \quad \text{for} \quad \frac{1}{m\left(SNR^{-1}+SIR^{-1}/\rho\right)} \geq 3 \tag{4.33}$$

and

$$\left(1+\sum_{k=0}^{\infty}\frac{\prod_{n=0}^{k-1}(m+0.5+n)\left(\frac{1}{1+SNR/m}\right)^{k}}{\prod_{n=0}^{k-1}(m+1+n)}\right)\approx 1 \quad \text{for} \quad \frac{SNR}{m} \geq 3. \tag{4.34}$$

With these substitutions in Equation (4.31), a more analytically appealing expression for the probability of bit error is obtained:

$$P_{b_{BPSK/QPSK}} \approx \frac{\rho}{\sqrt{1+m\left(SNR^{-1}+SIR^{-1}/\rho\right)}}\cdot\frac{\Gamma(m+0.5)}{2\sqrt{\pi}\Gamma(m+1)\left(1+\frac{1}{m\left(SNR^{-1}+SIR^{-1}/\rho\right)}\right)^{m}}$$
$$+\frac{(1-\rho)}{\sqrt{1+m\cdot SNR^{-1}}}\cdot\frac{\Gamma(m+0.5)}{2\sqrt{\pi}\Gamma(m+1)(1+SNR/m)^{m}}. \tag{4.35}$$

Equations (4.31) and (4.35) are plotted in Figure 17 for $m=5$. From Figure 17 we see that this approximation is fairly tight for $SIR=13$ dB, which implies that the approximation is accurate for larger SIR.

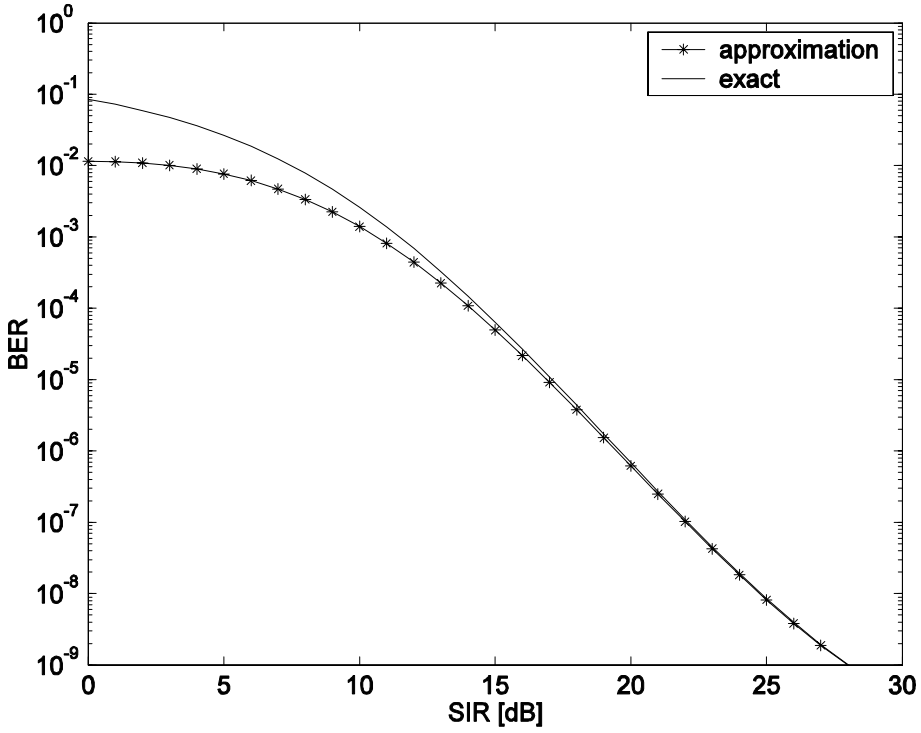

Figure 17. Comparison of Equation (4.31) and (4.35)

2. 16 and 64-QAM Modulation

To obtain data rates between 24 and 54 Mbps, *IEEE 802.11a* uses the bandwidth efficient M-ary QAM. The derivation of an analytic expression for the performance of QAM with pulsed-noise jamming in Nakagami fading channels is similar to that of BPSK/QPSK, but the conditional probability of bit error for QAM in the presence of pulse jamming is obtained from Equation (4.11):

$$P_b\left(e_b\right)=\frac{\rho\cdot 4\left(\sqrt{M}-1\right)}{q\sqrt{M}}Q\left(\sqrt{\frac{3qe_b}{(M-1)\cdot(N_0+N_I/\rho)}}\right)+(1-\rho)\cdot\frac{4\left(\sqrt{M}-1\right)}{q\sqrt{M}}Q\left(\sqrt{\frac{3qe_b}{(M-1)N_0}}\right) \quad (4.36)$$

Now substituting Equation (4.36) into

$$P_b=\int_0^\infty P_b\left(e_b\right)\cdot f_{E_b}\left(e_b\right)de_b \quad (4.37)$$

we find

$$P_b\left(e_b\right)=\int_0^{\infty}\left[\frac{\rho\cdot 4\left(\sqrt{M}-1\right)}{q\sqrt{M}}Q\left(\sqrt{\frac{3qe_b}{(M-1)\cdot(N_0+N_I/\rho)}}\right)+(1-\rho)\cdot\frac{4\left(\sqrt{M}-1\right)}{q\sqrt{M}}Q\left(\sqrt{\frac{3qe_b}{(M-1)N_0}}\right)\right]$$
$$\times\frac{m^m}{\Gamma(m)\left(E_b\right)^m}e_b^{\,m-1}e^{-\frac{me_b}{E_b}}de_b \tag{4.38}$$

We can use the mathematical equality given by Equation (4.25) to obtain an analytical solution for this rather complicated integral by making the following substitutions from Equation (4.25) into Equation (4.38):

$$\begin{aligned}
d_1&=\rho\cdot\frac{4\left(\sqrt{M}-1\right)}{\sqrt{M}}\\
c_1&=\frac{3q}{\left(M-1\right)\cdot\left(N_o+N_I/\rho\right)}\\
b_1&=m\\
t_1&=e_b\\
a_1&=\frac{m}{E_b}\\
\psi_1&=\frac{c_1}{2a_1}=\frac{3q}{2m\left(M-1\right)\left(SNR^{-1}+SIR^{-1}/\rho\right)}
\end{aligned} \tag{4.39}$$

for the first term and

$$\begin{aligned}
d_2&=(1-\rho)\cdot\frac{4\left(\sqrt{M}-1\right)}{\sqrt{M}}\\
c_2&=\frac{3q}{\left(M-1\right)\cdot N_o}\\
b_2&=m\\
t_2&=e_b\\
a_2&=\frac{m}{E_b}\\
\psi_2&=\frac{c_2}{2a_2}=\frac{3q\cdot SNR}{2m\left(M-1\right)}
\end{aligned} \tag{4.40}$$

for the second term. We obtain the final result

$$P_{bQAM} = \frac{4\rho\left(\sqrt{M}-1\right)}{q\sqrt{M}} \frac{\Gamma(m+0.5)}{\sqrt{1+\left[\frac{2m(M-1)}{3q}\left(SNR^{-1}+SIR^{-1}/\rho\right)\right]}\cdot 2\sqrt{\pi}\cdot\Gamma(m+1)\left[1+\frac{3q}{2m(M-1)\left(SNR^{-1}+SIR^{-1}/\rho\right)}\right]^{m}}$$

$$\times\left[1+\sum_{k=1}^{\infty}\frac{\prod_{n=0}^{k-1}(m+0.5+n)\left(\frac{1}{1+\frac{3q}{2m(M-1)\left(SNR^{-1}+SIR^{-1}/\rho\right)}}\right)^{k}}{\prod_{n=0}^{k-1}(m+1+n)}\right]$$

$$+\frac{(1-\rho)4\left(\sqrt{M}-1\right)}{q\sqrt{M}} \frac{\Gamma(m+0.5)}{\sqrt{1+\left[\frac{2m(M-1)}{3q\cdot SNR}\right]}\cdot 2\sqrt{\pi}\cdot\Gamma(m+1)\left[1+\frac{3q\cdot SNR}{2m(M-1)}\right]^{m}}\left[1+\sum_{k=1}^{\infty}\frac{\prod_{n=0}^{k-1}(m+0.5+n)\left(\frac{1}{1+\frac{3q\cdot SNR}{2m(M-1)}}\right)^{k}}{\prod_{n=0}^{k-1}(m+1+n)}\right]. \quad (4.41)$$

Consequently, Equation (4.41) represents an analytic expression for the performance of square constellation QAM in Nakagami fading with pulsed-noise jamming.

Just as for BPSK/QPSK we can simplify Equation (4.41) by noting the dominance term of the first term in the summations and substituting

$$\left(1+\sum_{k=0}^{\infty}\frac{\prod_{n=0}^{k-1}(m+0.5+n)\left(\frac{1}{1+\frac{3q}{2m(M-1)\left(SNR^{-1}+SIR^{-1}/\rho\right)}}\right)^{k}}{\prod_{n=0}^{k-1}(m+1+n)}\right)\approx 1 \quad \text{for} \quad \frac{3q}{2m(M-1)\left(SNR^{-1}+SIR^{-1}/\rho\right)}\geq 3 \quad (4.42)$$

and

$$\left(1+\sum_{k=0}^{\infty}\frac{\prod_{n=0}^{k-1}(m+0.5+n)\left(\frac{1}{1+\frac{3q\cdot SNR}{2m(M-1)}}\right)^{k}}{\prod_{n=0}^{k-1}(m+1+n)}\right)\approx 1 \quad \text{for} \quad \frac{3q\cdot SNR}{2m(M-1)}\geq 3. \quad (4.43)$$

With this substitution in Equation (4.41), a more analytically appealing expression for the probability of bit error is obtained:

$$P_{bQAM} = \frac{4\rho\left(\sqrt{M}-1\right)}{q\sqrt{M}} \frac{\Gamma\left(m+0.5\right)}{\sqrt{1+\left[\frac{2m\left(M-1\right)}{3q}\left(SNR^{-1}+SIR^{-1}/\rho\right)\right]}\cdot 2\sqrt{\pi}\cdot\Gamma\left(m+1\right)\left[1+\frac{3q}{2m\left(M-1\right)\left(SNR^{-1}+SIR^{-1}/\rho\right)}\right]^{m}}$$

$$+\frac{\left(1-\rho\right)4\left(\sqrt{M}-1\right)}{q\sqrt{M}} \frac{\Gamma\left(m+0.5\right)}{\sqrt{1+\left[\frac{2m\left(M-1\right)}{3q\cdot SNR}\right]}\cdot 2\sqrt{\pi}\cdot\Gamma\left(m+1\right)\left[1+\frac{3q\cdot SNR}{2m\left(M-1\right)}\right]^{m}}. \tag{4.44}$$

Finally, because of the Nakagami-m distributed fading, Equation (4.14) is also a conditional probability $P_{b\max}\left(a_c\right)$; hence, in order to obtain the worst case probability of bit error $P_{b\max}$ when a_c is random, we must average the conditional probability of bit error over the probability density function (PDF)

$$P_{b\max} = \int_0^{\infty} \frac{0.0221\cdot\left(M-1\right)\left(\sqrt{M}-1\right)}{q\cdot\sqrt{M}\cdot e_b/N_I}\cdot\frac{m^m}{\Gamma\left(m\right)\left(E_b\right)^m} e_b^{\,m-1} e^{-\frac{me_b}{E_b}}\, de_b. \tag{4.45}$$

This integral is evaluated numerically.

The performance of QAM with Nakagami fading channels in the presence of pulsed-noise jamming is plotted in Figures 18 and 19, where m as a parameter in the range of $1/2 \le m \le 5$. Note that $SNR = 28$ dB for 16QAM and $SNR = 31$ dB for 64QAM obtained from Figure 15 are used in Equation (4.44). What we see in both Figures 18 and 19 indicates the same general trend of improved performance for higher values of m. However, for small m, performance is significantly degraded. We can verify by inspection of our results that BPSK and QPSK have superior performance to M-QAM. On the other hand, when the allocated bandwidth is limited and higher data rates are required, QAM modulation is preferable over BPSK or QPSK. The design engineers must balance these requirements.

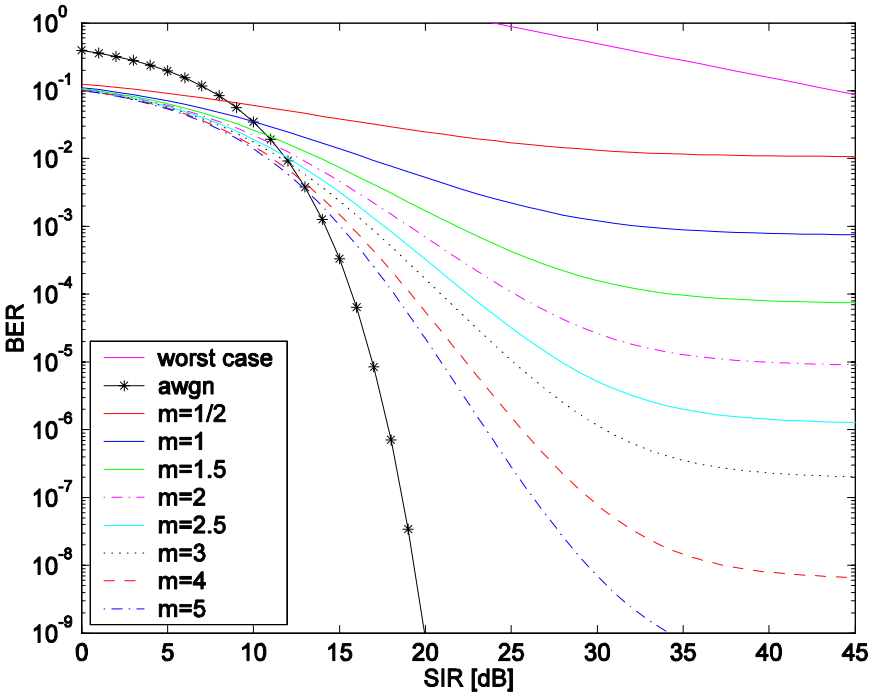

Figure 18. The performance of 16QAM in Nakagami fading with pulsed-noise jamming with $SNR = 28$ dB and $\rho = 0.5$.

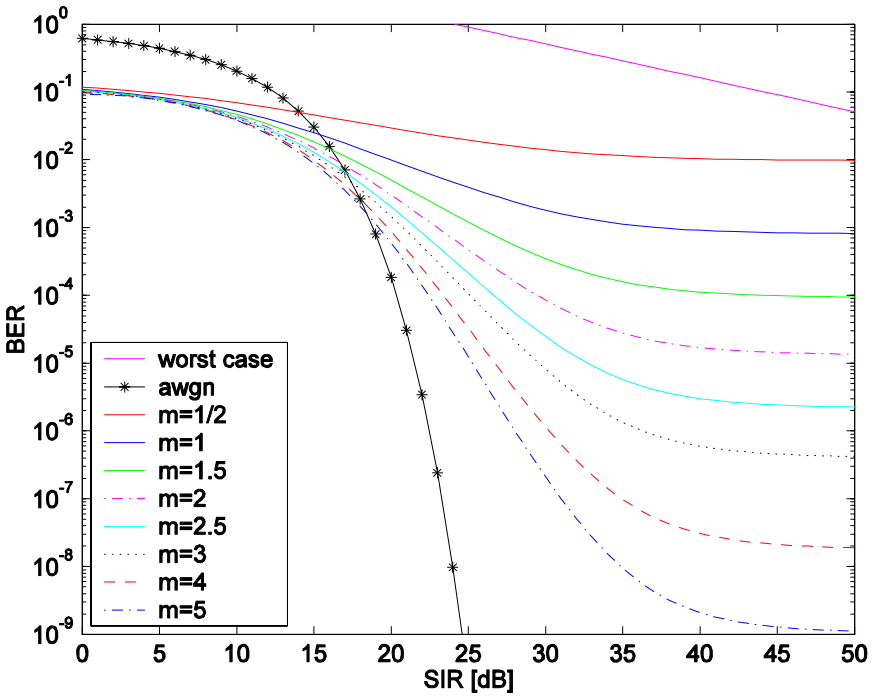

Figure 19. The performance of 64QAM in Nakagami fading with pulsed-noise jamming with $SNR = 31$ dB and $\rho = 0.5$.

By way of comparison, in Figure 20 we overlay the results of Figures 16, 18 and 19 for the case of $m = 1$ to view their performance relative to each other. As discussed earlier, $SNR = 26,\ 28$, and 31 dB for BPSK/QPSK, 16QAM, and 64QAM, respectively, which yields $P_b = 10^{-3}$ when $SIR \to \infty$, are used in plotting Figure 20 where $\rho = 0.5$.

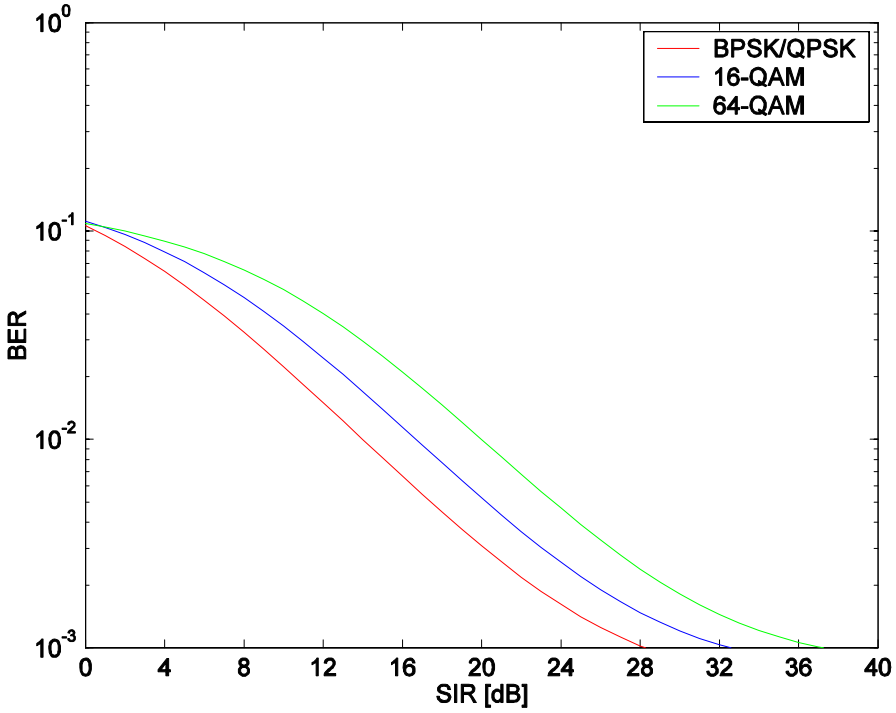

Figure 20. All modulations in Nakagami fading with pulsed-noise jamming. $(m = 1)$

In Figure 20, we see the performance trends are as expected. BPSK outperforms 16QAM which outperforms 64QAM. As indicated in Figure 20, 16QAM requires SIR approximately 4 dB greater than that of BPSK and QPSK in order to achieve the same BER of 10^{-3} for $m = 1$. This is also true for 16QAM and 64QAM.

C. UNCODED OFDM SYSTEM PERFORMANCE

Having found the analytic expressions for P_b for BPSK/QPSK, 16QAM and 64QAM performance in Nakagami fading channels with pulsed-noise jamming, we are

ready to analyze OFDM system performance without FEC coding for the *IEEE 802.11a* standard. However, there are several issues that need to be discussed first.

First of all, as specified by the *IEEE 802.11a* standard, one OFDM symbol utilizes 48 sub-carriers for data transmission, and each sub-carrier is separated by 312.5 kHz. When channel coherence bandwidth is less than or equal to the sub-carrier spacing Δf_{sc}, then each sub-carrier will encounter independent fading. In this case, it is reasonable to consider 48 independent sub-carriers in the OFDM system; however, this condition may not be true for all fading environments since conditions are much more variable with respect to reflection, diffraction and scattering factors. For instance, signal levels vary greatly depending on whether interior doors are open or closed inside a building. Recalling Equation (2.3), if the coherence bandwidth is defined as the bandwidth over which the frequency correlation function is above 0.9, then $B_c \approx 1/50\sigma_\tau$, where σ_τ is the rms delay spread. According to [9], depending on the existence or absence of a clear LOS path, the reported rms delay spread values are 30 ns for small/medium-size office buildings and less than 120 ns for large office buildings, respectively. This result indicates that rms delay varies from 30 ns to 120 ns in different circumstances. Substituting these values into Equation (2.3), we obtain a range of values for coherence bandwidth as $666.67 \geq B_c \geq 166.67$ kHz. In this case, the lower range of B_c is less than Δf_{sc}, while the upper range of B_c is approximately equivalent to $2\Delta f_{sc}$. Therefore, we can assume 48 independent sub-carriers for large office buildings where $\Delta f_{sc} \geq B_c$, and 24 independent sub-carriers for small/medium-size office buildings where $\Delta f_{sc} \leq B_c \leq 2\Delta f_{sc}$.

Secondly, *IEEE 802.11a* is standardized for WLAN indoor transmissions. Consequently, we must consider that we are transmitting from a lap-top computer and link to the LAN through an access point from different corners in a building. At the same time we encounter pulsed-noise jamming during our transmissions. We must also allow for both line-of-sight (LOS) and non-LOS transmission since both are reasonable. Hence, we assume that m can be modeled as a uniformly distributed random variable since the uniform random variable is used to model situations in which all values within an interval are equally likely to occur [12]. As previously discussed, the value of $m = 1$ corresponds

to Rayleigh fading. Values $m > 1$ indicate better fading conditions than Rayleigh and usually specify LOS is available between workstation and access point, while higher values of m indicate less severe fading. If we let $m \to \infty$ there is no fading. Consequently, the assumption $0.5 \le m \le 5$ is reasonable for any office building.

Finally, we use the following process in order to analyze composite OFDM performance: first we evaluate each sub-carrier's performance under the effect of pulsed-noise jamming using Equation (4.35) or Equation (4.44), 48 times for the 48 independent sub-carrier case and 24 times for the 24 independent sub-carrier case. Since m is considered to be uniformly distributed, its value will be different in each trial. We then average each independent sub-carrier's performance under the effect of pulsed-noise jamming to estimate the overall OFDM system performance. We now investigate the performance of the *IEEE 802.11a* standard without FEC coding given the preceding assumptions.

1. BPSK/QPSK Modulated OFDM

As we discussed above, to examine the performance of a BPSK/QPSK modulated OFDM transmission with Nakagami fading in the presence of pulsed-noise jamming, we need to evaluate Equation (4.35) either 48 or 24 times. Then we average all sub-carrier's performance results to obtain the overall OFDM performance. BPSK/QPSK modulated OFDM performance for both 48 and 24 independent sub-carriers over composite Nakagami fading channels with pulsed-noise jamming where m is assigned randomly from a uniform distribution over the range $0.5 \le m \le 5$ is plotted in Figure 21 for one trial.

We plot the results against the two endpoints in the uniform distribution. As we can see, there is a performance difference between 48 and 24 independent sub-carriers. In fact this difference is randomly distributed since m is modeled as a random variable. For some perspective, although m is allowed to vary from $1/2$ to 5, it seems that the negative effects of the lower fading figure dominate the overall OFDM system performance. We see in Figure 21 that for low values of E_b / N_J, the performance trend for the independent 48 sub-carriers appears to be near the midpoint between $m = 1/2$ and

$m = 5$. However, system performance is improved when we use 24 independent sub-carriers.

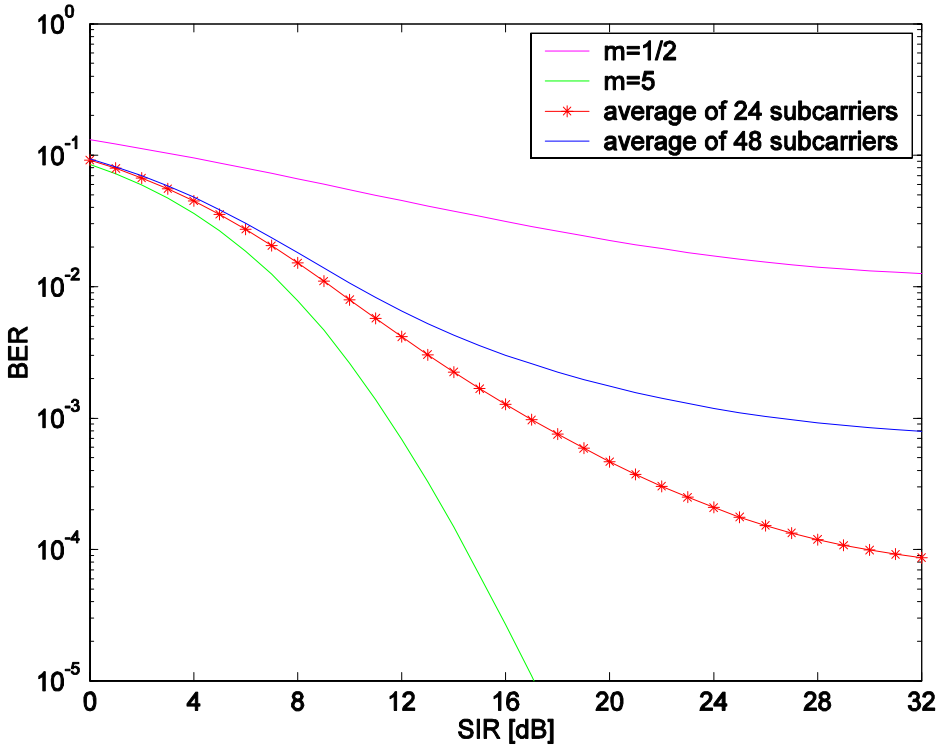

Figure 21. BPSK/QPSK modulated OFDM in composite Nakagami fading channels with pulsed-noise jamming, $SNR = 26$ dB and $\rho = 0.5$.

An average probability of bit error can be obtained by evaluating the BPSK/QPSK modulated OFDM performance for ten trials for both 48 and 24 independent sub-carriers. The minimum, maximum, and mean values for the E_b / N_I required for $P_b = 10^{-3}$ obtained from ten trials for BPSK/QPSK modulated OFDM when m is modeled as a uniform random variable that varies from 1/2 to 5 is shown in Table 3.

Uncoded BPSK/QPSK	48 sub-carriers [dB]	24 sub-carriers [dB]	Difference [dB]
Minimum	17.60	15.50	2.10
Maximum	29.80	23.00	6.80
Mean	23.59	17.83	5.76

Table 3. Uncoded BPSK/QPSK modulated OFDM performance statistics for E_b / N_I at $P_b = 10^{-3}$ where $1/2 \le m \le 5$.

The difference in the mean value of E_b / N_I between 48 and 24 independent sub-carrier's performance is 5.76 dB. This indicates that BPSK/QPSK modulated OFDM with 24 sub-carriers has better performance in the presence of pulsed-noise jamming with respect to the assumptions that have been made.

Since the negative effects of the lower fading figure dominate the overall OFDM performance, in order to investigate more severe fading conditions, we narrow the scope of the fading figure in Figure 22 and assume that m is modeled as a uniform random variable that varies from 1/2 to 2. In addition, while evaluating the composite BPSK/QPSK modulated OFDM performance with pulsed-noise jamming, we increase SNR to 32 dB because of the more severe fading conditions; otherwise, we cannot achieve $P_b = 10^{-3}$ which is required by many wireless communications systems as previously mentioned. We see in Figure 22 that the performance trend for the average of both 48 and 24 independent sub-carriers appears to be near the midpoint where $m = 1,$ so that the resulting composite signal is fairly well approximated as a Rayleigh fading channel.

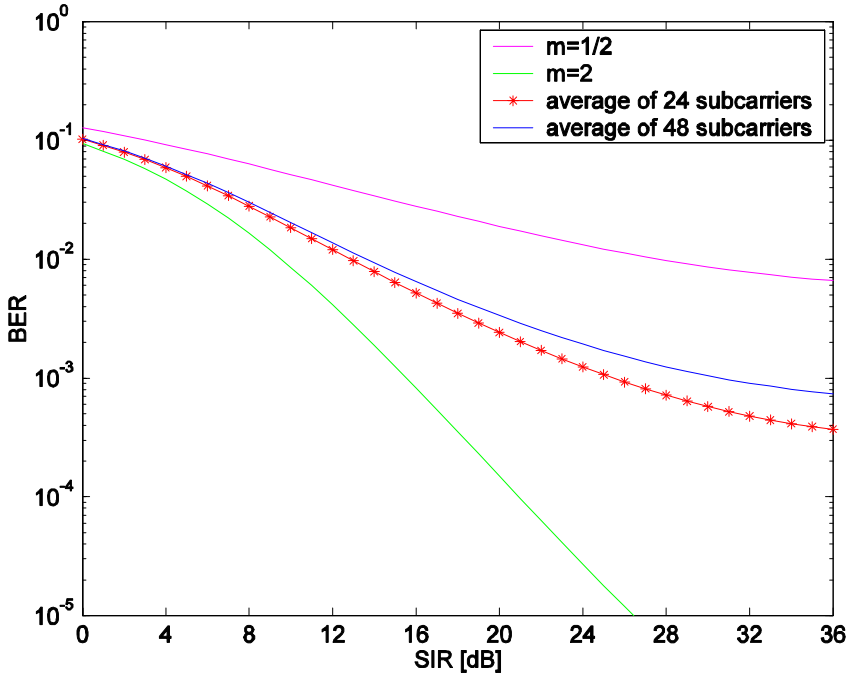

Figure 22. BPSK/QPSK modulated OFDM in composite Nakagami fading channels with pulsed-noise jamming, $SNR = 32$ dB, $\rho = 0.5$, and $1/2 \le m \le 2$.

An average probability of bit error can be obtained by evaluating the BPSK/QPSK modulated OFDM performance for ten trials for both 48 and 24 independent sub-carriers. The minimum, maximum, and mean values for the E_b / N_I required for $P_b = 10^{-3},$ obtained from ten trials for BPSK/QPSK modulated OFDM when m is modeled as a uniform random variable that varies from 1/2 to 2 is shown in Table 4.

Uncoded BPSK/QPSK	48 sub-carriers [dB]	24 sub-carriers [dB]	Difference [dB]
Minimum	25.50	24.00	1.50
Maximum	37.00	28.70	8.30
Mean	31.61	26.36	5.25

Table 4. Uncoded BPSK/QPSK modulated OFDM performance statistics for E_b / N_I at $P_b = 10^{-3}$ where $1/2 \le m \le 2.$

The difference in the mean value of E_b / N_I between 48 and 24 independent sub-carrier's performance is 5.25 dB, which is smaller than the 5.76 dB obtained for BPSK/QPSK modulated OFDM when m is modeled as a uniform random variable that varies from 1/2 to 5.

2. 16QAM and 64QAM Modulated OFDM

In order to investigate the performance of 16QAM and 64QAM modulated OFDM transmissions with Nakagami fading in the presence of pulsed-noise jamming, we follow an approach similar to that for BPSK/QPSK. This time we need to evaluate Equation (4.35) either 48 or 24 times. 16QAM and 64QAM modulated OFDM performance for both 48 and 24 independent sub-carriers over composite Nakagami fading channels with pulsed-noise jamming where m is assigned randomly from a uniform distribution over the range $0.5 \le m \le 5$ is plotted in Figure 23 and 24, respectively. Note that $SNR = 28$ dB and 31 dB obtained from Figure 15 which yields $P_b = 10^{-3}$ for 16QAM and 64QAM, respectively, are used in plotting the Figure 23 and 24.

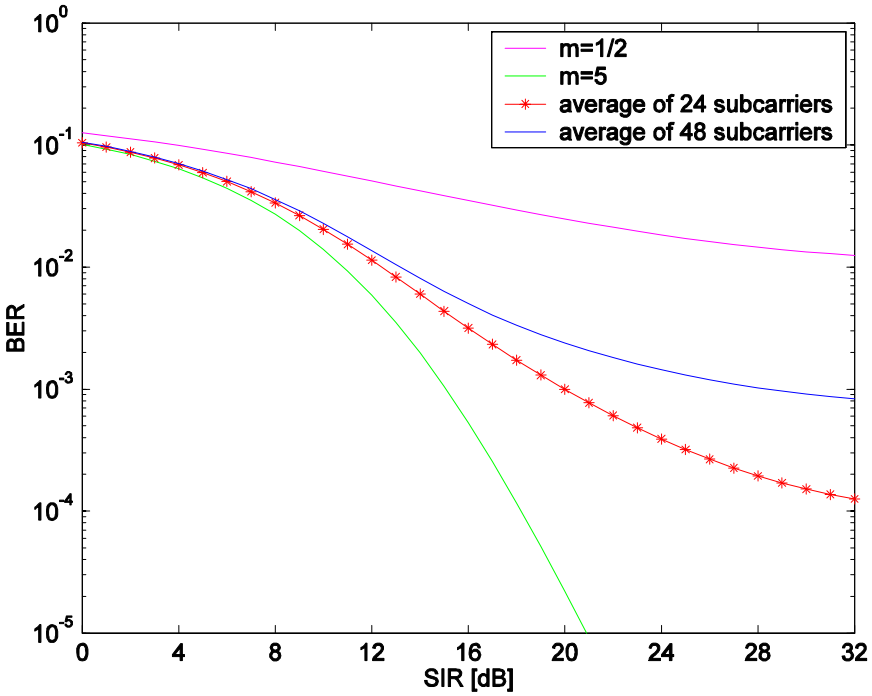

Figure 23. 16QAM modulated OFDM in composite Nakagami fading channels with pulsed-noise jamming, $SNR = 28$ dB and $\rho = 0.5$.

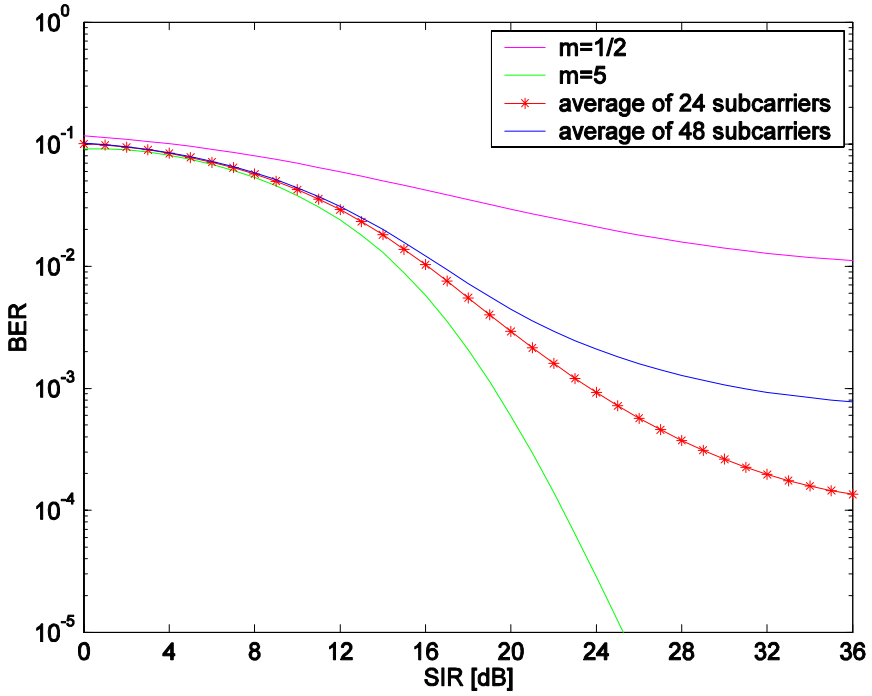

Figure 24. 64QAM modulated OFDM in composite Nakagami fading channels with pulsed-noise jamming, $SNR = 31$ dB and $\rho = 0.5$.

Basically, the curves reflect a slight degradation in performance relative to BPSK/QPSK. The minimum, maximum, and mean values for the E_b / N_I required for $P_b = 10^{-3}$ obtained from ten trials for 16QAM and 64QAM modulated OFDM are shown in Table 5 and 6, respectively. The difference in the mean value of E_b / N_I between 48 and 24 independent sub-carrier's performance is 6.33 dB for 16QAM and 5.35 for 64QAM.

Uncoded 16QAM	**48 sub-carriers [dB]**	**24 sub-carriers [dB]**	**Difference [dB]**
Minimum	22.70	16.80	5.90
Maximum	40.00	32.50	7.50
Mean	29.71	23.38	6.33

Table 5. Uncoded 16QAM modulated OFDM performance statistics. $(1/2 \le m \le 5)$

Uncoded 64QAM	**48 sub-carriers [dB]**	**24 sub-carriers [dB]**	**Difference [dB]**
Minimum	24.20	20.80	3.40
Maximum	43.50	34.10	9.40
Mean	31.23	25.88	5.35

Table 6. Uncoded 64QAM modulated OFDM performance statistics. $(1/2 \le m \le 5)$

The performance degrades from BPSK/QPSK to 16QAM to 64QAM. While considering the OFDM performance under the effect of pulsed-noise jamming, SNR is an important parameter. Furthermore, performance is not acceptable regardless of the modulation type or the number of independent sub-carriers without FEC. The results are summarized for the fading figure m that varies from 1/2 to 5 in Table 7.

Uncoded OFDM System Performance	**BPSK/QPSK [dB]**		**16QAM [dB]**		**64QAM [dB]**	
	48 Subc	**24 Subc**	**48 Subc**	**24 Subc**	**48 Subc**	**24 Subc**
Minimum	17.60	15.50	22.70	16.80	24.20	20.80
Maximum	29.80	23.00	40.00	32.50	43.50	34.10
Mean	23.59	17.83	29.71	23.38	31.23	25.88

Table 7. Overall uncoded OFDM performance statistics. $(1/2 \le m \le 5)$

Just as we did in the previous section, in order to investigate the negative effects of more severe fading, we narrow the scope of the fading figure and assume that m is modeled as a uniform random variable that varies from 1/2 to 2. While evaluating the composite 16QAM and 64QAM modulated OFDM performance with pulsed-noise jamming, we also increase SNR to 34 and 37 dB, respectively, because of the more severe fading conditions. The results are plotted in Figures 25 and 26 where m is in the range of $1/2 \le m \le 2$. As we can see, there is a slight performance difference between 48 and 24 independent sub-carriers at $P_b = 10^{-3}$, and the performance trend for the average of both 48 and 24 independent sub-carriers appears to be near the midpoint where $m = 1$, a Rayleigh fading channel.

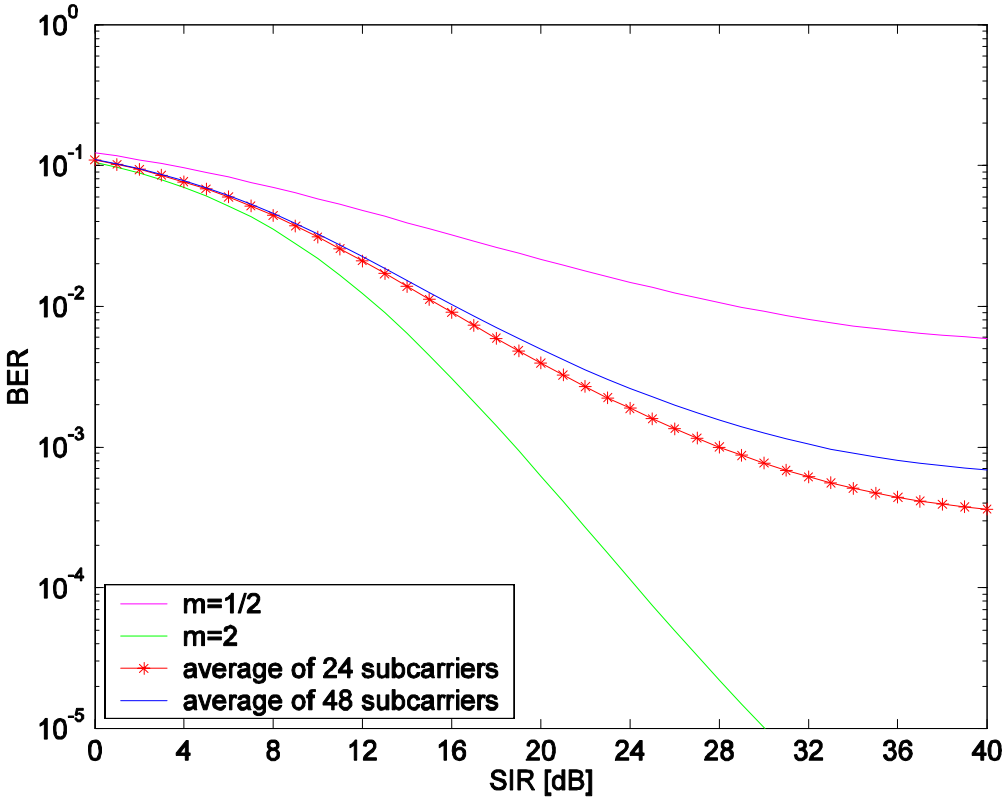

Figure 25. 16QAM modulated OFDM in composite Nakagami fading channels with pulsed-noise jamming, $SNR = 34$ dB, $\rho = 0.5$, and $1/2 \le m \le 2$.

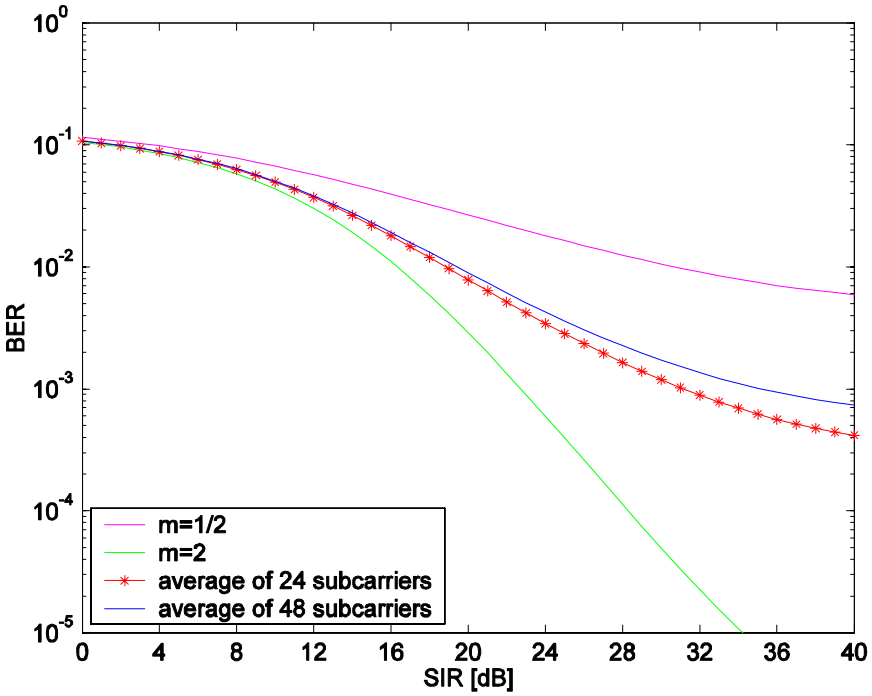

Figure 26. 64QAM modulated OFDM in composite Nakagami fading channels with pulsed-noise jamming, $SNR = 37$ dB, $\rho = 0.5$, and $1/2 \le m \le 2$.

The minimum, maximum, and mean values for the E_b / N_I required for $P_b = 10^{-3}$ obtained from ten trials for 16QAM and 64QAM modulated OFDM when m is modeled as a uniform random variable that varies from 1/2 to 2 are shown in Tables 8 and 9, respectively.

Uncoded 16QAM	48 sub-carriers [dB]	24 sub-carriers [dB]	Difference [dB]
Minimum	28.20	22.90	5.30
Maximum	40.75	33.50	7.25
Mean	33.77	29.04	4.73

Table 8. Uncoded 16QAM modulated OFDM performance statistics. $(1/2 \le m \le 2)$

Uncoded 64QAM	48 sub-carriers [dB]	24 sub-carriers [dB]	Difference [dB]
Minimum	31.25	26.50	4.75
Maximum	42.30	36.00	6.30
Mean	36.50	32.06	4.44

Table 9. Uncoded 64QAM modulated OFDM performance statistics. $(1/2 \le m \le 2)$

The difference in the mean value of E_b / N_I between 48 and 24 independent sub-carrier's performance is 4.73 dB for 16QAM and 4.44 dB for 64QAM, respectively, which are smaller than the 6.33 dB and 5.35 dB obtained for 16QAM and 64QAM modulated OFDM when m is modeled as a uniform random variable that varies from 1/2 to 2. As before, the results are summarized in Table 10.

Uncoded OFDM System Performance	**BPSK/QPSK [dB]**		**16QAM [dB]**		**64QAM [dB]**	
	48 Subc	**24 Subc**	**48 Subc**	**24 Subc**	**48 Subc**	**24 Subc**
Minimum	25.50	24.00	28.20	22.90	31.25	26.50
Maximum	37.00	28.70	40.75	33.50	42.30	36.00
Mean	31.61	26.36	33.77	29.04	36.50	32.06

Table 10. Overall uncoded OFDM performance statistics. $\left(1/2 \le m \le 2\right)$

D. SUMMARY OF UNCODED OFDM PERFORMANCE

In this chapter, we derived analytic expressions in order to investigate the uncoded OFDM performance in the presence of worst-case, pulsed-noise jamming for either pure or composite Nakagami fading channels. Next we examine the assumption that we have 48 independent sub-carriers for large office buildings where $\Delta f_c \ge B_c$ and 24 independent sub-carriers for small/medium-size office buildings where $\Delta f_{sc} \le B_c \le 2\Delta f_{sc}$.

Then we evaluated uncoded OFDM performance for both pure and composite Nakagami fading channels under the effect of hostile jamming. Consistent with the results that we obtained, the performance is dominated by the small values of m, which corresponds to more severe fading conditions. The values of E_b / N_I required to achieve a certain probability of bit error are well beyond what is achievable in any communications system. The performance of uncoded BPSK/QPSK modulated OFDM in the presence of pulsed-noise jamming is better than uncoded 16QAM and 64QAM; however, the performance is not acceptable regardless of the modulation type or the number of independent sub-carriers without FEC.

V. PERFORMANCE ANAYSIS WITH FEC CODING

In Chapter IV, we emphasized that the performance of OFDM without coding over composite Nakagami fading channels in the presence of pulsed-noise jamming is not acceptable regardless of the modulation type or the number of independent sub-carriers. In this chapter, we investigate the performance of an *IEEE 802.11a* system with FEC coding both for a pure and a composite Nakagami fading channel that is attacked by a hostile pulsed-noise jammer. Before the analysis, we first address the concept of error control coding (especially FEC coding), the definition of coding, and the implementation of FEC coding in Section A. We then investigate the performance of OFDM with respect to Viterbi hard decision decoding (HDD) for the modulation schemes as specified by *IEEE 802.11a* in Section B. Finally, we examine the performance of OFDM with Viterbi soft decision decoding (SDD); however, SDD with M-QAM modulation is beyond the scope of this thesis owing to the complexity of analyzing the probability bit error for SDD of a binary code transmitted with non-binary modulation.

A. ERROR CONTROL CODING

Because digital systems offer error control coding, data processing, and other flexibilities not possible for analog systems, digital communication systems are becoming more attractive. Communications system performance can be improved significantly by implementing error control coding. There are two basic error control strategies [13], automatic repeat request (ARQ) and forward error correction (FEC) coding. In an ARQ system, the receiver checks for errors but does not correct them; it simply requests the transmitter to resend the incorrectly received data. Unlike an ARQ system, a FEC coding system does correct the data errors at the receiver. Since *IEEE 802.11a* PHY uses FEC coding, ARQ systems are not considered in this thesis.

1. Forward Error Correcting (FEC) Coding

The purpose of FEC coding is to increase the robustness of a channel by adding a certain number of redundant bits to the actual data bits in a particular pattern such that

recovery of the actual data bits is enhanced. There are basically two types of FEC codes, convolutional and block codes. With block codes, a block of k data bits is encoded into a block of n coded bits, where $n > k$. The $n - k$ redundant bits in a codeword are called *parity bits*, which are used to check the codeword for errors during the decoding process. If errors exist due to the presence of noise, the decoder will ideally detect and correct them. Convolutional codes use linear shift-registers to add redundancy into the entire data stream. Convolutional codes operate on serial data, one or a few bits at a time. Block codes operate on relatively large (i.e., up to a couple of hundred bytes) message blocks. Since *IEEE 802.11a* PHY uses convolutional codes, block codes are not considered in this thesis. This section continues with the general concepts of convolutional coding: convolutional encoding and Viterbi decoding, but not the Viterbi algorithm. More information on the Viterbi algorithm can be found in a number of publications on FEC coding such as [8, 10, 13, 14, and 15].

a. Convolutional Encoding

Convolutional encoding is a technique that adds redundancy to the data systematically. The information bits are processed by the shift registers and the encoded output bits are obtained by the modulo-2 summation of the input bits and the contents of the shift registers. A general convolutional encoder can be implemented with k shift registers and n modulo-2 adders. The convolutional encoder specified by the *IEEE 802.11a* standard has six shift registers and two modulo-2 adders. The constraint length is $v = 7$. The constraint length represents the number of k data bit shifts over which a single data bit can influence the encoder output. However, the definition of constraint length is not standardized in the literature. In [14], the constraint length v is defined as the length of the shift register, while in [15] it is defined as the length of the shift register plus one. The second definition is used in this thesis. Convolutional codes are specified by two parameters, r and v, where $r = k / n$ is the code rate, n is the total number of coded bits generated by k input bits, and v is the constraint length of the code. The typical range of values for r and v are

$$\frac{1}{4} \le r \le \frac{7}{8} \tag{5.1}$$

and

$$2 \le v \le 9. \tag{5.2}$$

Note that higher coding gain is generally achieved by either increasing v or decreasing r.

b. Viterbi Decoding

In modern digital communication systems, the Viterbi decoding algorithm is a computationally efficient and easily achievable algorithm used for the optimum decoding of convolutional codes. The Viterbi algorithm decodes a convolutional code by choosing a path through the code trellis, which yields a code word that differs from the received code word in the fewest possible places [13]. The Viterbi algorithm searches all possible paths in the trellis in order to compute the path metrics. Each state (node) in the trellis diagram is assigned a value that is determined from $s = 0$ at the time $t = 0$ to a particular state K at $t \ge 0$. At each state, the path with the best metric is the survivor, while the other entering paths are non-survivors. The selected metric represents the survivor path and the remaining metrics represent the non-survivor paths. The best value may be either the smallest or the largest, depending on hard or soft decision decoding and the metric chosen. The path selected by the Viterbi algorithm is the maximum-likelihood (ML) path. At any given state, we can only continue backward on a path that survived upon entry into that node. Since each node has only one entering survivor, our trace-back operation always yields a ML path.

Hard decision and soft decision decoding are the two possible ways to generate the branch metric for a Viterbi decoder. In hard decision decoding each received signal is examined and a decision is made as to whether the signal represents a transmitted bit zero or a bit one. For a hard decision decoding, the Viterbi algorithm is a minimum Hamming distance decoder. Hamming distance is obtained by choosing a path through the trellis which yields a codeword that differs from the received codeword in the fewest possible places. In soft decision decoding, the receiver takes advantage of the side information generated by the receiver quantization circuitry. Additionally, the Viterbi

decoding can be separated as HDD or SDD with respect to the quantization levels at the receiver. A 2-level quantization corresponds to HDD, while an infinite-level quantization corresponds to true SDD. Practically, it has been found that an 8-level quantization matched filter output is almost as good as when the matched filter output is unquantized [13].

2. Implementation of (FEC) Coding

In a system using FEC coding, for every k information data bits, n coded bits are transmitted such that $n > k$. Since the transmission time is the same for both coded and uncoded bits,

$$kT_b = nT_{b_c} \tag{5.3}$$

where T_{b_c} is the duration of a coded bit and T_b is the duration of a data bit. The coded bit rate is

$$R_{b_c} = \frac{1}{T_{b_c}}. \tag{5.4}$$

Substituting Equation (5.4) into Equation (5.3), we get

$$R_{b_c} = \frac{n}{k} \cdot R_b = \frac{R_b}{r} \tag{5.5}$$

where $r = k/n$ is the code rate. Since FEC coding adds redundancy to the original data, the trade-off of using FEC coding is the need for increased bandwidth. As seen in Equation (5.5), this bandwidth expansion is a function of the code rate. In addition to the transmission time, the average transmitted power is the same whether coded or uncoded bits are transmitted. Consequently,

$$P_c = E_{b_c} R_{b_c} = E_b R_b \tag{5.6}$$

where E_b is the average energy of the uncoded data bit, and E_{b_c} is the average energy of the coded data bit. Equation (5.6) can be rewritten as

$$E_{b_c} R_{b_c} = E_b R_b$$
$$E_{b_c} = \frac{R_b}{R_{b_c}} \cdot E_b = r E_b \tag{5.7}$$

since $r = R_b / R_{b_c}$. Hence, with Equations (5.3), (5.5) and (5.7), we can obtain the relationship between coded and uncoded system in terms of T_b, R_b or E_b.

3. Coding Gain

Coding gain is defined as the difference in the signal-to-noise ratios required by a FEC coded communication system and the same uncoded communications system to achieve a specific probability of bit error [13]:

$$G[dB] = \left(\frac{E_b}{N_o}\right)_{uncoded} [dB] - \left(\frac{E_b}{N_o}\right)_{coded} [dB] \tag{5.8}$$

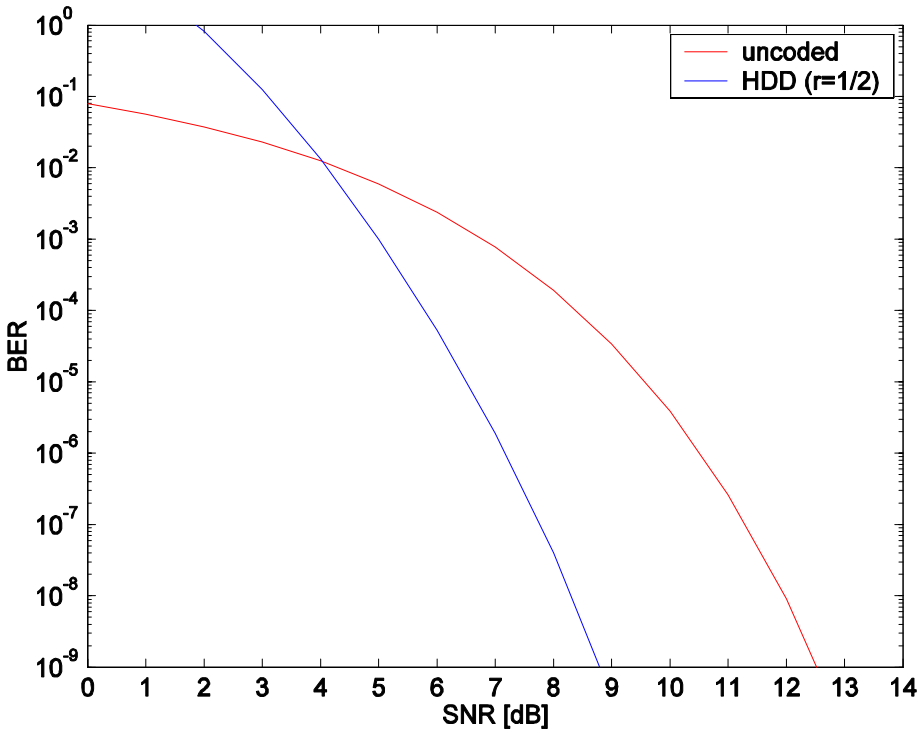

Figure 27. Uncoded vs. hard decision decoded BPSK in AWGN. $(r = 1/2, \nu = 7)$

Coding gain varies with different types of modulation and FEC coding. The addition of FEC coding may improve the system in terms of better performance, lower power requirements, and higher achievable data rates. In order to illustrate these points, uncoded BPSK versus coded BPSK in AWGN is plotted in Figure 27.

B. HARD DECISION DECODING (HDD)

In this section, we apply HDD to the analytic expressions obtained in Chapter IV for the modulations used in *IEEE 802.11a* and then investigate the performance of OFDM in frequency-selective, slow Nakagami fading channels in the presence of pulsed-noise jamming.

1. BPSK/QPSK with HDD (6, 9, 12, and 18 Mbps)

For data rates of 6 and 12 Mbps, the *IEEE 802.11a* standard calls for BPSK and QPSK modulation, respectively, with rate $r = 1/2$ convolutional coding. For data rates of 9 and 18 Mbps, the standard requires BPSK and QPSK, respectively, at a code rate $r = 3/4$.

The probability of bit error with HDD cannot be precisely obtained; hence, an upper bound on the probability of bit error is used in order to examine the performance of HDD. The commonly used upper bound on probability of bit error is [10]

$$P_b < \frac{1}{k} \sum_{d=d_{free}}^{\infty} B_d P_d \tag{5.9}$$

where d_{free} is the free distance of the convolutional code, B_d is the total number of information bit ones on all weight d paths, P_d is the probability of selecting a weight d output sequence as the transmitted code sequence, and k is the number of information bits. The quantities B_d and d_{free} are parameters of the convolutional code, and P_d is determined by the modulation type, the channel, and whether hard or soft decision decoding is used. The values of B_d for the constraint length seven $(v = 7)$ convolutional

code specified in the *IEEE 802.11a* standard are listed in Table 11 with respect to code rates.

Rate	d_{free}	$B_{d_{free}}$	$B_{d_{free}+1}$	$B_{d_{free}+2}$	$B_{d_{free}+3}$	$B_{d_{free}+4}$
1/2	10	36	0	211	0	1404
2/3	6	1	81	402	1487	6793
3/4	5	21	252	1903	11995	72115

Table 11. Weight structure of the best convolutional codes. [After Ref.14]

It is generally accepted that the first five terms in Equation (5.9) dominate for $P_b < 10^{-2}$. Therefore, Equation (5.9) can be rewritten as

$$P_b < \frac{1}{k} \sum_{d=d_{free}}^{d_{free}+4} B_d P_d . \tag{5.10}$$

Equation (5.10) is valid for both HDD and SDD; however, P_d is different for hard and soft decision decoding. For HDD and d odd, the probability of selecting a code word that is Hamming distance d from the correct code word is given by [10]

$$P_d = \sum_{i=\frac{d+1}{2}}^{d} \binom{d}{i} p^i (1-p)^{d-i} \tag{5.11}$$

where p is the channel transition probability. If d is even, the incorrect path is selected when the number of errors is greater than $d/2$. If the number of errors equals $d/2$, there is a tie between the metrics in the two paths, which can be resolved by flipping a fair coin; hence, the incorrect path is selected half of the time. As a result, the probability of selecting the incorrect path when d is even is given by [10]

$$P_d = \frac{1}{2} \binom{d}{\frac{d}{2}} p^{\frac{d}{2}} (1-p)^{\frac{d}{2}} + \sum_{i=\frac{d}{2}+1}^{d} \binom{d}{i} p^i (1-p)^{d-i} . \tag{5.12}$$

Since from Equation (5.7) we know that $E_{b_c} = rE_b$, we can replace E_{b_c} in Equation (4.5) with rE_b and obtain:

$$p = \rho \cdot Q\left(\sqrt{\frac{2rE_b}{N_o + N_I/\rho}}\right) + (1-\rho)\cdot Q\left(\sqrt{\frac{2rE_b}{N_o}}\right). \tag{5.13}$$

Note that the channel transition probability is nothing more than the uncoded probability of bit error in AWGN under the effect of pulsed-noise jamming with a minor modification to allow for the code rate. The channel transition probability is obtained by replacing the portion of Equation (4.24) that represents the uncoded probability of bit error for BPSK/QPSK with Equation (5.13) and re-evaluating the integral in its new form

$$p = \int_0^\infty \left\{ \rho \cdot Q\left(\sqrt{\frac{2a_c^2 T_b \cdot r}{N_o + N_I/\rho}}\right) + (1-\rho)\cdot Q\left(\sqrt{\frac{2a_c^2 T_b \cdot r}{N_o}}\right)\right\} \cdot \frac{m^m}{\Gamma(m) E_b^{\,m}} e_b^{\,m-1} e^{-\frac{me_b}{E_b}} de_b. \tag{5.14}$$

noting that as before $E_b = a_c^2 T_b$.

We obtain an analytic solution for Equation (5.14) by noting the mathematical relationships given in Equation (4.25) through (4.29) and setting $b_1 = m$, $a_1 = m/E_b$, $c_1 = \dfrac{2r}{N_o + N_I/\rho}$, $t_1 = e_b$, $d_1 = \rho$, $\psi_1 = c_1/2a_1 = \dfrac{rE_b}{(N_o + N_I/\rho)\cdot m}$ for the first term of the integrand and $b_2 = m$, $a_2 = m/E_b$, $c_2 = \dfrac{2r}{N_o}$, $t_2 = e_b$, $d_1 = (1-\rho)$, $\psi_2 = c_2/2a_2 = \dfrac{rE_b}{N_o \cdot m}$ for the second term. Equation (5.14) is now in a form suitable for analytical resolution by comparison with Equation (4.25). If we define $SNR = \dfrac{E_b}{N_o}$ as the signal-to-noise ratio and $SIR = \dfrac{E_b}{N_I}$ as the signal-to-interference ratio, respectively, then we obtain

$$p = \frac{\rho}{\sqrt{1+\frac{m}{r}\left(SNR^{-1}+SIR^{-1}/\rho\right)}}\frac{\Gamma\left(m+0.5\right)}{2\sqrt{\pi}\Gamma\left(m+1\right)\left(1+\frac{r}{m\left(SNR^{-1}+SIR^{-1}/\rho\right)}\right)^{m}}$$
$$\times\left(1+\sum_{k=0}^{\infty}\frac{\prod_{n=0}^{k-1}\left(m+0.5+n\right)\left(\frac{1}{1+r\cdot\left[m\left(SNR^{-1}+SIR^{-1}/\rho\right)\right]^{-1}}\right)^{k}}{\prod_{n=0}^{k-1}\left(m+1+n\right)}\right) \tag{5.15}$$
$$+\frac{\left(1-\rho\right)}{\sqrt{1+\frac{m}{r}SNR^{-1}}}\frac{\Gamma\left(m+0.5\right)}{2\sqrt{\pi}\Gamma\left(m+1\right)\left(1+\frac{rSNR}{m}\right)^{m}}\left(1+\sum_{k=0}^{\infty}\frac{\prod_{n=0}^{k-1}\left(m+0.5+n\right)\left(\frac{m}{m+rSNR}\right)^{k}}{\prod_{n=0}^{k-1}\left(m+1+n\right)}\right).$$

Finally, we estimate the average channel probability of bit error. Since the *IEEE 802.11a* standard uses OFDM, Equation (5.15) is also the transition probability for the i^{th} sub-channel for BPSK/QPSK with pulsed-noise jamming. Hence, the overall transition probability is the average of the transition probability on each of the N OFDM sub-channels:

$$p = \frac{1}{N}\sum_{i=1}^{n} p_i \tag{5.16}$$

where p_i is the transition probability for the i^{th} sub-carrier and N represents either 48 or 24 independent sub-carriers for *IEEE 802.11a* systems.

Since thermal noise is not neglected in Equation (5.15), now we need to estimate the required signal-to-noise ratio. Therefore, considering all modulation types used in *IEEE 802.11a*, OFDM system performance for 48 independent sub-carriers over composite Nakagami fading channels with HDD is plotted by using the results provided in [5] in Figures 28, 29 and 30 with respect to different code rates, where *m* is uniformly distributed between $0.5 < m < 3$.

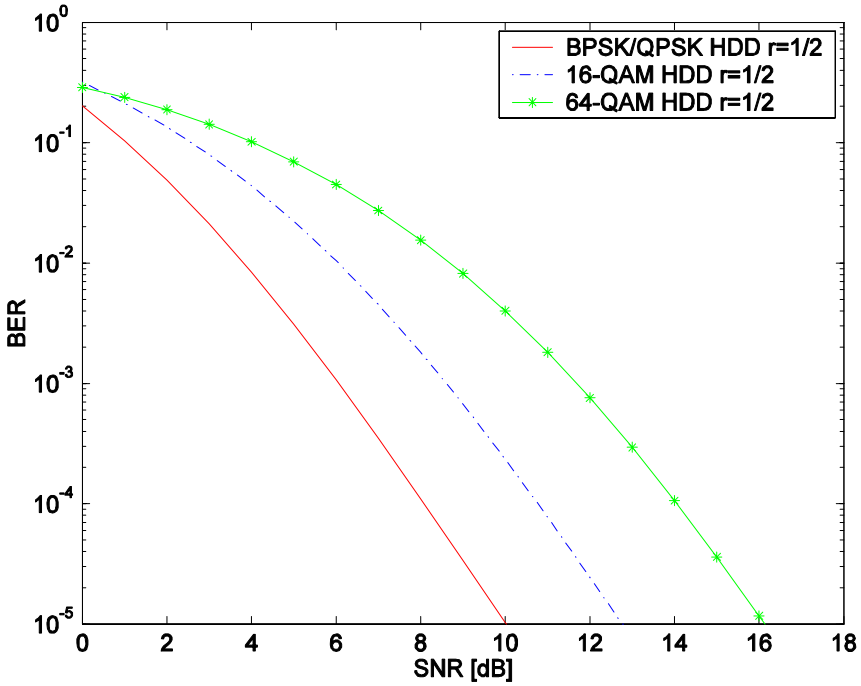

Figure 28. Performance of BPSK/QPSK, 16QAM and 16QAM with HDD $(r = 1/2)$ in Nakagami fading.

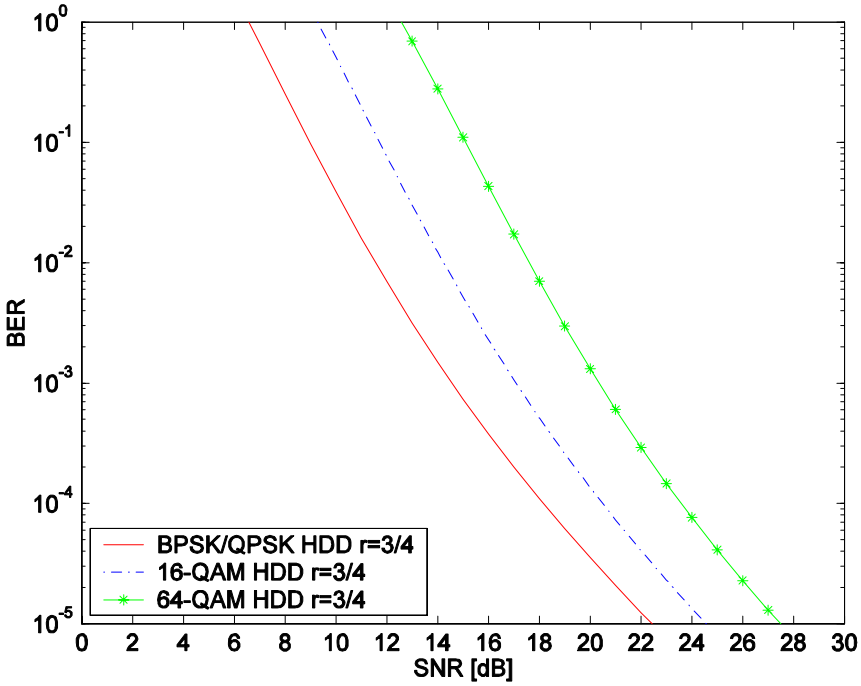

Figure 29. Performance of BPSK/QPSK, 16QAM and 16QAM with HDD $(r = 3/4)$ in Nakagami fading.

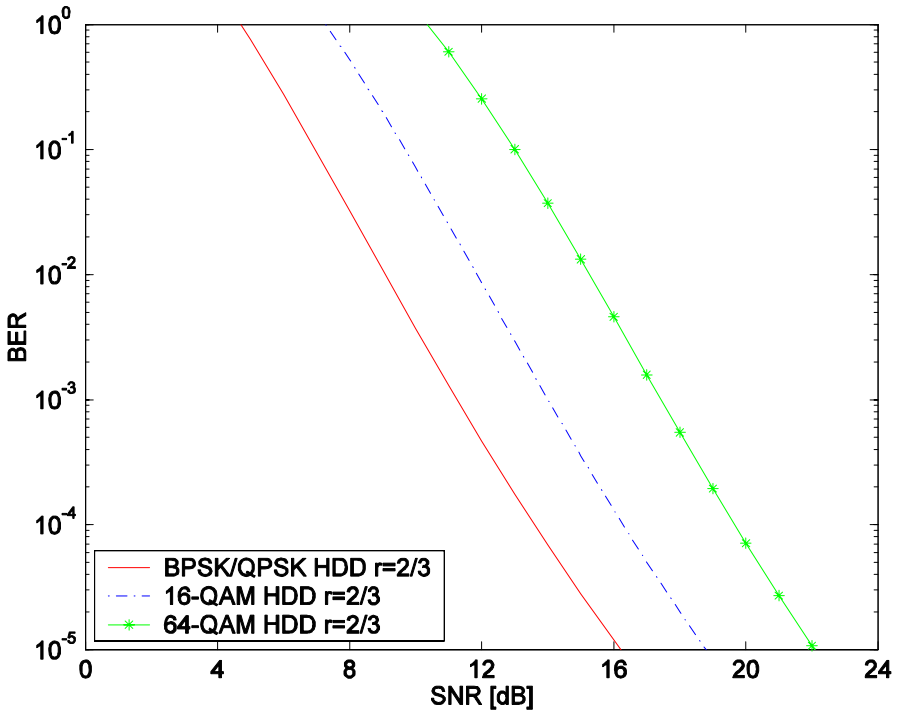

Figure 30. Performance of BPSK/QPSK, 16QAM and 16QAM with HDD $(r = 2/3)$ in Nakagami fading.

For practical applications, $P_b = 10^{-5}$ is a good benchmark required by many wireless communications systems with FEC coding. Consequently, $P_b = 10^{-5}$ is chosen. Hence, the corresponding *SNR* required to obtain at $P_b = 10^{-5}$ when only AWGN is present will be used in evaluating Equation (5.15) with the code rates as specified in the *IEEE 802.11a* standard. In order to make a direct comparison, the same SNR will be used in the sub-channel equations while investigating the improvement in performance for either pure or composite OFDM both for uncoded and coded cases.

Using Equation (5.15) in Equation (5.11) or (5.12) and substituting the result into Equation (5.10) at code rate $r = 1/2$ and its corresponding weight structure as shown in Table 11, we obtain the performance of BPSK/QPSK with hard decision Viterbi decoding over Nakagami fading channels in the presence of pulsed-noise jamming. The results of this analysis are plotted in Figure 31 for $1/2 \le m \le 5$ and $\rho = 0.5$. The corresponding *SNR*=10 dB value obtained from Figure 28 for BPSK/QPSK is used for

the convolutional code rate $r = 1/2$. Recall that this accounts for the *IEEE 802.11a* target data rates of six Mbps for BPSK and 12 Mbps for QPSK.

Although not shown here, the approximation for Equation (4.31) obtained in Equation (4.35) can no longer be used. The approximation remains valid with the addition of the code rate as in Equation (5.14); however, the results obtained for P_b become unreliable after using Equation (5.15) in Equation (5.11) or (5.12) and substituting the result into Equation (5.10). Hence, hereafter the full expression for the channel transition probability will be used in our analysis.

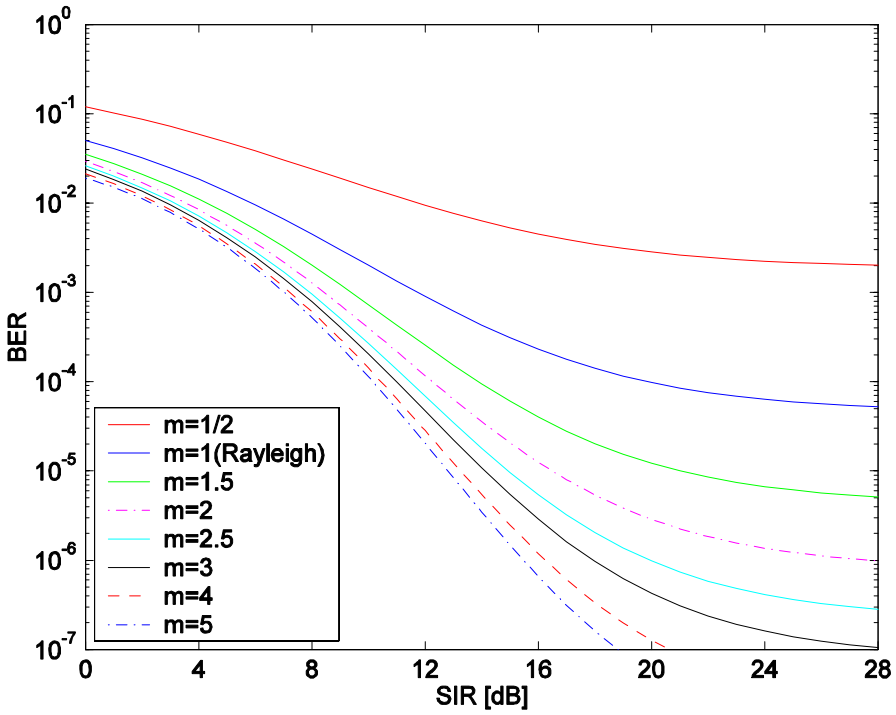

Figure 31. Performance of BPSK/QPSK with HDD $(r = 1/2)$ over Nakagami fading in pulsed-noise jamming where $SNR = 10$ dB, $\rho = 0.5$.

In order to gain some perspective on the performance improvement, in Figure 32 we compare Figure 31 with Figure 16, which is the performance of BPSK/QPSK over Nakagami fading in the presence of pulsed-noise jamming without FEC coding. As we can see, the FEC coding provides significant performance improvement for Nakagami fading channels under the effect of pulsed-noise jamming.

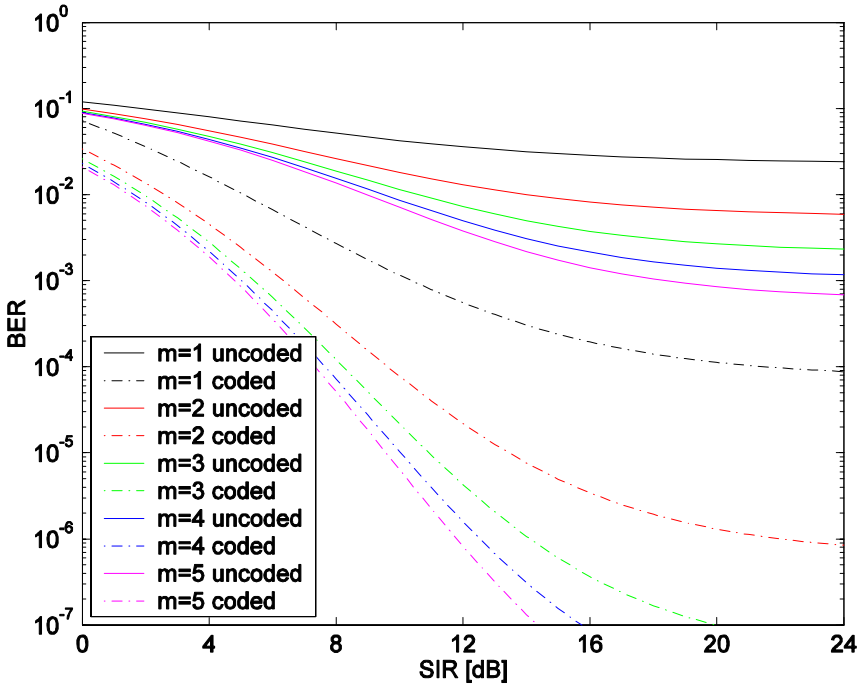

Figure 32. Uncoded versus HDD $(r = 1/2)$ BPSK/QPSK over Nakagami fading with pulsed-noise jamming where $SNR = 10$ dB and $\rho = 0.5$.

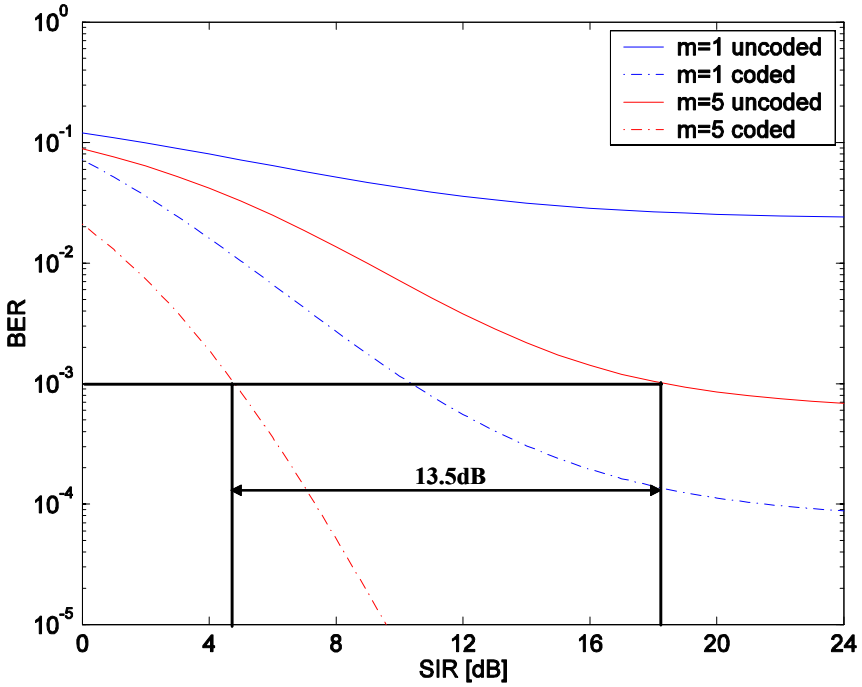

Figure 33. Range of coding gain for HDD BPSK/QPSK. $(r = 1/2)$

In Figure 33 we illustrate the range of coding gain obtained with HDD and BPSK/QPSK. As we can see, for $m = 5$ the coding gain is 13.5 dB and $E_b / N_I = 4.8$ dB with HDD $(r = 1/2)$ and BPSK/QPSK modulation at $P_b = 10^{-3}$. Note that the highest coding gain is achieved at higher values of m, and $P_b = 10^{-3}$ represents the low end of acceptable performance for WLAN applications.

Until now, we have only examined the sub-carrier performance of BPSK/QPSK with HDD over Nakagami fading channels in the presence of pulsed-noise jamming. We now turn our attention to analyzing the performance of OFDM under fading conditions with a pulsed jammer.

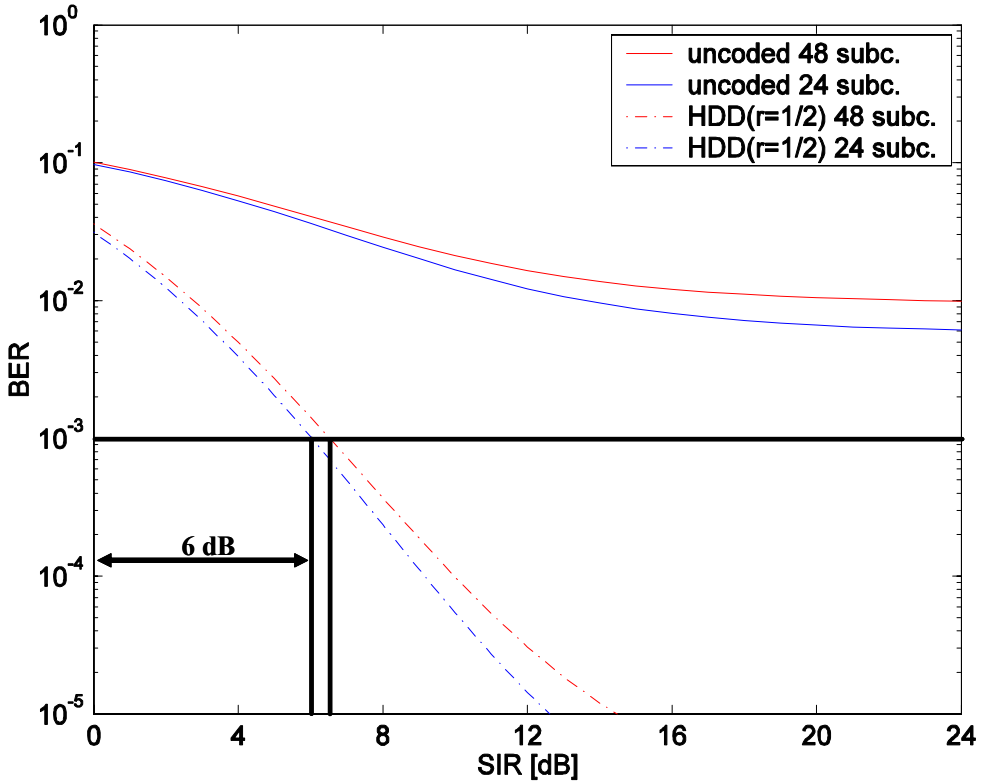

Figure 34. HDD $(r = 1/2)$ versus uncoded BPSK/QPSK modulated OFDM performance over a composite Nakagami fading channel with pulsed-noise jammer, $SNR = 10$ dB and $\rho = 0.5$.

In order to evaluate composite OFDM performance, Equation (5.15) is used in Equation (5.16) as p_i to obtain the average probability of bit error on each of the N OFDM sub-carriers for BPSK/QPSK. We then use Equation (5.16) in Equation (5.11) or (5.12) and substitute the result into Equation (5.10) at code rate $r = 1/2$. BPSK/QPSK modulated OFDM with HDD $(r = 1/2)$ performance for both 48 and 24 independent sub-carriers cases over a composite Nakagami fading channel with pulsed-noise jamming is plotted in Figure 34 for one trial, where m is assumed to be a uniform random variable over the range $1/2 \le m \le 5$.

As we can see, the coding gain is remarkable, and values of SIR are 6.5 and 6 dB for 48 and 24 independent sub-carriers, respectively, at $P_b = 10^{-3}$. Without FEC coding, we cannot achieve even $P_b = 10^{-2}$ with the same SIR. In terms of absolute performance at $P_b = 10^{-3}$, we see in Figure 34 that the composite OFDM system requires a received average SIR per bit of 6.5 and 6 dB for 48 and 24 independent sub-carriers, respectively. In fact, these values are randomly distributed because m is modeled as a random variable. Hence, as we did in Chapter IV, an average probability of bit error is obtained by evaluating the BPSK/QPSK modulated OFDM performance with HDD $(r = 1/2)$ for ten trials for both 48 and 24 independent sub-carriers. The minimum, maximum, and mean value for the E_b / N_I required for $P_b = 10^{-3}$ obtained from ten trials for BPSK/QPSK modulated OFDM with HDD $(r = 1/2)$ performance is shown in Table 12.

HDD(1/2) BPSK/QPSK	48 sub-carriers [dB]	24 sub-carriers [dB]	Difference [dB]
Minimum	6.25	5.70	0.55
Maximum	8.00	6.45	1.55
Mean	6.78	6.20	0.60

Table 12. HDD$(r = 1/2)$ BPSK/QPSK modulated OFDM performance statistics for E_b / N_I at $P_b = 10^{-3}$.

The difference in the mean value of E_b / N_I between 48 and 24 independent sub-carrier's performance is 0.6 dB, which is much smaller than the 5.76 dB obtained for uncoded BPSK/QPSK modulated OFDM.

We now repeat analysis for code rate $r = 3/4$ to investigate performance for 9-Mbps BPSK and 18-Mbps QPSK as specified in the *IEEE 802.11a* standard. The results of this analysis for a single sub-carrier are given in Figure 35 for the usual range of m. Note that the corresponding $SNR = 22.5$ dB value obtained from Figure 29 for BPSK/QPSK is used for convolutional code rate $r = 3/4$ while evaluating Equation (5.15).

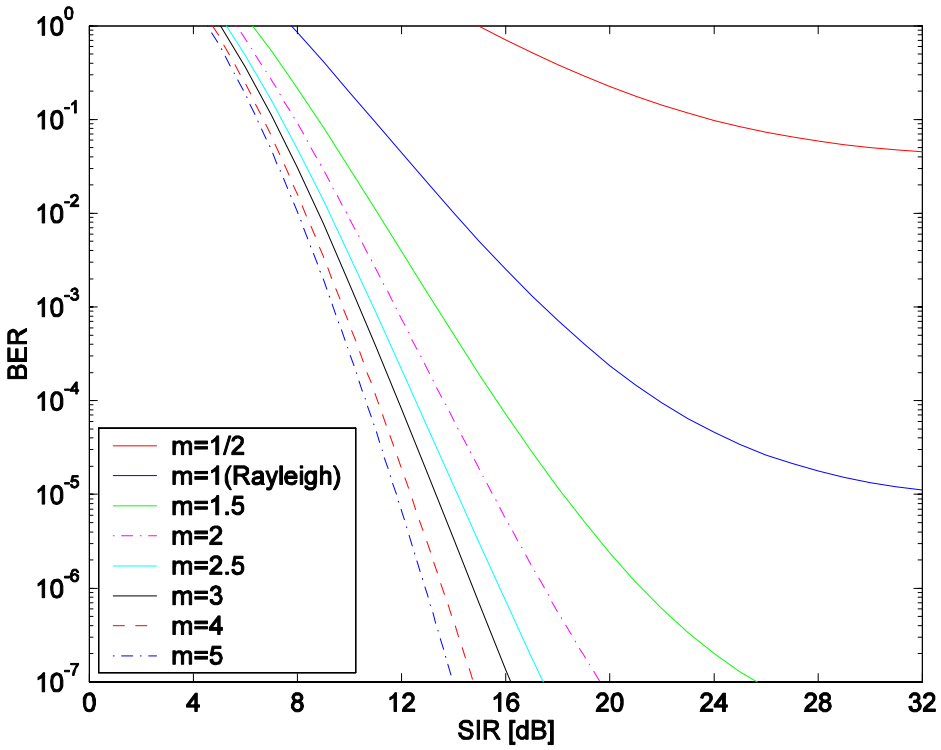

Figure 35. Performance of BPSK/QPSK with HDD $(r = 3/4)$ over Nakagami fading in pulsed-noise jamming where $SNR = 22.5$ dB and $\rho = 0.5$.

In Figure 36, we overlay the uncoded BPSK/QPSK performance onto those in Figure 35 to see the improvement in performance of BPSK/QPSK when applying HDD with code rate $r = 3/4$ over Nakagami fading channels in the presence of pulsed-noise jamming.

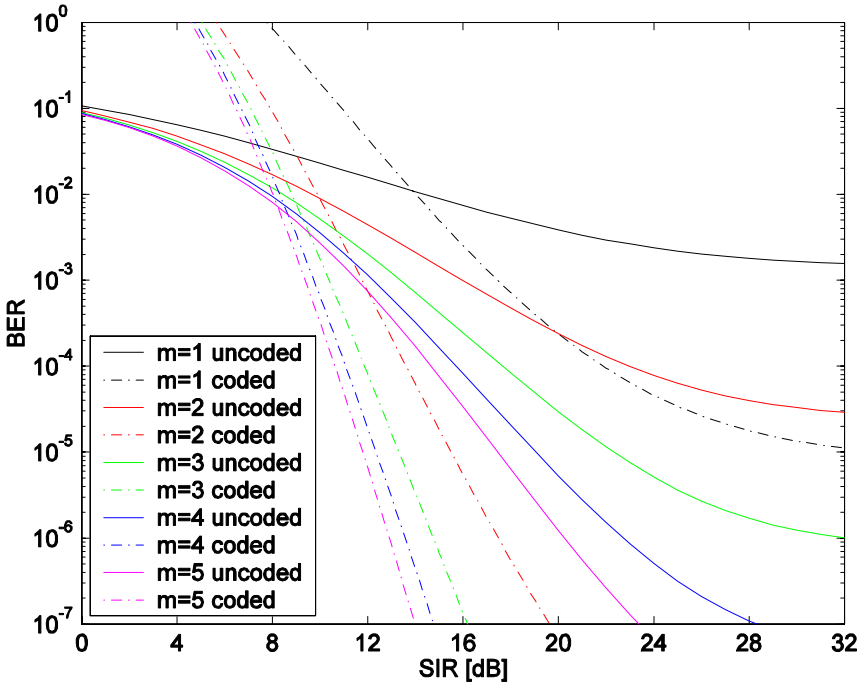

Figure 36. Uncoded vs. HDD $(r = 3/4)$ BPSK/QPSK over Nakagami fading with pulsed-noise jamming where $SNR = 22.5$ dB and $\rho = 0.5$.

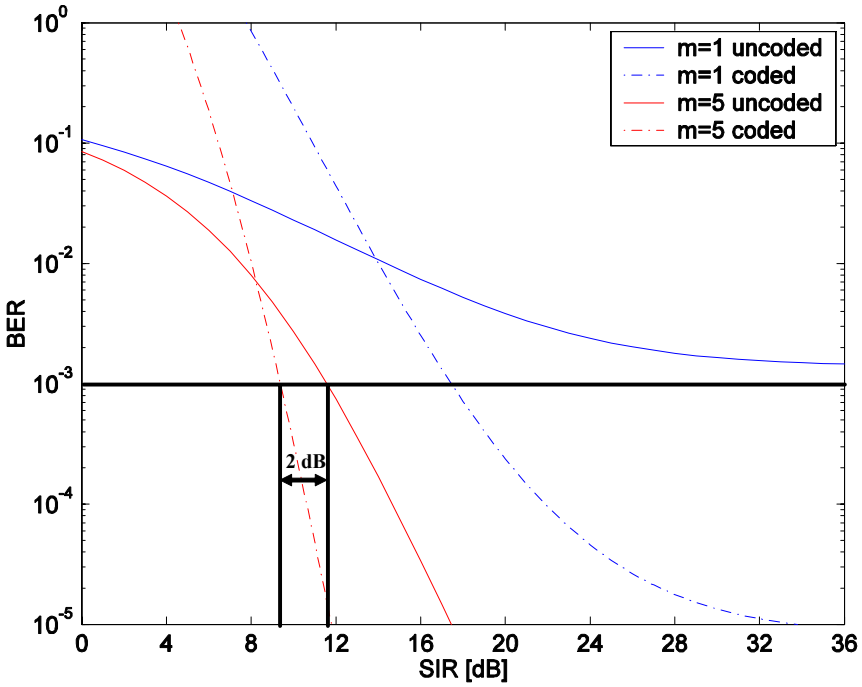

Figure 37. Range of coding gain for HDD BPSK/QPSK. $(r = 3/4)$

As we did for $r = 1/2$, the HDD$(r = 3/4)$ and uncoded BPSK/QPSK modulated OFDM performance over a Nakagami fading channel under the effect of hostile pulsed-noise jamming are plotted in Figure 37. As we can see, the coding gain is reduced to 2 dB and E_b / N_I is degraded to 9.4 dB at $P_b = 10^{-3}$ when $m = 5$.

BPSK/QPSK modulated OFDM with HDD $(r = 3/4)$ performance for both 48 and 24 independent sub-carriers cases over a composite Nakagami fading channel in the presence of pulsed-noise jamming where m is assumed to be a uniform random variable over the range $0.5 \le m \le 5$ is plotted in Figure 38 for one trial.

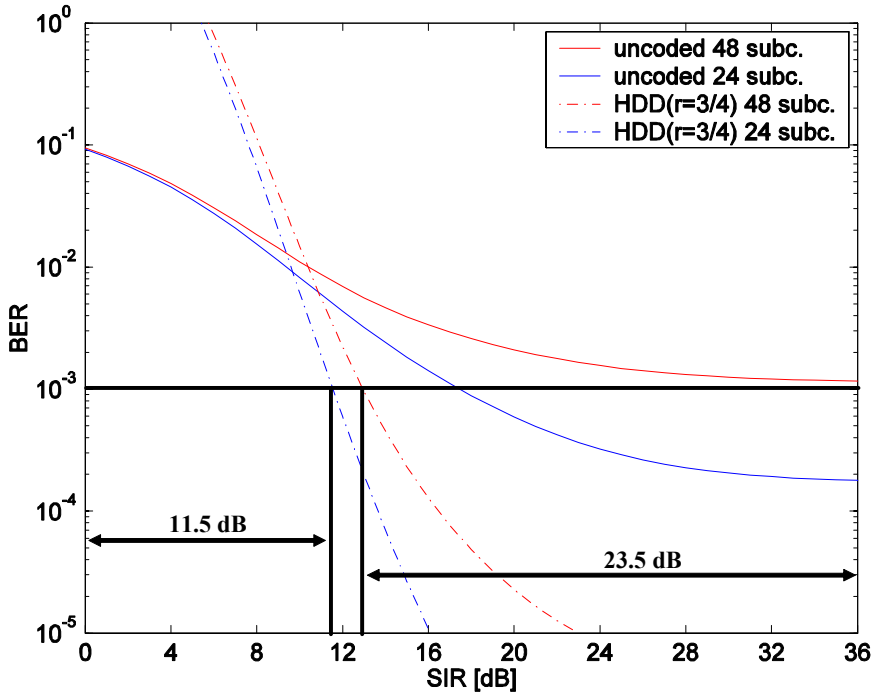

Figure 38. HDD$(r = 3/4)$ vs. uncoded BPSK/QPSK modulated OFDM performance over a composite Nakagami fading channel with pulsed-noise jamming where $SNR = 22.5$ dB and $\rho = 0.5$.

As we can see, the coding gain is 23.5 dB, and the required SIR is 12.5 and 11.5 dB, respectively, for 48 and 24 independent sub-carriers at $P_b = 10^{-3}$. Proceeding as before, we evaluate BPSK/QPSK modulated OFDM performance with HDD $(r = 3/4)$ for ten trials for both 48 and 24 independent sub-carriers to obtain an average probability

of bit error. The minimum, maximum, and mean for the E_b / N_I required for $P_b = 10^{-3}$ obtained from ten trials for BPSK/QPSK modulated OFDM with HDD $(r = 3/4)$ performance is shown in Table 13.

HDD(3/4) BPSK/QPSK	48 sub-carriers [dB]	24 sub-carriers [dB]	Difference [dB]
Minimum	11.60	10.30	1.30
Maximum	14.70	13.30	1.40
Mean	13.11	11.92	1.20

Table 13. HDD $(r = 3/4)$ BPSK/QPSK modulated OFDM performance statistics for E_b / N_I at $P_b = 10^{-3}$

The difference in the mean value of E_b / N_I between 48 and 24 independent sub-carrier's performance is 1.2 dB, which is again much smaller than the 5.76 dB obtained for uncoded BPSK/QPSK modulated OFDM.

2. 16QAM with HDD (24 and 36 Mbps)

For data rates of 24 and 36 Mbps, the *IEEE 802.11a* standard calls for 16QAM modulation, with convolutional coding at the rates $r = 1/2$ and $r = 3/4$, respectively. Proceeding as for BPSK/QPSK, we first examine the 16QAM sub-carrier performance and then perform the analysis for 16QAM modulated OFDM over a composite Nakagami fading channel in the presence of pulsed-noise jamming. Although achievable data rates are higher and bandwidth efficiency greater, MQAM performance is poorer than that of BPSK and QPSK. Consequently, we expect the performance of 16QAM with HDD will be inferior to that of BPSK/QPSK with HDD.

The channel transition probability for M-QAM over a Nakagami fading channel in the presence of pulsed-noise jamming can be obtained from the probability of bit error in AWGN with an added factor accounting for the code rate as follows:

$$p = \frac{\rho \cdot 4\left(\sqrt{M}-1\right)}{q\sqrt{M}} Q\left(\sqrt{\frac{3qr \cdot E_b}{(M-1)\cdot(N_0 + N_I/\rho)}}\right) + (1-\rho)\cdot \frac{4\left(\sqrt{M}-1\right)}{q\sqrt{M}} Q\left(\sqrt{\frac{3qr \cdot E_b}{(M-1)N_0}}\right). \quad (5.17)$$

Using Equation (5.17), we now evaluate

$$p = \int_0^{\infty} \left(\frac{\rho \cdot 4\left(\sqrt{M}-1\right)}{q\sqrt{M}} Q\left(\sqrt{\frac{3qre_b}{(M-1)\cdot(N_0+N_I/\rho)}} \right) + (1-\rho)\cdot \frac{4\left(\sqrt{M}-1\right)}{q\sqrt{M}} Q\left(\sqrt{\frac{3qre_b}{(M-1)N_0}} \right) \right) \times \frac{m^m}{\Gamma(m)(E_b)^m} e_b^{m-1} e^{-\frac{me_b}{E_b}} de_b. \tag{5.18}$$

Given the mathematical relationship in Equation (4.25), we make the following substitutions:

$$\begin{aligned} d_1 &= \rho \cdot \frac{4\left(\sqrt{M}-1\right)}{\sqrt{M}} \\ c_1 &= \frac{3qr}{(M-1)\cdot(N_o+N_I/\rho)} \\ b_1 &= m \\ t_1 &= e_b \\ a_1 &= \frac{m}{E_b} \\ \psi_1 &= \frac{c_1}{2a_1} = \frac{3qr}{2m(M-1)\left(SNR^{-1}+SIR^{-1}/\rho\right)} \end{aligned} \tag{5.19}$$

for the first term and

$$\begin{aligned} d_2 &= (1-\rho)\cdot \frac{4\left(\sqrt{M}-1\right)}{\sqrt{M}} \\ c_2 &= \frac{3qr}{(M-1)\cdot N_o} \\ b_2 &= m \\ t_2 &= e_b \\ a_2 &= \frac{m}{E_b} \\ \psi_2 &= \frac{c_2}{2a_2} = \frac{3qr\cdot SNR}{2m(M-1)} \end{aligned} \tag{5.20}$$

for the second term. We then obtain the final result

$$p=\frac{4\rho\left(\sqrt{M}-1\right)}{q\sqrt{M}}\frac{\Gamma\left(m+0.5\right)}{\sqrt{1+\left[\frac{2m\left(M-1\right)}{3qr}\left(SNR^{-1}+SIR^{-1}/\rho\right)\right]}\cdot 2\sqrt{\pi}\cdot\Gamma\left(m+1\right)\left[1+\frac{3qr}{2m\left(M-1\right)\left(SNR^{-1}+SIR^{-1}/\rho\right)}\right]^{m}}$$

$$\times\left[1+\left[\sum_{k=1}^{\infty}\frac{\prod_{n=0}^{k-1}\left(m+0.5+n\right)\left(\frac{1}{1+\frac{3qr}{2m\left(M-1\right)\left(SNR^{-1}+SIR^{-1}/\rho\right)}}\right)^{k}}{\prod_{n=0}^{k-1}\left(m+1+n\right)}\right]\right]+\frac{\left(1-\rho\right)4\left(\sqrt{M}-1\right)}{q\sqrt{M}}$$

$$\times\frac{\Gamma\left(m+0.5\right)}{\sqrt{1+\left[\frac{2m\left(M-1\right)}{3qr\cdot SNR}\right]}\cdot 2\sqrt{\pi}\cdot\Gamma\left(m+1\right)\left[1+\frac{3qr\cdot SNR}{2m\left(M-1\right)}\right]^{m}}\left[1+\left[\sum_{k=1}^{\infty}\frac{\prod_{n=0}^{k-1}\left(m+0.5+n\right)\left(\frac{1}{1+\frac{3qr\cdot SNR}{2m\left(M-1\right)}}\right)^{k}}{\prod_{n=0}^{k-1}\left(m+1+n\right)}\right]\right].$$

(5.21)

Equation (5.21) represents an analytic expression for the channel transition probability.

Substituting Equation (5.21) into Equation (5.11) for d odd or Equation (5.12) for d even and taking the results for P_d into Equation (5.10), we obtain the performance of M-QAM over Nakagami fading channels under the effect of pulsed-noise jamming with HDD. In Figure 39, we plot the sub-channel performance of 16QAM $\left(q=4\right)$ with HDD $\left(r=1/2\right)$ over Nakagami fading channels with pulsed-noise jamming where m is modeled as a uniform random variable over the range $1/2\le m\le 5$. Note that *SNR=13* dB obtained from Figure 28 for 16QAM is used for a convolutional code rate $r=1/2$ while evaluating Equation (5.21).

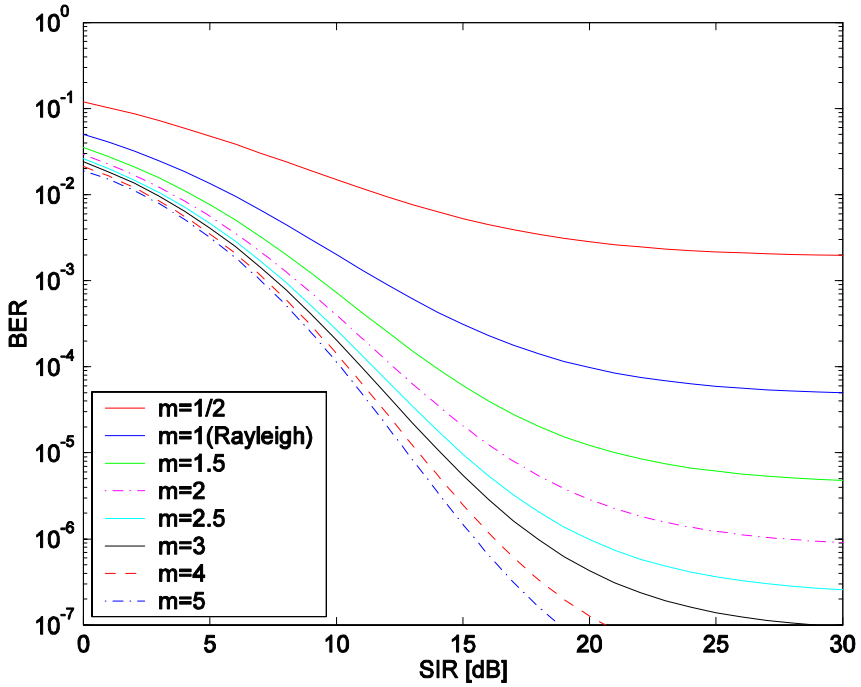

Figure 39. Performance of 16QAM with HDD$(r=1/2)$ over Nakagami fading in pulsed-noise jamming where $SNR=13$ dB and $\rho=0.5$.

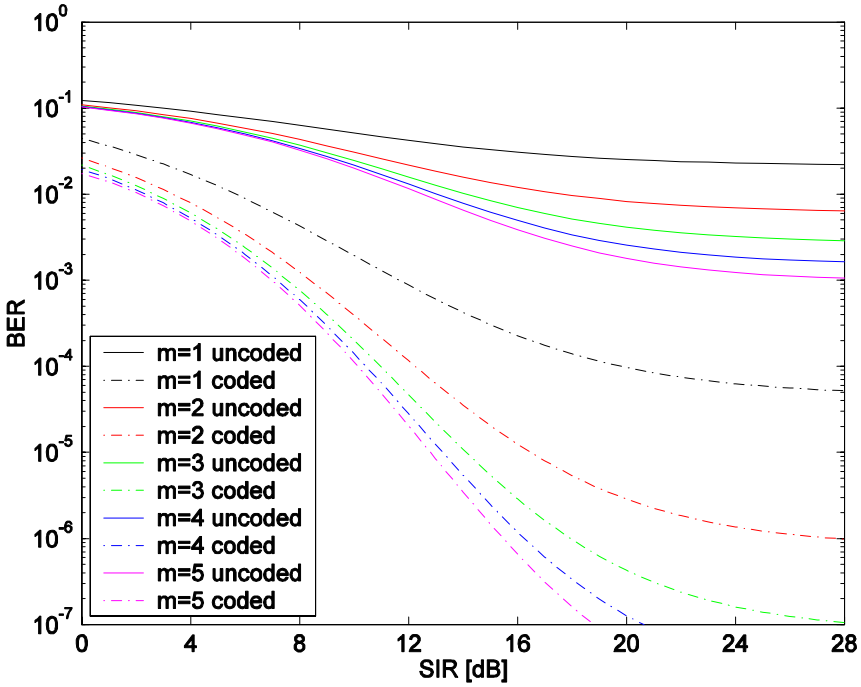

Figure 40. Uncoded vs. HDD$(r=1/2)$ 16QAM over Nakagami fading with pulsed-noise jamming where $SNR=13$ dB and $\rho=0.5$.

In order to gain some perspective on the improvement in performance, in Figure 40 we compare Figure 39 with Figure 18, which is the performance of 16QAM over Nakagami fading in the presence of pulsed-noise jamming without FEC coding. As we can see, FEC coding significantly improves performance for Nakagami fading channels under the effect of pulsed-noise jamming.

We now turn our attention to analyzing the performance of OFDM under fading conditions with a pulsed-jammer. In order to evaluate the composite OFDM performance, Equation (5.21) is used in Equation (5.16) as p_i to obtain the average transition probability on each of the N OFDM sub-carriers for 16QAM. We then use Equation (5.16) in Equation (5.11) or (5.12) and substitute the result into Equation (5.10) at code rate $r = 1/2$. 16QAM modulated OFDM with HDD $(r = 1/2)$ performance for both 48 and 24 independent sub-carriers cases over a composite Nakagami fading channel with pulsed-noise jamming is plotted in Figure 41 for one trial, where m is assumed to be a uniform random variable over the range $1/2 \le m \le 5$.

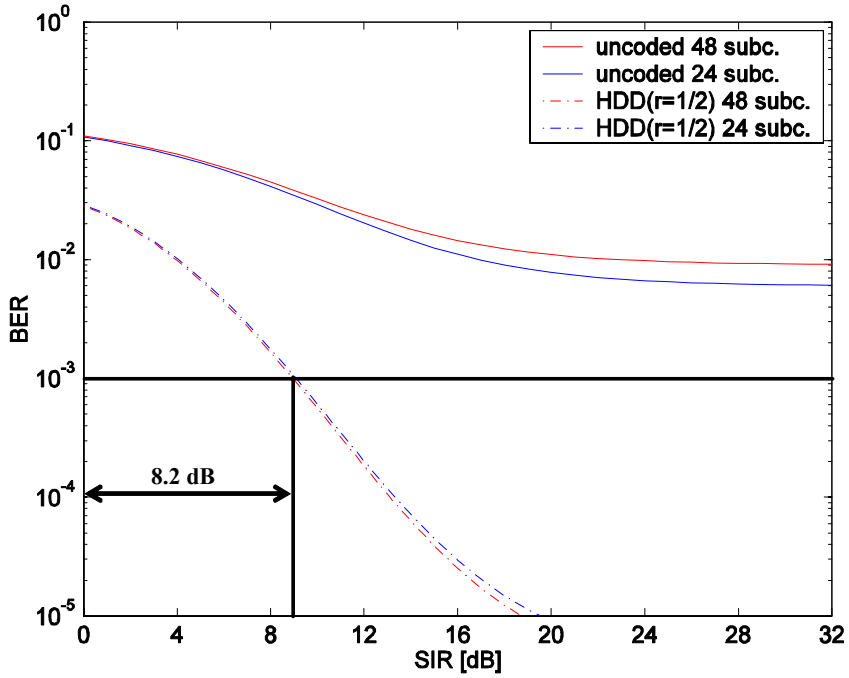

Figure 41. HDD $(r = 1/2)$ vs. uncoded 16QAM modulated OFDM performance over a composite Nakagami fading channel with pulsed-noise jamming where $SNR = 13$ dB and $\rho = 0.5$.

As we can see, the coding gain is remarkable, and the required SIR is 8.5 and 8.2 dB, respectively, for 48 and 24 independent sub-carriers at $P_b = 10^{-3}$. Without FEC coding, we cannot achieve $P_b = 10^{-2}$ with the same SIR. In terms of absolute performance at $P_b = 10^{-3}$, we see in Figure 41 that the composite OFDM system requires a received average SIR per bit of 8.5 and 8.2 dB for 48 and 24 independent sub-carriers, respectively. As before, these values are randomly distributed because m is modeled as a random variable. Hence, as we did before, an average probability of bit error is obtained by evaluating the 16QAM modulated OFDM performance with HDD $(r = 1/2)$ for ten trials for both 48 and 24 independent sub-carriers. The minimum, maximum, and mean for the E_b / N_I required for $P_b = 10^{-3}$ obtained from ten trials for 16QAM modulated OFDM with HDD $(r = 1/2)$ performance is shown in Table 14.

HDD(1/2) 16QAM	48 sub-carriers [dB]	24 sub-carriers [dB]	Difference [dB]
Minimum	8.30	7.60	0.70
Maximum	9.30	9.00	0.30
Mean	8.78	8.37	0.42

Table 14. HDD$(r = 1/2)$ 16QAM modulated OFDM performance statistics for E_b / N_I at $P_b = 10^{-3}$.

The difference in the mean value of E_b / N_I between 48 and 24 independent sub-carrier's performance is 0.4 dB, which is much smaller than the 6.33 dB obtained for uncoded 16QAM modulated OFDM.

Likewise, the same analysis is performed for the 36 Mbps data rate with code rate $r = 3/4$. In Figure 42, we plot the sub-channel performance of 16QAM $(q = 4)$ with HDD $(r = 3/4)$ over Nakagami fading channels with pulsed-noise jamming where m is modeled as a uniform random variable as before. Note that the corresponding $SNR = 24.5$ dB obtained from Figure 29 for 16QAM is used for convolutional code rate $r = 3/4$ while evaluating Equation (5.21).

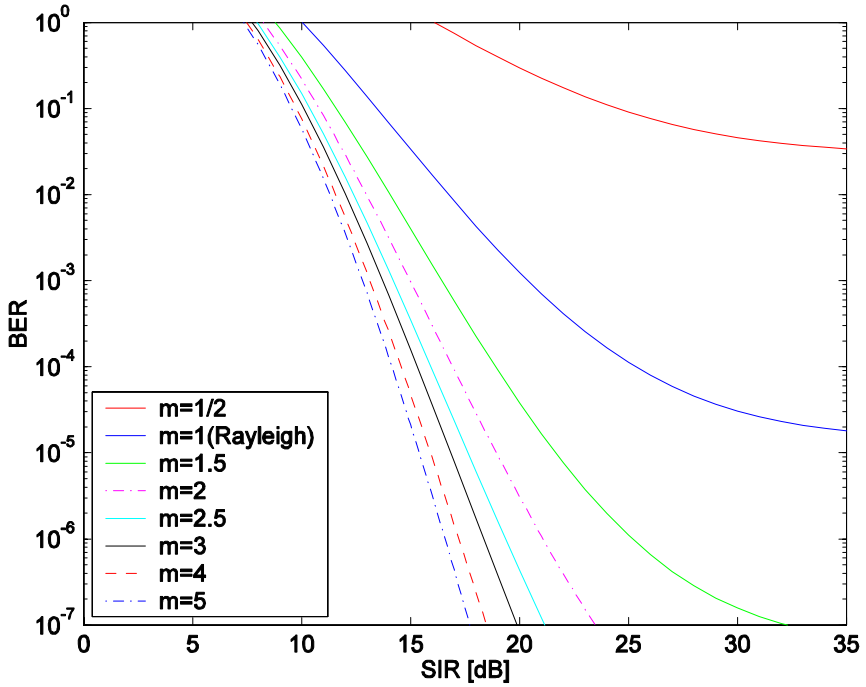

Figure 42. Performance of 16QAM with HDD $(r = 3/4)$ over Nakagami fading in pulsed-noise jamming, $SNR = 24.5$ dB and $\rho = 0.5$.

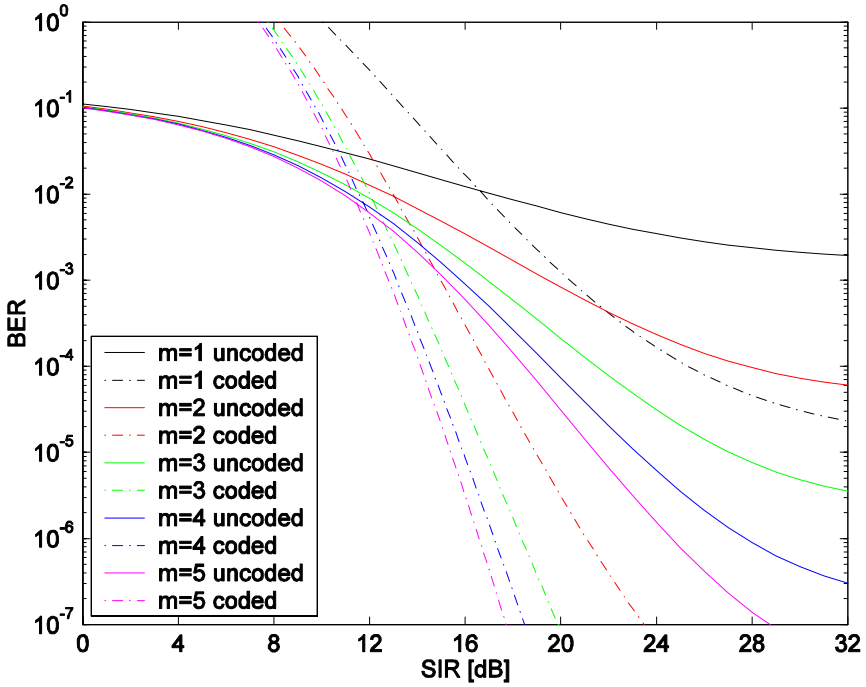

Figure 43. Uncoded vs. HDD $(r = 3/4)$ 16QAM over Nakagami fading with pulsed-noise jamming, $SNR = 24.5$ dB and $\rho = 0.5$.

In Figure 43, we overlay uncoded 16QAM performance onto the results shown in Figure 42 in order to see the improvement in performance of 16QAM when applying HDD with code rate $r = 3/4$ over the Nakagami fading channels in the presence of pulsed-noise jamming.

In the final part of our 16QAM performance analysis, we plot the performance of 16QAM modulated OFDM with HDD $(r = 3/4)$ performance for both 48 and 24 independent sub-carriers cases over a composite Nakagami fading channel with pulsed-noise jamming in Figure 44 for one trial, where m is assumed to be a uniform random variable over the range $1/2 \le m \le 5$.

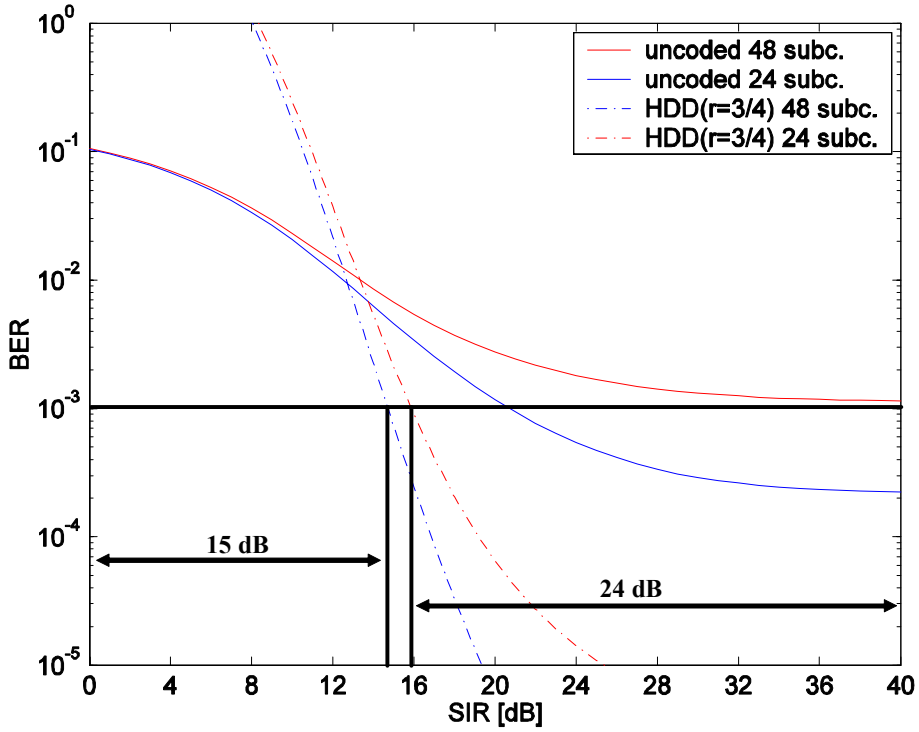

Figure 44. HDD $(r = 3/4)$ vs. uncoded 16QAM modulated OFDM performance over a composite Nakagami fading channel with pulsed-noise jamming, $SNR = 24.5$ dB and $\rho = 0.5$.

As we can see, the coding gain is remarkable, and the required SIR is 16 and 15 dB, respectively, for 48 and 24 independent sub-carriers at $P_b = 10^{-3}$. As before, an

average probability of bit error is obtained by evaluating the 16QAM modulated OFDM performance with HDD $(r = 3/4)$ for ten trials for both 48 and 24 independent sub-carriers. The minimum, maximum, and mean for the E_b / N_I required for $P_b = 10^{-3}$ obtained from ten trials for 16QAM modulated OFDM with HDD $(r = 3/4)$ performance is shown in Table 15.

HDD(3/4) 16QAM	48 sub-carriers [dB]	24 sub-carriers [dB]	Difference [dB]
Minimum	14.80	13.70	1.10
Maximum	17.40	16.10	1.30
Mean	16.05	15.04	1.01

Table 15. HDD$(r = 3/4)$ 16QAM modulated OFDM performance statistics for E_b / N_I at $P_b = 10^{-3}$.

The mean value of E_b / N_I for 48 and 24 independent sub-carriers is 16.05 and 15.04 dB, respectively, and the difference is 1.01 dB, which again is much smaller than the 6.33 dB obtained for uncoded 16QAM modulated OFDM.

3. 64QAM with HDD (48 and 54 Mbps)

The equations describing the performance of 64QAM in HDD are the same as those developed in the previous section since they were derived for the general case of square constellation M-QAM. Therefore, the analysis of 64QAM performance over Nakagami fading channels in the presence of pulsed-noise jamming proceeds in the same manner as 16QAM, except for using $q = 6$ (vice $q = 4$) and code rate $r = 2/3$ (vice $r = 1/2$) in Equation (5.21) for data rates of 48 Mbps. The sub-channel performance of 64QAM at 48 Mbps with m as a parameter in the range of $1/2 \le m \le 5$ over Nakagami fading channels under the effect of hostile pulsed-noise jamming with $\rho = 0.5$ is plotted in Figure 45. Note that the corresponding *SNR=22* dB obtained from Figure 30 for 64QAM is used for convolutional code rate $r = 2/3$ while evaluating Equation (5.21).

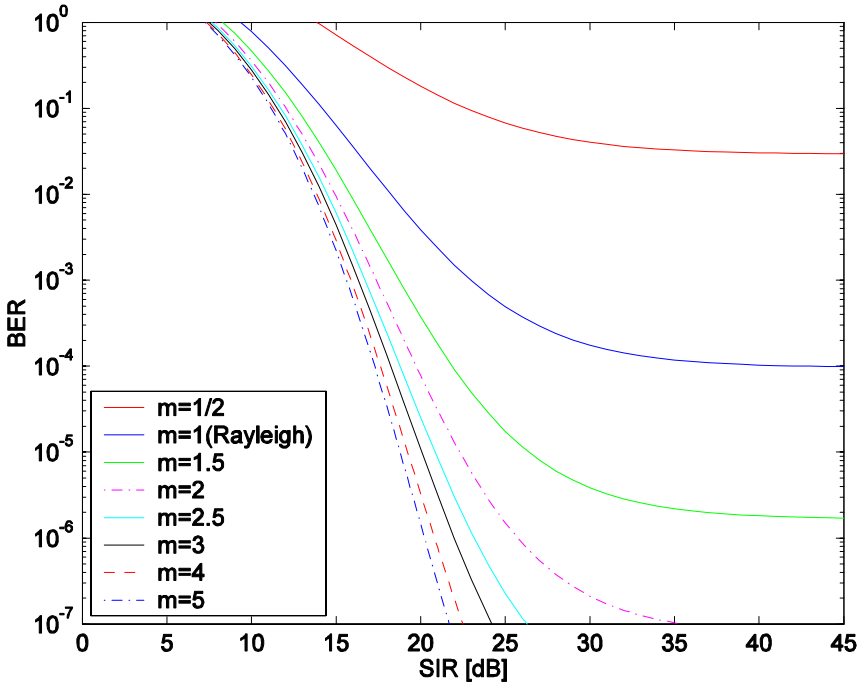

Figure 45. Performance of 64QAM with HDD $(r = 2/3)$ over Nakagami fading in pulsed-noise jamming where $SNR = 22$ dB and $\rho = 0.5$.

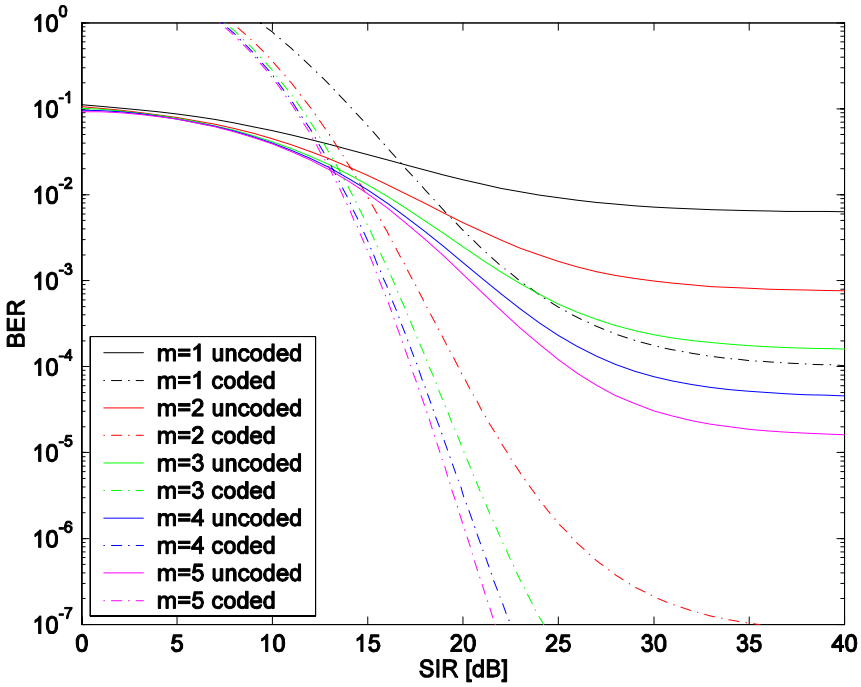

Figure 46. Uncoded vs. HDD $(r = 2/3)$ 64QAM over Nakagami fading with pulsed-noise jamming where $SNR = 22$ dB and $\rho = 0.5$.

In order to gain some perspective on the performance improvement, in Figure 46 we overlay the uncoded and HDD $(r = 2/3)$ 64QAM performance over a Nakagami fading channel with pulsed-noise jamming.

In Figure 47, we plot the performance of 64QAM modulated OFDM with HDD $(r = 2/3)$ for both 48 and 24 independent sub-carriers over a composite Nakagami fading channel in the presence of pulsed-noise jamming for one trial where $\rho = 0.5$ and m is assumed to be a uniform random variable over the range $1/2 \le m \le 5$.

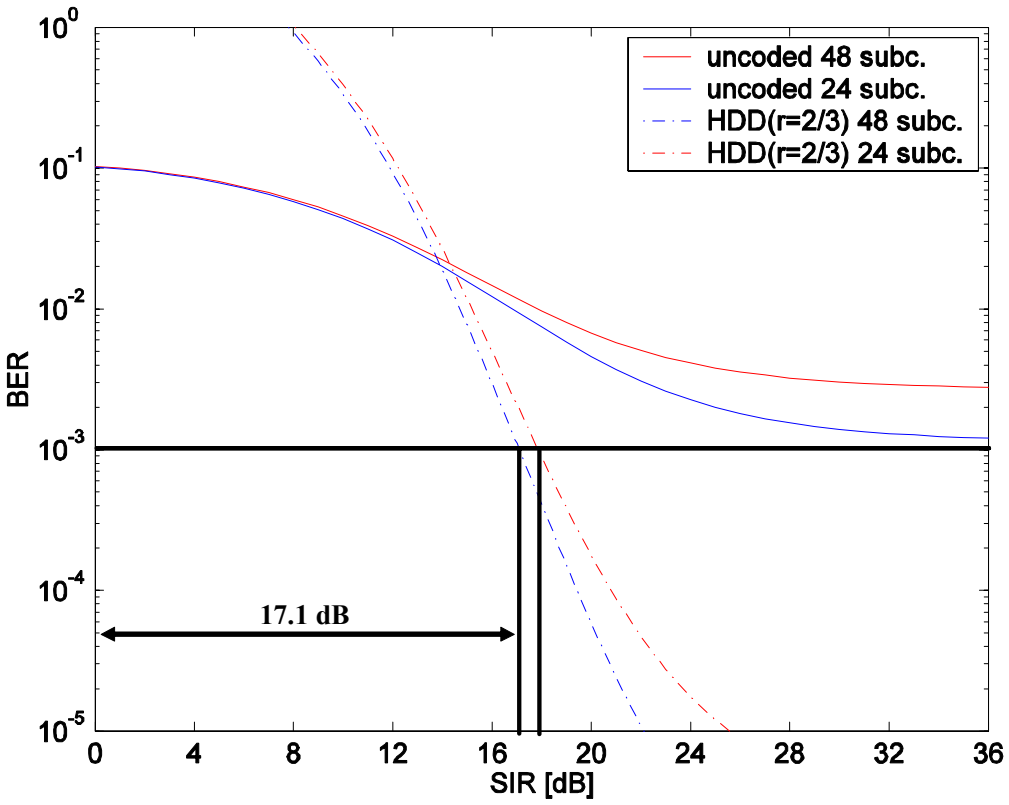

Figure 47. HDD $(r = 2/3)$ vs. uncoded 64QAM modulated OFDM performance over a composite Nakagami fading channel with pulsed-noise jamming where $SNR = 22$ dB and $\rho = 0.5$.

As we can see, the coding gain is remarkable, and the required SIR is 17.9 and 17.1 dB, respectively, for 48 and 24 independent sub-carriers at $P_b = 10^{-3}$. Without FEC coding, we cannot achieve even $P_b = 10^{-3}$ with the same SIR. In terms of absolute

performance at $P_b = 10^{-3}$, we see in Figure 47 that the composite OFDM system requires a received average SIR per bit of 17.9 and 17.1 dB for 48 and 24 independent sub-carriers, respectively. In fact, these values are randomly distributed because m is modeled as a random variable. Hence, as before, an average probability of bit error is obtained by evaluating the 64QAM modulated OFDM performance with HDD $(r = 2/3)$ for ten trials for both 48 and 24 independent sub-carriers. The minimum, maximum, and mean value for the E_b / N_I required for $P_b = 10^{-3}$ obtained from ten trials for 64QAM modulated OFDM with HDD $(r = 2/3)$ performance is shown in Table 16.

HDD(2/3) 64QAM	48 sub-carriers [dB]	24 sub-carriers [dB]	Difference [dB]
Minimum	17.42	16.70	0.72
Maximum	18.80	18.20	0.60
Mean	17.95	17.34	0.61

Table 16. HDD$(r = 2/3)$ 64QAM modulated OFDM performance statistics for E_b / N_I at $P_b = 10^{-3}$.

The difference in the mean value of E_b / N_I between 48 and 24 independent sub-carrier's performance is 0.61 dB, which is much smaller than the 5.35 dB obtained for uncoded 64QAM modulated OFDM.

At this point, only the 54 Mbps data rate remains to be examined. In order to achieve this data rate, *IEEE 802.11a* uses 64QAM with a code rate of $r = 3/4$. The sub-channel performance of 64QAM at 54 Mbps with m as a parameter in the range of $1/2 \le m \le 5$ over Nakagami fading channels under the effect of hostile pulsed-noise jamming with $\rho = 0.5$ is plotted in Figure 48. Note that the corresponding *SNR=27.5* dB obtained from Figure 30 for 64QAM is used for the convolutional code rate $r = 3/4$ while evaluating Equation (5.21).

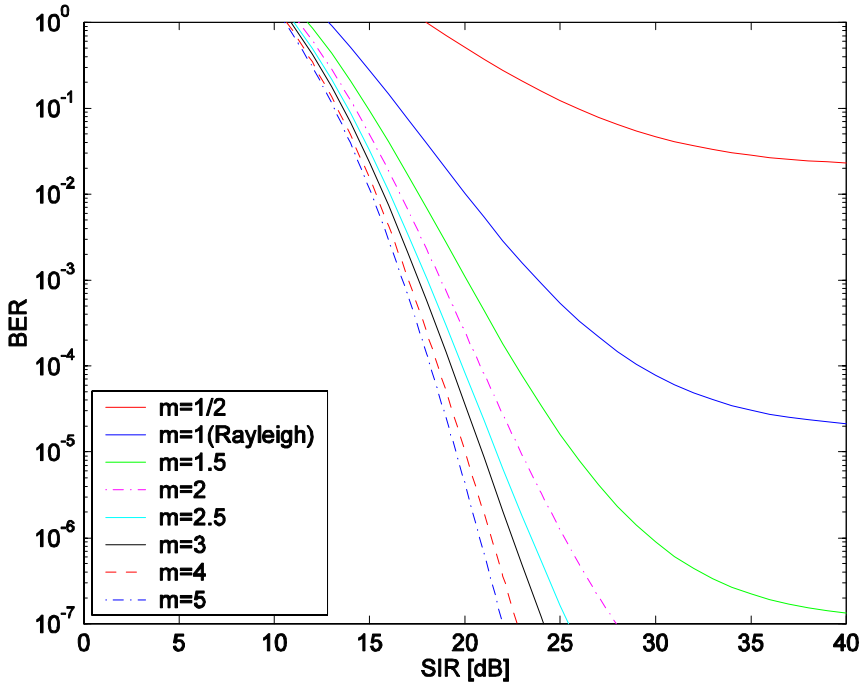

Figure 48. Performance of 64QAM with HDD $(r = 3/4)$ over Nakagami fading in pulsed-noise jamming where $SNR = 27.5$ dB and $\rho = 0.5$.

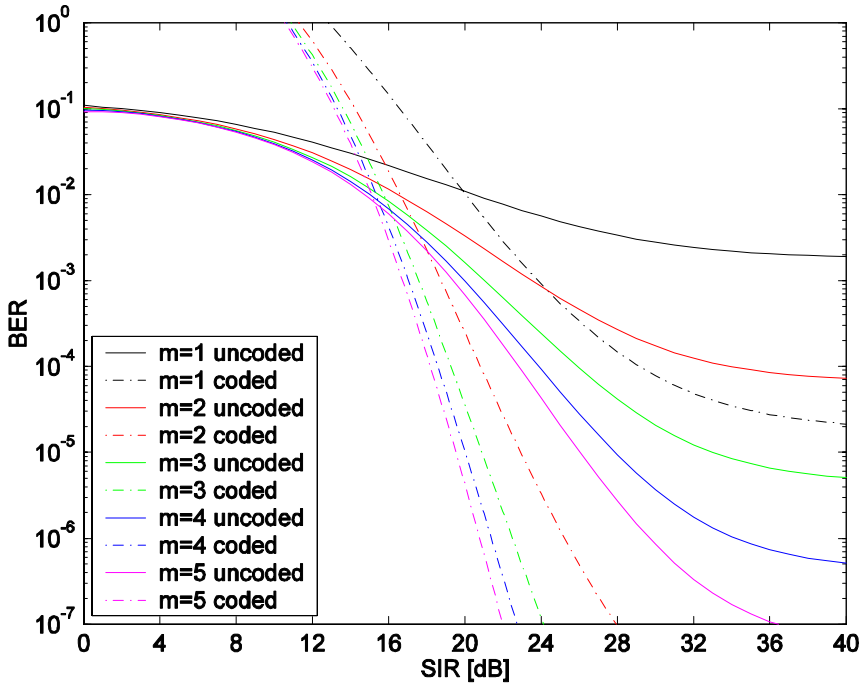

Figure 49. Uncoded vs. HDD $(r = 3/4)$ 64QAM over Nakagami fading with pulsed-noise jamming where $SNR = 27.5$ dB and $\rho = 0.5$.

In Figure 49, we overlay the uncoded 16QAM performance onto the results shown in Figure 48 to see the improvement in performance of 16QAM when applying HDD with code rate $r = 3/4$ over Nakagami fading channels in the presence of pulsed-noise jamming.

In Figure 50, we plot the performance of 64QAM modulated OFDM with HDD $(r = 3/4)$ for both 48 and 24 independent sub-carriers over a composite Nakagami fading channel in the presence of pulsed-noise jamming for one trial where $\rho = 0.5$ and m is assumed to be a uniform random variable over the range $1/2 \le m \le 5$.

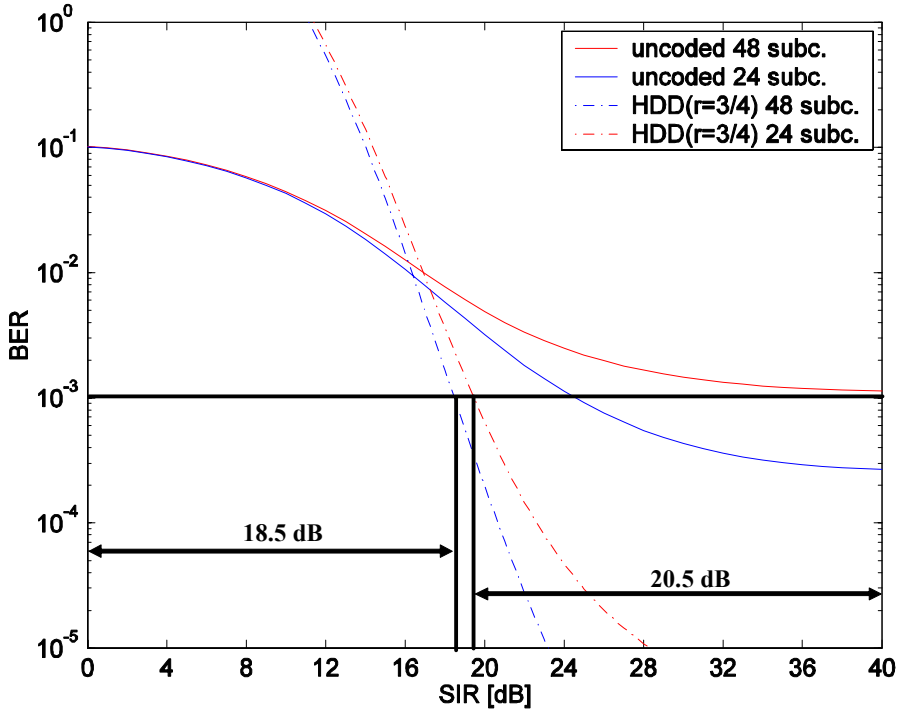

Figure 50. HDD $(r = 3/4)$ vs. uncoded 64QAM modulated OFDM performance over a composite Nakagami fading channel with pulsed-noise jamming, $SNR = 27.5$ dB and $\rho = 0.5$.

As we can see, the coding gain is remarkable, and the required SIR is 19.5 and 18.5 dB, respectively, for 48 and 24 independent sub-carriers at $P_b = 10^{-3}$. In terms of absolute performance at $P_b = 10^{-3}$, we see in Figure 50 that the composite OFDM system

requires a received average SIR per bit of 19.5 and 18.5 dB for 48 and 24 independent sub-carriers, respectively. As before, an average probability of bit error is obtained by evaluating the 64QAM modulated OFDM performance with HDD $(r = 3/4)$ for ten trials for both 48 and 24 independent sub-carriers. The minimum, maximum, and mean E_b / N_I required for $P_b = 10^{-3}$ obtained from ten trials for 64QAM modulated OFDM with HDD $(r = 3/4)$ performance is shown in Table 17.

HDD(2/3) 64QAM	48 sub-carriers [dB]	24 sub-carriers [dB]	Difference [dB]
Minimum	18.50	18.00	0.50
Maximum	20.50	22.40	-1.90
Mean	19.34	19.28	0.06

Table 17. HDD$(r = 3/4)$ 64QAM modulated OFDM performance statistics for E_b / N_I at $P_b = 10^{-3}$.

The difference in the mean value of E_b / N_I between the 48 and 24 independent sub-carrier's performance is 0.06 dB, which is much smaller than the 5.35 dB obtained for uncoded 64QAM modulated OFDM.

4. HDD Summary

In this section, we investigated the performance of BPSK/QPSK, 16QAM, and 64QAM modulated OFDM with FEC coding at the data rates specified in the *IEEE 802.11a* standard over the Nakagami fading channels in the presence of pulsed-noise jamming where m is modeled as a uniformly distributed random variable in the range of $1/2 \le m \le 5$. This analysis is based on the receiver using hard decision Viterbi decoding. We assume that the channel coherence bandwidth is such that we have $N = 48$ independent sub-channels, although very similar results are obtained if we assume $N = 24$ independent sub-channels. Since the coded and uncoded results cannot be compared for a sufficiently low probability of bit errors, we expressed the coding gain in terms of absolute performance at $P_b = 10^{-3}$, which represents the low end of acceptable performance for WLAN applications. The absolute performance required for $P_b = 10^{-3}$ with HDD

over frequency-selective, slow, composite Nakagami fading channels under the effect of hostile pulsed-noise jamming is summarized in Table 18, where the results represent an average.

Data Rate (Mbps)	Modulation	Code Rate	48 Sub-carriers	24 Sub-carriers
			Absolute Performance in SIR [dB]	Absolute Performance in SIR [dB]
6/12	BPSK/QPSK	1/2	6.78	6.20
9/18	BPSK/QPSK	3/4	13.11	11.92
24	16QAM	1/2	8.78	8.37
36	16QAM	3/4	16.05	15.04
48	64QAM	2/3	17.95	17.34
54	64QAM	3/4	19.34	19.28

Table 18. *IEEE 802.11a* system performance statistics for HDD at $P_b = 10^{-3}$.

For a specific modulation type, regardless of the channel conditions, the SIR required to achieve a fixed probability of bit error increases as the code rate increases. Furthermore, the SIR ranges from 6.2 to 19.34 dB. However, contrary to expectations, the SIR required to achieve a specific P_b does not monotonically decrease when the bit rate decreases. For instance, a larger SIR is required for a bit rate of 18 Mbps than for 24 Mbps.

C. SOFT DECISION DECODING (SDD)

In the previous section, we showed that OFDM system performance is improved significantly by adding FEC coding. We now investigate the performance of the *IEEE 802.11a* standard with Viterbi soft decision decoding. SDD with M-QAM is beyond the scope of this thesis owing to the complexity of analyzing the probability of the bit error with SDD for a binary code transmitted with a non-binary modulation. In addition, due to the difficulty of analyzing the probability of the bit error for two different noise levels

(i.e., when the pulsed-noise jammer is on or off) for SDD with BPSK/QPSK, perfect side information is assumed.

1. BPSK/QPSK with SDD (6 and 12 Mbps)

As addressed earlier, Equation (5.10) is valid as the upper bound for both HDD and SDD, except the probability that the decoder will select a code word that is a Hamming distance d from the correct code word P_d in Equation (5.10) is determined by the type of the modulation, channel, and whether HDD or SDD is used. Therefore, we need to find P_d in order to examine the performance of BPSK/QPSK with SDD over Nakagami fading channels in the presence of pulsed-noise jamming. Assuming that the correct path is the all-zero path and that the r^{th} path differs from the correct path in d bits, then a decoding error occurs when [13]

$$\sum_{l=1}^{d} r_l > 0, \tag{5.22}$$

where l is the index and runs over the set of d bits in which the correct path and the r^{th} path differ, r_l is the demodulator output, and d is the number of bits that the r^{th} path differs from the correct path. Since the demodulator outputs r_l are modeled as independent random variables, then P_d is given by the probability that the sum of the d independent random variables is greater than zero, and P_d can be written as

$$P_d = P_r\left(\sum_{l=1}^{d} r_l > 0\right) \tag{5.23}$$

where P_d is equivalent to the probability of bit error for coherent binary signaling with d^{th}-order diversity [13].

For BPSK/QPSK with SDD over Nakagami fading channels, P_d is conditioned on the received signal amplitude a_c; hence, we obtain the average P_d from

$$P_d = \int_0^\infty P_d\left(a_c\right) f_{A_c}\left(a_c\right) da_c = \int_0^\infty P_d\left(e\right) f_E\left(e\right) de. \tag{5.24}$$

In addition, optimum performance is obtained by using a maximal ratio combiner (MRC) receiver designed for the pulsed-noise jammer with perfect side information. For perfect side information, we assume we know which bits are jammed and which are not. Perfect side information is not realistic, but it gives us a standard against which to measure receivers which have imperfect side information. We assume, except when all bits are jammed, that the jammed bits are disregarded so that for $i < d$ the decision statistic for the BPSK/QPSK receiver consists of the summation of the signals of only the unjammed bits, where i represents the number of bits that are jammed. Therefore, we need to obtain $(d-i)$-fold diversity for BPSK/QPSK over Nakagami fading.

Recall that in Chapter IV, we define $e_b = a_c^2 \cdot T_b$. In this case, we must adjust this definition to reflect the summation of $(d-i)$ Nakagami-squared random variables by defining

$$e = \sum_{k=1}^{d-i} \left(a_c^2\right)_k \cdot T_b. \tag{5.25}$$

Consequently, Equation (4.1) can be expressed

$$P_d(e) = Q\left(\sqrt{\frac{2r \cdot e}{N_o}}\right) \tag{5.26}$$

where the average energy of the $(d-i)$ sequence of uncoded data bits e is equal to the $(d-i)$ sequence of average energy of the coded data bits e_c; hence, $e_c = r \cdot e$ as previously discussed in the derivation of Equation (5.7). Note that Equation (5.26) is a conditional probability. Therefore, we need to obtain the PDF of the sum of $(d-i)$ Nakagami-squared random variables. In [5], the expression for the sum of d independent Nakagami-squared random variables is given as

$$f_\Gamma(\gamma) = \frac{m^{md}}{\Gamma(md)\,\bar{\gamma}^{md}} \gamma^{md-1} e^{-\left(\frac{m\gamma}{\bar{\gamma}}\right)} \tag{5.27}$$

where $\bar{\gamma} = E[\gamma]$. We obtain the PDF of the sum of $(d-i)$ independent Nakagami-squared random variables by making the following substitutions in Equation (5.27):

$$
\begin{aligned}
d &= d - i \\
e &= \gamma \\
E &= \bar{\gamma}.
\end{aligned} \tag{5.28}
$$

We obtain the final result for the sum of $(d-i)$ independent Nakagami-squared random variables in terms of e, E, and $d-i$ as

$$
f_E(e) = \frac{m^{m(d-i)}}{\Gamma\left[m(d-i)\right] E^{m(d-i)}} E^{m(d-i)-1} e^{-\left(\frac{me}{E}\right)}. \tag{5.29}
$$

Substituting Equations (5.29) and (5.26) into Equation (5.24) to obtain P_d, we must evaluate the integral

$$
P_d = \int_0^{\infty} Q\left(\sqrt{\frac{2r \cdot e}{N_o}}\right) \cdot \frac{m^{m(d-i)}}{\Gamma\left[m(d-i)\right] E^{m(d-i)}} E^{m(d-i)-1} e^{-\left(\frac{me}{E}\right)} de. \tag{5.30}
$$

If we compare Equation (5.30) to Equations (4.25) through (4.29), we can evaluate this integral by setting

$$
\begin{aligned}
a &= m / E \\
b &= m(d-i) \\
t &= e \\
c &= 2r / N_o \\
\psi &= \frac{c}{2a} = \frac{r \cdot E}{m N_o} = \frac{r}{m} SNR.
\end{aligned} \tag{5.31}
$$

As a result, we get

$$
P_d(i) = \frac{1}{\sqrt{1 + \frac{m}{r} SNR^{-1}}} \frac{\Gamma\left[m(d-i) + 0.5\right]}{2\sqrt{\pi} \cdot \Gamma\left[m(d-i)+1\right] \left(1 + \frac{rSNR}{m}\right)^{m(d-i)}} \left(1 + \sum_{k=0}^{\infty} \frac{\prod_{n=0}^{k-1} \left[m(d-i) + 0.5 + n\right] \left(\frac{1}{1 + \frac{rSNR}{m}}\right)^k}{\prod_{n=0}^{k-1} \left[m(d-i) + 1 + n\right]} \right) \tag{5.32}
$$

as the probability of selecting a path that is a Hamming distance d from the correct path when i of the d bits are jammed for BPSK/QPSK.

For $i = d$, all bits are used to compute the decision statistic. At this point the total noise power spectral density increases from N_o to $N_I / \rho + N_o$ as we discussed in the derivation of Equation (4.5). In this case, $P_d\left(i = d\right)$ is obtained from the probability of bit error of BPSK/QPSK with d-fold diversity. Therefore, Equation (5.30) can be written as

$$P_d\left(d\right) = \int_0^\infty Q\left(\sqrt{\frac{2r \cdot e}{N_o + N_I / \rho}}\right) \cdot \frac{m^{md}}{\Gamma\left(md\right) E^{md}} E^{md-1} e^{-\left(\frac{me}{E}\right)} de. \tag{5.33}$$

As before, this integral is solved by using Equations (4.25) through (4.29) and making the following substitutions

$$\begin{aligned} a &= m / E \\ b &= md \\ t &= e \\ c &= \frac{2r}{\left(N_o + N_I / \rho\right)} \\ \psi &= \frac{c}{2a} = \frac{r \cdot E}{m\left(N_o + N_I / \rho\right)} = \frac{r}{m\left(SNR^{-1} + SIR^{-1} / \rho\right)}. \end{aligned} \tag{5.34}$$

Consequently, we obtain the final result

$$\begin{aligned} P_d\left(d\right) = & \frac{1}{\sqrt{1 + \frac{m}{r}\left(SNR^{-1} + SIR^{-1} / \rho\right)}} \cdot \frac{\Gamma\left(md + 0.5\right)}{2\sqrt{\pi} \cdot \Gamma\left(md + 1\right)\left(1 + \frac{r}{m\left(SNR^{-1} + SIR^{-1} / \rho\right)}\right)^{md}} \\ & \times \left(1 + \sum_{k=0}^{\infty} \frac{\prod_{n=0}^{k-1}\left(md + 0.5 + n\right)\left(\frac{1}{1 + \frac{r}{m\left(SNR^{-1} + SIR^{-1} / \rho\right)}}\right)^k}{\prod_{n=0}^{k-1}\left(md + 1 + n\right)}\right). \end{aligned} \tag{5.35}$$

Since whether or not a bit is jammed is independent of whether other bits are jammed or not, the probability that i of d bits are jammed is

$$\rho^i (1-\rho)^{d-i} \tag{5.36}$$

where i is the number of jammed bits and ρ represents the probability that the bit is jammed, which is determined by the fraction of the time the jammer is turned on.

The number of the different ways that i of d bits can be jammed is an example of Bernolli trials and is given by the binomial coefficient

$$\binom{d}{i}. \tag{5.37}$$

Hence, the probability of the event i of d bits jammed is [16]

$$P_r(i \text{ bits jammed}) = \binom{d}{i} \rho^i (1-\rho)^{d-i}. \tag{5.38}$$

The probability of selecting a path that is a Hamming distance d from the correct path when i of the d bits are jammed for BPSK/QPSK is the sum of the probability of selecting a path that is a Hamming distance d from the correct path when i of the d bits are jammed for BPSK/QPSK that 1 bit is jammed and $d-1$ are not, the probability of the bit error that 2 bits are jammed and $d-2$ are not, etc. and can be written as

$$P_d = \sum_{i=0}^{d} P_r(i \text{ bits jammed}) P_d(i) = \sum_{i=0}^{d} \binom{d}{i} \rho^i (1-\rho)^{d-i} \cdot P_d(i) \tag{5.39}$$

where $P_d(i)$ is represented by Equation (5.32) when $i < d$. If all the bits are jammed $(i = d)$, we substitute Equation (5.35) into Equation (5.39).

Consequently, we obtain an upper bound on the probability of the bit error for BPSK/QPSK with SDD over Nakagami fading channels in the presence of a pulsed-noise jammer with perfect side information by substituting Equation (5.39) and the coefficients of B_d listed in Table 11 into Equation (5.10).

Since thermal noise is not neglected in Equations (5.32) and (5.35), we need to estimate the required signal-to-noise ratio (SNR). Therefore, with respect to the two different code rates $\left(r = 1/2,\ r = 3/4\right)$ used in the *IEEE 802.11a* standard for BPSK/QPSK, OFDM performance for 48 independent sub-carriers over composite Nakagami fading channels with SDD is plotted in Figure 51 by using the results provided in [5]. As we can see, $SNR = 6$ dB is required for code rate $r = 1/2$ in order to achieve the $P_b = 10^{-5}$ bit error probability.

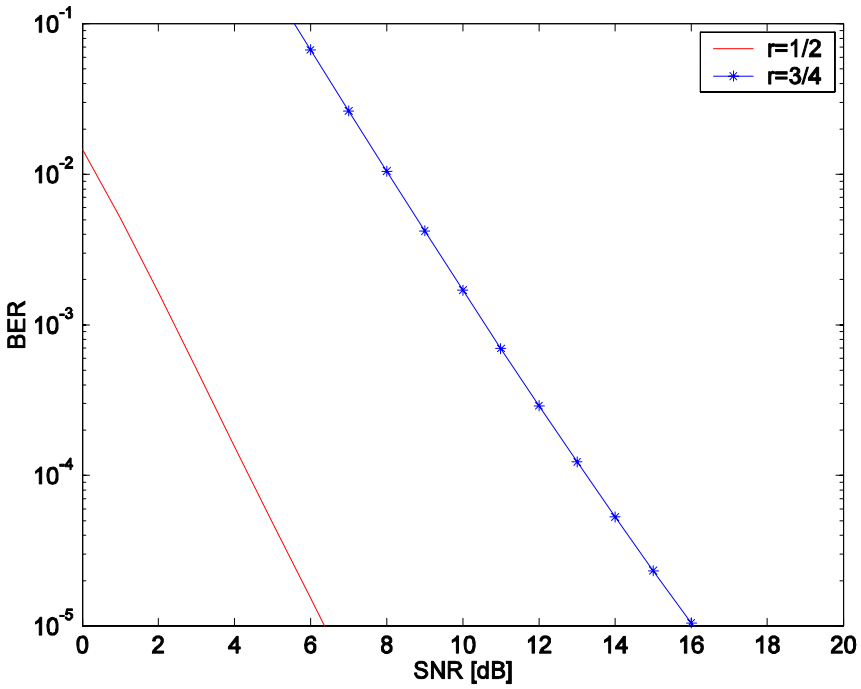

Figure 51. Performance of BPSK/QPSK with SDD in Nakagami fading.

Looking at Equation (5.39) more closely, we notice that for small SNR, P_d is dominated by the $i = d - 1$ term. If we plot the performance of BPSK/QPSK with respect to SIR, we get constant probability of bit error curves. Thus, in order to investigate the effects of pulsed-noise jamming in Nakagami fading channels for BPSK/QPSK with SDD $\left(r = 1/2\right)$, instead of using $SNR = 6$ dB in Equations (5.32) and (5.35), we plot sub-channel performance by assuming $SNR = 20$ dB and $SNR = 30$ dB in Figures 52 and 53, respectively, where $\rho = 0.5$ and m is a parameter in the range of $1/2 \le m \le 3$.

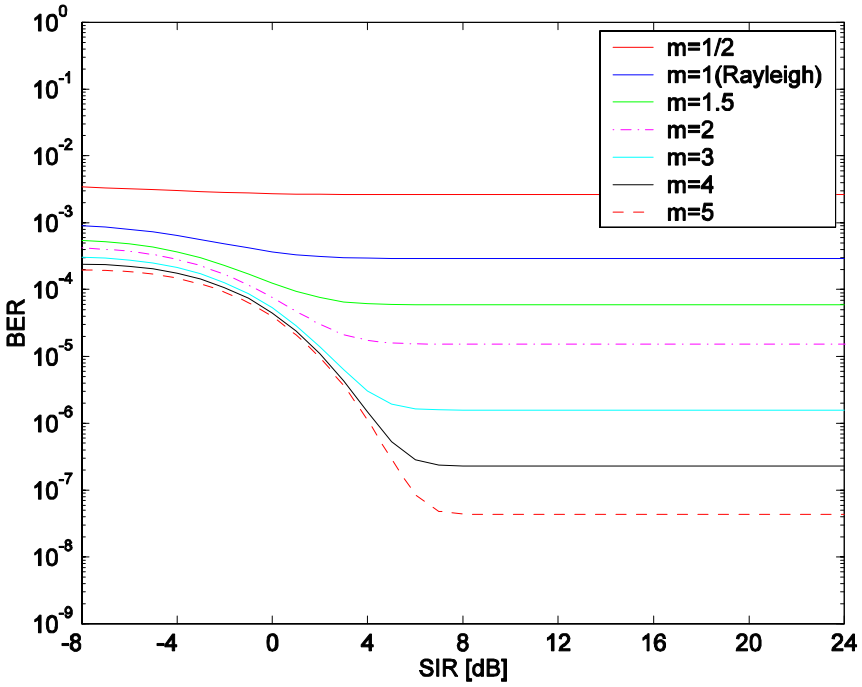

Figure 52. Performance of BPSK/QPSK with SDD $(r = 1/2)$ over a Nakagami fading channel with pulsed-noise jamming, $SNR = 20$ dB and $\rho = 0.5$.

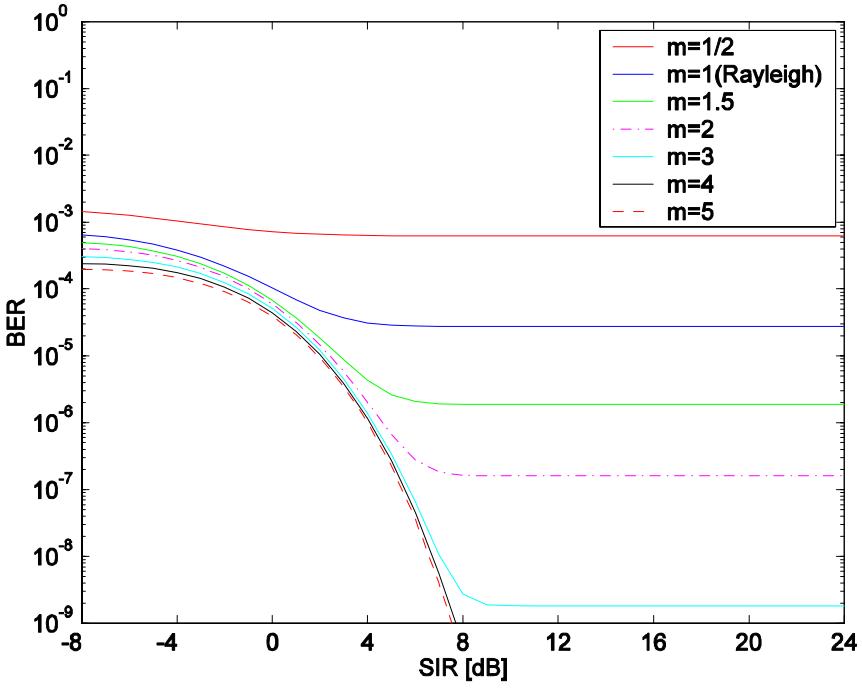

Figure 53. Performance of BPSK/QPSK with SDD $(r = 1/2)$ over a Nakagami fading channel with pulsed-noise jamming, $SNR = 30$ dB and $\rho = 0.5$.

We consider the worst case $\rho_{wc} = 1$ for the SDD receiver where all jammed bits are used to compute the decision statistics. In Figure 54, we plot the performance of BPSK/QPSK with SDD $(r = 1/2)$ for the worst case by substituting Equation (5.35) into Equation (5.39) for different values of the fading figure m. Note that the corresponding $SNR = 6$ dB value obtained from Figure 51 is used in Equation (5.35) in this case.

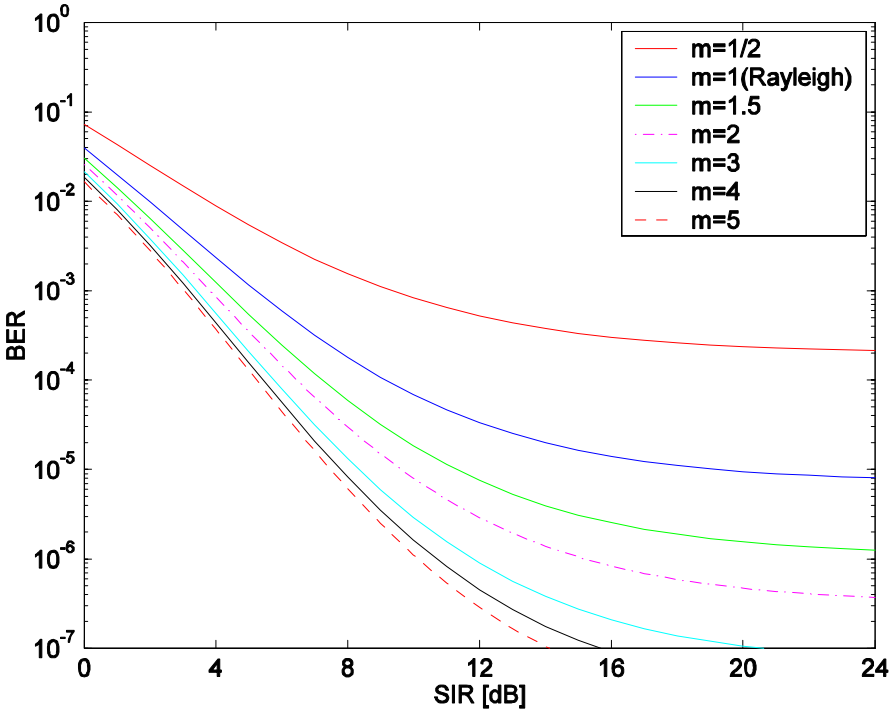

Figure 54. Performance of BPSK/QPSK with SDD $(r = 1/2)$ over a Nakagami fading channel with pulsed-noise jamming, $SNR = 6$ dB and $\rho = 1$.

As discussed earlier, we assume that the receiver has perfect side information for SDD. If we compare the performance of BPSK/QPSK with SDD versus HDD, we cannot make a direct comparison since we used two different noise levels in the HDD analysis. However, we can compare the results by assuming $\rho = 1$ for HDD. Therefore, in order to gain some perspective on the improvement in performance, in Figure 55 we compare Figure 54 with Figure 31, which is the performance of BPSK/QPSK with HDD over a Nakagami fading channel in the presence of pulsed-noise jamming, but this time with $\rho = 1$.

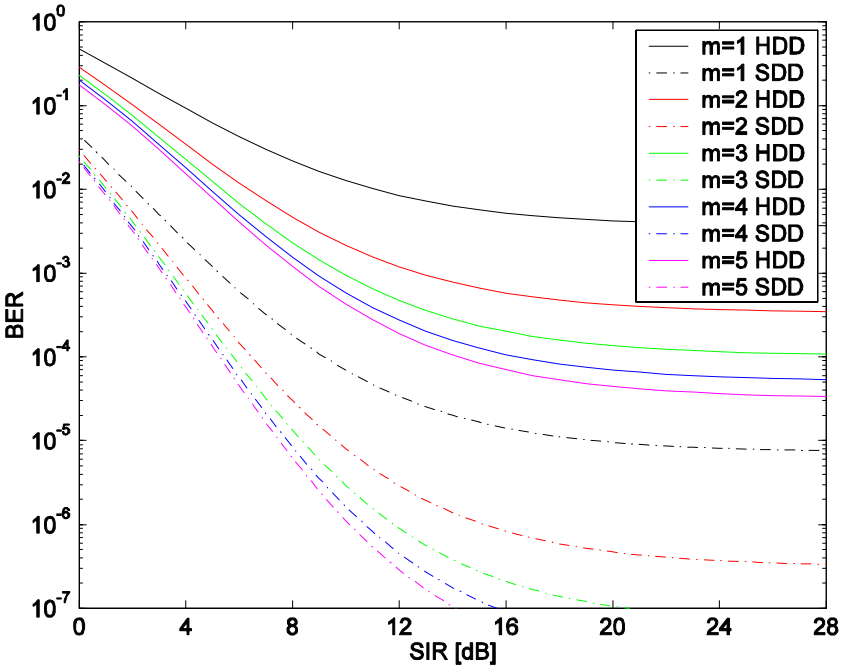

Figure 55. SDD vs. HDD$(r=1/2)$ BPSK/QPSK performance over Nakagami fading with pulsed-noise jamming where $SNR=6$ dB and $\rho=1$.

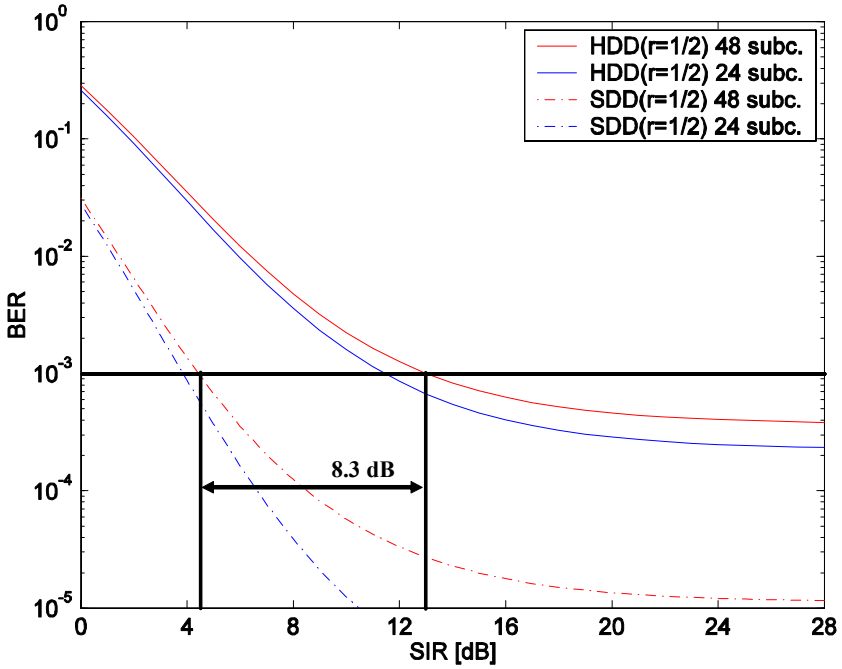

Figure 56. SDD vs. HDD$(r=1/2)$ BPSK/QPSK modulated OFDM performance over a composite Nakagami fading channel with pulsed-noise jamming where $SNR=6$ dB and $\rho=1$.

After examining sub-channel performance, we investigate the performance of BPSK/QPSK modulated OFDM with SDD over Nakagami fading channels in the presence of the worst case $\rho_{wc} = 1$ pulsed-noise jamming. In Figure 56, we overlay SDD and HDD performance, both with $r = 1/2$ code, for BPSK/QPSK modulated OFDM for both 48 and 24 independent sub-carriers over a composite Nakagami fading channel for one trial, where m is assumed to be a random variable over the range $1/2 \le m \le 5$.

As we can see, the coding gain for SDD relative to HDD is 8.3 dB. Just as before, an average probability of bit error is obtained by evaluating BPSK/QPSK modulated OFDM performance with SDD $(r = 1/2)$ for ten trials for both 48 and 24 independent sub-carriers. The minimum, maximum, and mean for the E_b / N_I required for $P_b = 10^{-3}$ obtained from ten trials for BPSK/QPSK modulated OFDM with SDD $(r = 1/2)$ is shown in Table 19.

SDD(1/2) BPSK/QPSK	48 sub-carriers [dB]	24 sub-carriers [dB]	Difference [dB]
Minimum	4.06	3.34	0.72
Maximum	4.82	4.53	0.29
Mean	4.37	3.98	0.39

Table 19. SDD $(r = 1/2)$ BPSK/QPSK modulated OFDM performance statistics for E_b / N_I at $P_b = 10^{-3}$.

The mean of E_b / N_I for 48 and 24 independent sub-carriers are 4.37 dB and 3.98 dB, respectively. The difference in the mean value of E_b / N_I between 48 and 24 independent sub-carrier's performance is 0.39 dB.

By way of summarizing the results for BPSK/QPSK for 6 and 12 Mbps data rates, we overlay the performance curves for SDD, HDD, and uncoded BPSK/QPSK modulated OFDM over a composite Nakagami fading channel in the presence of pulsed-noise jamming in Figure 57 where $\rho = 1$ and $SNR = 6$ dB. As we can see, the coding gain is remarkable. Without FEC, we cannot achieve even $P_b = 10^{-2}$. In terms of absolute performance, the composite OFDM system requires a received average SIR per bit of 4.4 dB with SDD.

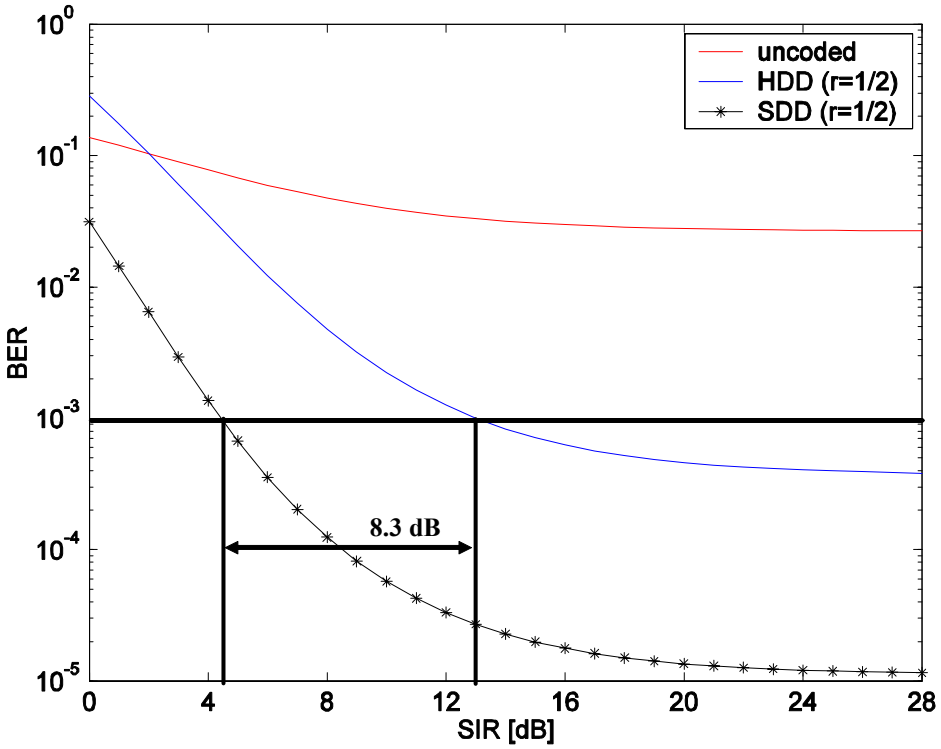

Figure 57. SDD, HDD and uncoded BPSK/QPSK modulated OFDM performance over a composite Nakagami fading channel with pulsed-noise jamming where $SNR = 6$ dB and $\rho = 1$.

2. BPSK/QPSK with SDD (9 and 18 Mbps)

We perform the same analysis for code rate $r = 3/4$ to obtain the performance curves for 9 Mbps BPSK modulated OFDM and 18 Mbps QPSK modulated OFDM used in the *IEEE 802.11a* standard. The results of this analysis for a single sub-carrier are shown in Figure 58 for the usual range of m. However, as discussed in the previous subsection, in order to investigate the effects of pulsed-noise jamming in Nakagami fading channels for BPSK/QPSK with SDD $(r = 3/4)$, instead of using $SNR = 16$ dB obtained from Figure 51 in Equations (5.32) and (5.35), we plot the sub-channel performance by assuming $SNR = 30$ dB in Figures 58 where $\rho = 0.5$.

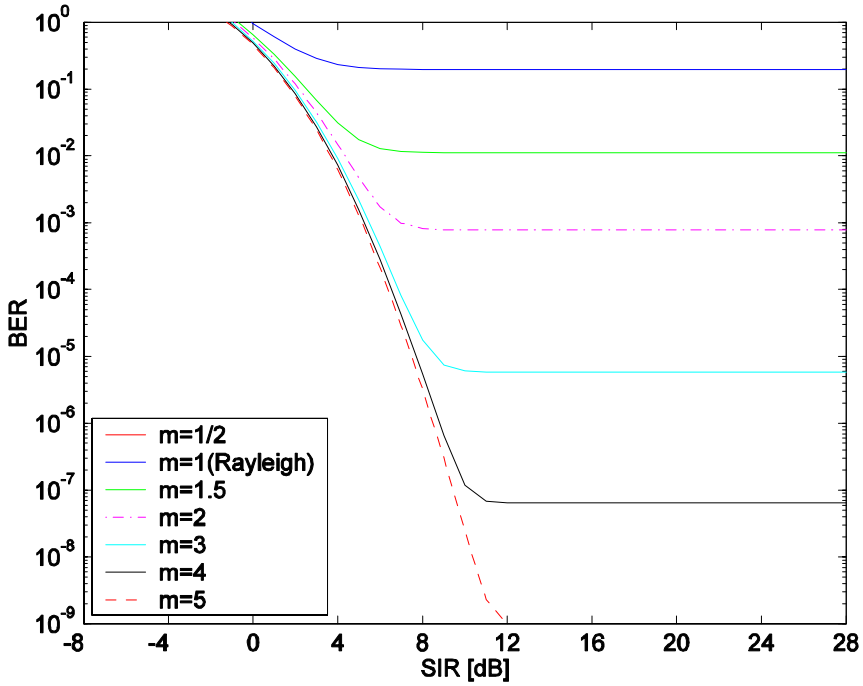

Figure 58. Performance of BPSK/QPSK with SDD $(r = 3/4)$ over a Nakagami fading channel with pulsed-noise jamming, $SNR = 30$ dB and $\rho = 0.5$.

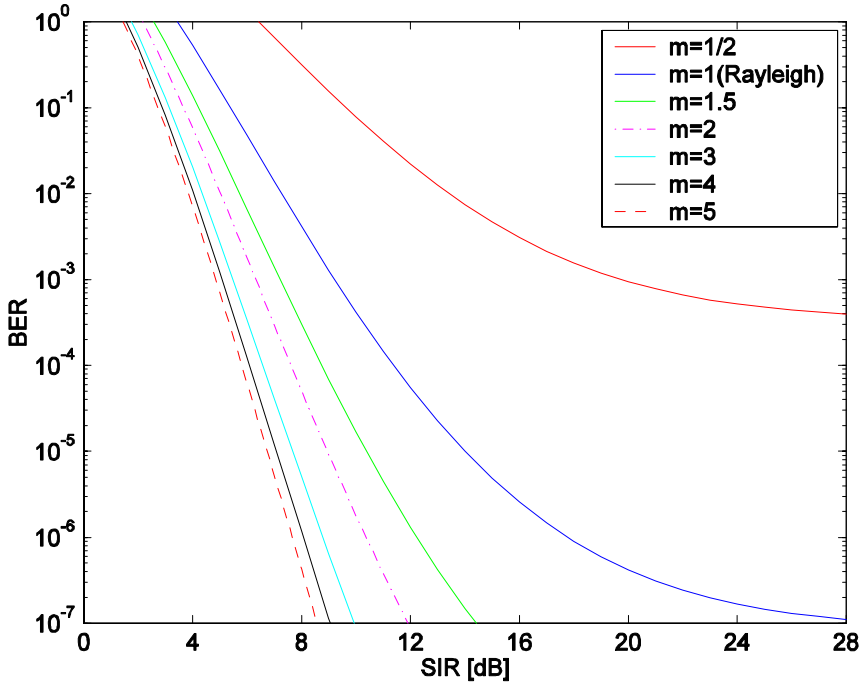

Figure 59. Performance of BPSK/QPSK with SDD $(r = 3/4)$ over a Nakagami fading channel with pulsed-noise jamming, $SNR = 16$ dB and $\rho = 1$.

As before, we consider the worst case $\rho_{wc}=1$ for the SDD receiver where all jammed bits are used to compute the decision statistics. In Figure 59, we plot the performance of BPSK/QPSK with SDD $(r=3/4)$ for the worst case by substituting Equation (5.35) into Equation (5.39) for different values of the fading figure m. Note that the corresponding $SNR=16$ dB obtained from Figure 51 is used in Equation (5.35).

In Figure 60, we overlay the BPSK/QPSK with HDD $(r=3/4)$ performance over those in Figure 35 to see the improvement in performance of BPSK/QPSK when applying SDD with a code rate $(r=3/4)$ over the Nakagami fading channels in the presence of pulsed-noise jamming but this time with $\rho=1$. Looking at Figure 60 more closely, we see that there is a significant improvement in sub-channel performance with SDD$(r=3/4)$ for $m=1$ at $P_b=10^{-5}$, which is better than the performance obtained for HDD$(r=3/4)$ where we cannot achieve even $P_b=10^{-3}$ regardless of the SIR that is used.

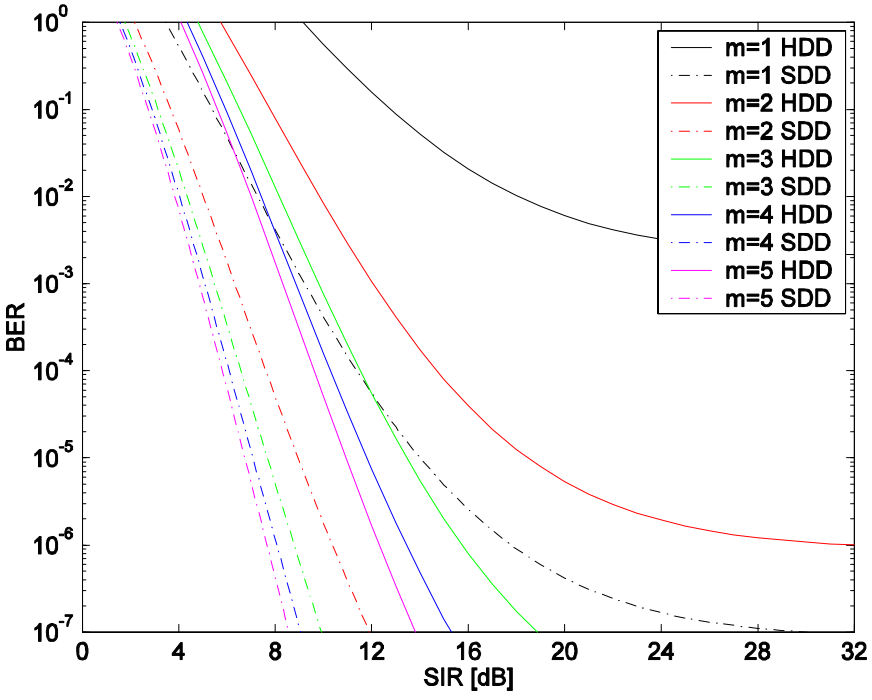

Figure 60. SDD vs. HDD$(r=3/4)$ BPSK/QPSK performance over Nakagami fading with pulsed-noise jamming, $SNR=16$ dB and $\rho=1$.

After examining sub-channel performance, we investigate the performance of BPSK/QPSK modulated OFDM with SDD $(r = 3/4)$ over the Nakagami fading channels in the presence of the worst case $\rho_{wc} = 1$ pulsed-noise jamming. In Figure 61, we overlay SDD and HDD performance, both with $r = 3/4$ code, for BPSK/QPSK modulated OFDM for both 48 and 24 independent sub-carriers over a composite Nakagami fading channel for one trial, where m is assumed to be a uniform random variable over the range $1/2 \le m \le 5$.

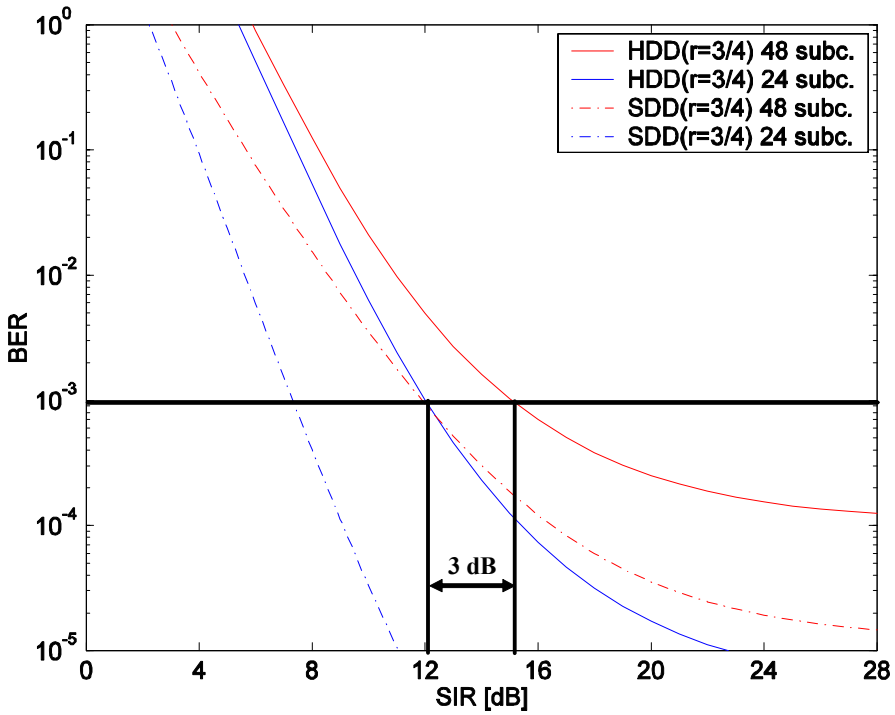

Figure 61. SDD vs. HDD $(r = 3/4)$ BPSK/QPSK modulated OFDM performance over a composite Nakagami fading channel with pulsed-noise jamming where $SNR = 16$ dB and $\rho = 1$.

As we can see the coding gain for SDD relative to HDD is 3dB. There is a degradation in the coding gain with respect to the code rate $r = 1/2$. An average probability of bit error is obtained by evaluating the BPSK/QPSK modulated OFDM performance with SDD $(r = 3/4)$ for ten trials for both 48 and 24 independent sub-carriers. The minimum, maximum, and mean for the E_b / N_I required for $P_b = 10^{-3}$

obtained from ten trials for BPSK/QPSK modulated OFDM with SDD $(r = 3/4)$ is shown in Table 20.

SDD(3/4) BPSK/QPSK	48 sub-carriers [dB]	24 sub-carriers [dB]	Difference [dB]
Minimum	8.30	5.75	2.55
Maximum	12.15	11.83	0.32
Mean	10.86	8.94	1.92

Table 20. SDD $(r = 3/4)$ BPSK/QPSK modulated OFDM performance statistics for E_b / N_I at $P_b = 10^{-3}$.

The mean of E_b / N_I for 48 and 24 independent sub-carriers are 11.9 dB and 7.3 dB, respectively. The difference in the mean of E_b / N_I between 48 and 24 independent sub-carrier's performance is 1.92 dB.

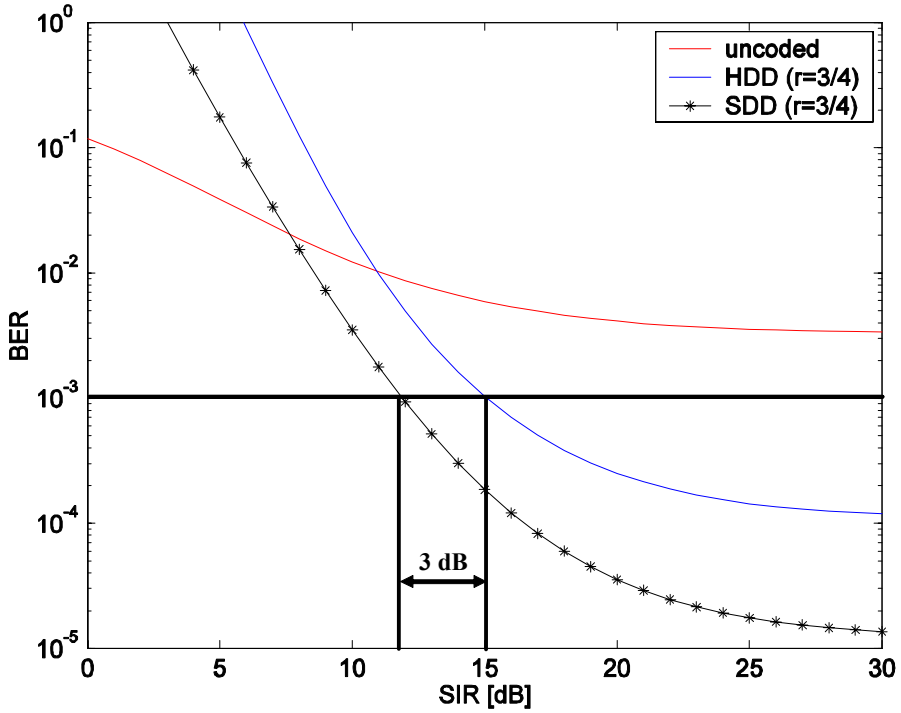

Figure 62. SDD, HDD and uncoded BPSK/QPSK modulated OFDM performance over a composite Nakagami fading channel with pulsed-noise jamming where $SNR = 16$ dB and $\rho = 1$.

By way of summarizing the results for BPSK/QPSK for 9 and 18 Mbps data rates, we overlay the performance curves for SDD, HDD, and uncoded BPSK/QPSK modulated OFDM over a composite Nakagami fading channel in the presence of pulsed-noise jamming in Figure 62, where $\rho = 1$ and $SNR = 16$ dB. As we can see, the coding gain is remarkable. In terms of absolute performance, the composite OFDM system requires a received average SIR per bit of 11.9 dB with SDD.

3. SDD Summary

As expected, even greater improvement in performance is obtained by employing soft decision Viterbi decoding. In order to compare the improvement obtained with SDD, we disregarded the two different noise levels and made the assumption that the jammer is on at all times. For BPSK/QPSK with code rate $r = 1/2$, SDD improves performance by 8.3 dB over a composite Nakagami fading channel with jamming. For BPSK/QPSK with code rate $r = 3/4$, SDD improves performance by 3 dB over a composite Nakagami fading channel with jamming. Moreover, there is a significant improvement in sub-channel performance with SDD$(r = 3/4)$ for $m = 1$ at $P_b = 10^{-5}$, which is better than the performance obtained for HDD$(r = 3/4)$.

VI. CONCLUSION

A. FINDINGS

There are several findings that result from the analysis of *IEEE 802.11a* based OFDM system performance over frequency-selective, slow, Nakagami fading channels in the presence of pulsed-noise jamming.

First, OFDM performance without FEC coding is dominated by the small values of the channel parameter m, which corresponds to more severe fading conditions. Furthermore, after averaging sub-carrier performance, we note that the performance trend for the average of both 48 and 24 independent sub-carriers appears to be near the midpoint where $m = 1$ so that the resulting composite signal is fairly well approximated as a Rayleigh fading channel. The values of E_b / N_I required to achieve a certain probability of bit error are well beyond what is achievable in any communications system. The performance of uncoded BPSK/QPSK modulated OFDM in the presence of pulsed-noise jamming is better than uncoded 16QAM and 64QAM; however, the performance is not acceptable regardless of the modulation type or the number of independent sub-carriers without FEC.

Second, for the performance with convolutional coding and Viterbi HDD, the OFDM system performance is improved significantly by adding FEC coding. The coded and uncoded results cannot be compared for a sufficiently low probability of bit errors without resorting to excessively large SNR and SIR for the uncoded system; therefore, we expressed the coding gain in terms of absolute performance at $P_b = 10^{-3}$, which represents the low end of acceptable performance for WLAN applications. The absolute performance in SIR ranges from 6.2 to 19.34 dB. Also, as expected, for a specific modulation type, regardless of the channel conditions, the SIR required to achieve a fixed probability of bit error increases as the code rate increases. However, contrary to expectations, the SIR required to achieve a specific P_b does not monotonically decrease when the bit rate decreases.

Third, for the performance with convolutional coding and Viterbi SDD with perfect side information, for BPSK/QPSK with code rate $r = 1/2$, SDD improves performance by 8.3 dB over a composite Nakagami fading channel with jamming. For BPSK/QPSK with code rate $r = 3/4$, SDD improves performance by 3 dB over a composite Nakagami fading channel with jamming. Moreover, there is a significant improvement in sub-channel performance with SDD$(r = 3/4)$ for $m = 1$ at $P_b = 10^{-5}$, which is better than the performance obtained for HDD$(r = 3/4)$.

Finally, in this thesis we assume the channel coherence bandwidth is such that we have either $N = 48$ or $N = 24$ independent sub-carriers. Without FEC coding, the difference in the mean value of E_b / N_I between 48 and 24 independent sub-carrier's performance is around 5.8 dB at $P_b = 10^{-5}$ and ranges from 0.06 dB through 1.2 dB for Viterbi HDD; that is, the difference in performance between 48 and 24 independent sub-carriers decreases when FEC coding is used. On the other hand, we assume that the receiver has perfect side information for SDD. Thus, if we compare the performance of BPSK/QPSK with SDD versus HDD, we cannot make a direct comparison since we do not assume side information in the HDD analysis.

B. RECOMMENDATION FOR FURTHER RESEARCH

There are several areas in which follow-on research is recommended. First, another type of distribution can be chosen to model m when computing the composite OFDM signal. Intuitively, it seems that a Gaussian distribution would be a better model. In this thesis, m was modeled as a uniform distribution over the assumed range of m since this provides a more consecutive result. Second, due to the difficulty of analyzing the probability of bit error for two different noise levels (i.e., when the pulsed-noise jammer is on or off) for SDD, we assume that the receiver has perfect side information. However, an approximate approach to analyze the performance without perfect side information by using numerical results is a natural outgrowth of this thesis. Third, the performance analysis of OFDM with pulsed-noise jamming in different fading conditions as described by another random distribution in place of the Nakagami-m distribution is

also an interesting topic for further research. Finally, the analysis of system performance with SDD for non-binary modulation techniques should be investigated.

C. CLOSING COMMENTS

WLANs are increasingly important in meeting the needs of next generation broadband wireless communications systems for both commercial and military applications. Therefore, an analysis such as this thesis will prove beneficial to those learning, utilizing or designing the OFDM based *IEEE 802.11a* 5 GHz WLAN standard systems under the effect of hostile jamming for military applications.

In addition to its well-known ability to mitigate the most severe multipath effects while achieving high data rates, OFDM will continue to gain broad-based acceptance as the signaling technique of the future.

THIS PAGE INTENTIONALLY LEFT BLANK

LIST OF REFERENCES

1. Wan, L. and Dubey, V.K., "Bit Error Probability of OFDM System Over Frequency-nonselective Fast Rayleigh Fading Channels," *IEEE Electronics Letters*, Volume 36, pp. 1306-07, 15 July 2000.

2. Wan, L. and Dubey, V.K., "BER Performance of OFDM System Over Frequency-nonselective Fast Ricean Fading Channels," *IEEE Communications Letters*, Volume 5, pp. 19–21, 1 January 2001.

3. David A. Wiegandt & Carl R. Nassar, "High-Performance 802.11a Wireless LAN via Carrier-Interferometry Orthogonal Frequency Division Multiplexing at 5 Ghz," *IEEE Global Telecommunications Conference*, 2001, Volume 6, pp.3579-3582.

4. Kao, Chihan, "Performance of the IEEE 802.11a Wireless LAN Standard over Frequency-selective, Slow, Ricean Fading Channels," Master's thesis, Naval Postgraduate School, Monterey, CA, 2002.

5. Patrick, A.Count, "Performance Analysis of OFDM in Frequency-selective, Slowly Fading Nakagami Channels," Master's thesis, Naval Postgraduate School, Monterey, CA, 2001.

6. Institute of Electrical and Electronics Engineers, 802.11a, *Wireless LAN Medium Access Control (MAC) and Physical Layer (PHY) Specifications: High-Speed Physical Layer Extension in the 5 GHz Band*, 16 September 1999.

7. Theodore S. Rappaport, *Wireless Communications Principles and Practice*, 2nd edition, Prentice Hall, Upper Saddle River, NJ, 2002.

8. Sklar, B., *Digital Communications: Fundamental and Applications.*, 2nd edition, Prentice Hall, Upper Saddle River, NJ, 2001.

9. Homayoun Hastemi, "The Indoor Radio Propagation Channel", *Proceedings of the IEEE*, Vol.81, No.7, July 1993.

10. Proakis, J.G., *Digital Communications*, 4rd edition, McGraw Hill, New York, NY, 2001.

11. Xiong, F., *Digital Modulation Techniques*, Artech House, Norwood, MA, 2000.

12. Leon-Garcia, A., *Probability and Random Processes for Electrical Engineering.* 2nd edition, Reading, MA, 1994.

13. Robertson, Clark, Notes for EC4580 (Coding and Information), Naval Postgraduate School, Monterey, CA, 2001 (unpublished).

14. Clark, G.C., Jr. and Cain, J.B., *Error-Correction Coding for Digital Communications,* Plenum Press, New York, NY, 1981.

15. Wicker, S.B., *Error Control Systems for Digital Communication and Storage,* Prentice Hall, Upper Saddle River, NJ, 1995.

16. Robertson, Clark, Notes for EC4560 (Spread Spectrum Communication Systems), Naval Postgraduate School, Monterey, CA, 2001 (unpublished).

17. Peterson, R.L. Ziemer, R.E. and Borth, D.E, *Introduction to Spread Spectrum Communications*, Prentice Hall, Upper Saddle River, NJ, 1995.

18. Beaulieu, N.C. and Abu-Dayya, A. A., "Analysis of Equal Gain Diversity on Nakagami Fading Channels," *IEEE Trans. Commun.,* Vol. COM-39, pp. 225-234, February 1991.

19. Van Nee, R. and Prasad R., *OFDM for Wireless Multimedia Communications*, Artech House, Norwood, MA, 2000.

20. Bahai, A.R.S., and Saltzberg, B.R., *Multi-Carrier Digital Communications: Theory and Applications of OFDM*, Kluwer Academic/Plenum, New York, NY, 1999.

21. May, T. Rohling, H., and Engels, V., "Performance Analysis of Viterbi Decoding for 64-DAPSK and 64-QAM Modulated OFDM Signals," *IEEE Transactions on Communications.* Vol. 46, No. 2, pp. 182-190, Feb 1998.

22. Gradshteyn, I.S. and Ryzhik, I.M., *Tables of Integrals, Series, and Products*, Academic Press, New York, NY, 1980.

INITIAL DISTRIBUTION LIST

1. Defense Technical Information Center
   Ft. Belvoir, Virginia

2. Dudley Knox Library
   Naval Postgraduate School
   Monterey, California

3. Chairman, Code EC
   Department of Electrical and Computer Engineering
   Naval Postgraduate School
   Monterey, California

4. Professor R. Clark Robertson, Code EC/RC
   Department of Electrical and Computer Engineering
   Naval Postgraduate School
   Monterey, California

5. Professor Tri Ha, Code EC/HA
   Department of Electrical and Computer Engineering
   Naval Postgraduate School
   Monterey, California

6. Deniz Kuvvetleri Komutanligi
   Personel Daire Baskanligi
   Bakanliklar, Ankara-06410, TURKEY

7. Deniz Harp Okulu Komutanligi
   Kutuphane
   Tuzla, Istanbul-81704, TURKEY

8. Kara Harp Okulu Komutanligi
   Kutuphane
   Bakanliklar, Ankara-06410, TURKEY

9. Hava Harp Okulu Komutanligi
   Kutuphane
   Yesilyurt, Istanbul, TURKEY

10. Irfan Kosa
    Gokay Sitesi, Baglar Mahallesi
    Yildiztepe 33. Sokak No:5
    Erenler, Adapazari, TURKEY